2022

Optimisation of the End-To-End Phantom for Real-time High Dose Rate Prostate Brachytherapy Verification

Nicholas Ambrosi
University of Wollongong

Optimisation of the End-To-End Phantom for Real-time High Dose Rate Prostate Brachytherapy Verification.

A thesis submitted in fulfilment of

the requirements for the award of the degree

Masters of Research - Medical and Radiation Physics

from

UNIVERSITY OF WOLLONGONG

By

Nicholas Ambrosi

B. Med. Rad Physics

School of Physics

Faculty of Engineering and Information Sciences

May, 2022

I certify that this thesis has not previously been submitted for any degree and is not being submitted as part of candidature for any degree.

I also certify that the thesis has been written by me and any help that I have received in preparing this thesis, and all sources used, have been acknowledged in this thesis.

Signature of candidate:

.....

Nicholas Ambrosi

May 19, 2022

Abstract

High dose rate (HDR) brachytherapy is a form of close range radiotherapy whereby dose is delivered by means of an internal radiation source. By doing so, a high level of dose conformity and accuracy can be achieved. However, due to the high source activity coupled with the close proximity of radio-sensitive organs such as the rectum, bladder and urethra, there exists the potential of incorrect dose delivery; the irradiation of these organs may consequently lead to post-treatment complications. As a result, the need for accurate forms of quality assurance methodology which can verify different aspects of the treatment delivery is paramount. These methodologies must be able to perform real-time dose analysis to monitor crucial organ exposure as well as accurately localise the HDR source within space to verify its position according to the treatment plan.

An End-to-end Phantom was developed with anatomically correct Gel Prostate phantoms to create an anthropomorphic representation of the clinical environment. This allowed the testing of clinically relevant treatment plans on the MP987 detector system to test its source localisation capabilities. It was shown that when comparing to the TPS defined dwell positions, the system was able to determine positions on average to within (3.69±0.14)mm, (3.70±0.15)mm, (3.53±0.12)mm and (0.30±0.06)s for the x, y, z and t coordinates respectively.

Preliminary tracking capabilities of the novel TRUSProbe Tracker were shown to achieve limited levels of accuracy based upon which axis is being investigated. However, the probes ability to perform *in-vivo* rectal dose measurements was shown to yield an overall difference

of (-2.34±6.3)% compared to the TPS. The capability of real-time dose measurements was shown to be plausible, with a catheter-by-catheter dose analysis producing a -2.4% difference.

Acknowledgements

I would like this opportunity to extend my warmest and most sincere gratitude and appreciation to those who have helped me during the course of my thesis; from data interpretation to a few words of encouragement each act of assistance has not gone unnoticed.

I would first and foremost wish to express my greatest thanks to my supervisor Dr. Dean Cutajar. If it wasn't for his resourcefulness and commitment we would not have gotten through the thesis.

Secondly, I would like to thank Distinguished Professor Anatoly Rosenfeld, Director of Medical and Radiation Physics as the University of Wollongong, as well as Marco Petasecca and Owen Brace for their input into the progression of the thesis. Their ideals have aided greatly in moving through periods of low momentum.

I would also like to thank my colleague Yashiv Dookie, for his abundance in knowledge of computer programming. If it wasn't for Yashiv, the full potential of the thesis would not have been reached. I appreciate your help and more importantly your friendship over the course of this wild ride.

Another individual whom deserves recognition is Joel Poder as well as the staff from St George Cancer Care Centre. His input and dedication to research is admirable and his help over the course of this thesis is appreciated.

Finally, I would like to thank my friends and family for their constant support and encouragement over this time. They have been the backbone to my efforts and without them I would not have made it through. Thank you.

Contents

List of Figures

List of Tables

List of Abbreviations

BT Brachytherapy

HDR High Dose Rate

LDR Low Dose Rate

E2E End-to-End

TRUS Trans Rectal Ultra Sound

US Ultra Sound

TPS Treatment Planning System

QA Quality Assurance

CT Computed Tomography

MOSFET Metal oxide semiconductor field effect transistors

MP Magic Plate

IMRT Intensity modulated radiation therapy

SSD Source to surface distance

SDD Source to detector distance

MU Monitor units

IVTV *in-vivo* treatment verification

TPT TRUSProbe Tracker

Chapter 1

Introduction

Among Australian males, prostate cancer remains one of the leading causes of death, with an estimated 17,729 new cases and 3,500 deaths in 2018 [1]. Additionally, 1 in 31 males will die from prostate cancer by the age of 85 [1]. This high level of occurrence can be seen on the world scale, with an estimated 1.1 million new patients in 2015 and approximately 307,000 deaths which accounts for 6.6% of the total male deaths [2, 3]. Despite it's severity, early detection as well as an effective treatment course which factors in patient specific parameters can aid in curing prostate cancers. Typically, treatment options for prostate cancer patients include radical prostatectomy or a course of radiation treatment [3].

Brachytherapy (short range therapy) is a form of radiotherapy which involves the use of an internal radiation source to achieve dose delivery. A therapeutic radionuclide seed, typically ^{192}Ir, is placed within/close the treatment volume by means of a flexible steel rod connected to a mechanically driven remote afterloader. This allows a radiation dose delivery directly

to the targeted area. The precise positioning of the source allows clinicians to achieve high level of dose conformity and accuracy, minimising exposure to healthy tissues. The breast, prostate, cervix and skin are common organs in which brachytherapy is used to treat cancers. Brachytherapy generally is delivered using two distinct methods; low dose rate (LDR) and high dose rate (HDR). LDR Brachytherapy involves the implantation of low dose rate radiation seeds into the treatment volume. The seeds remain permanently implanted in the volume while delivering dose over an extended period of time. After the treatment is finished, the seeds remain within the treatment volume [4]. HDR Brachytherapy employs catheters which are temporarily inserted directly into the target volume. The positioning of these catheters are accurately verified and a treatment plan is generated based on these positions. Using these catheters, high dose rate radiation pellets are inserted. The positioning of the seeds within the catheter and the time in which they are in position are all controlled by computer guidance systems to accurately deliver precise dose treatment volumes [5].

The treatment of prostate tumours using HDR source involves a template being placed over the area between the scrotum and anus. Catheters are inserted through this template into the prostate. Their positioning is verified using a CT scan and a treatment plan is developed. Using this treatment plan, the treatment seeds are inserted into the catheters and the dose is delivered. The use of CT verification involves the movement of the patient out of dorsal lithotomy. This movement can result in a shift in the catheters, which in turn will cause uncertainty in the dose delivered to the patient [5].

In order to streamline the prostate brachytherapy treatment, Trans Rectal Ultra Sound (TRUS) probes have been implemented for catheter localisation and treatment planning.

By doing so, the patient can remain in the same position for the entirety of the treatment which reduces the chances of catheter movement. One problem associated with real-time brachytherapy is the difficulty associated with locating the catheters using the TRUS probe. There is an inherent distortion when the catheters are reconstructed on the US image, which in turn can result in an overestimation of the prescribed dose to the prostate and/or dose delivery to healthy tissue (urethra, bladder, rectal wall).

There is a need to validate catheter position in the intraoperative environment from start to finish of the procedure: End-to-End.

1.1 Project Aims

The aim of this thesis is to develop a system which can accurately verify each component of a real-time HDR prostate brachytherapy procedure: *in-vivo* treatment verification (IVTV). Included within the constraints of IVTV are the notions of *in-vivo* dosimetry as well as accurate HDR source localisation. This thesis proposes to achieve this aim through the following objectives:

- Review current literature surrounding current modalities of .
- Development of an anthropomorphic gel phantom to be used in clinically relevant end-to-end studies.
- Evaluating the feasibility for the use of a 2D diode array in the use of source localisation

in HDR pBT.

- The development and initial feasibility testing of a novel IVTV tool used for TRUS based HDR pBT.

Chapter 2

Literature Review

The aim of the following chapter is to establish a comprehensive outline of HDR prostate brachytherapy, whilst providing key context of prostate anatomy and treatment options for prostate cancer. The uncertainties associated with HDR brachytherapy and will also be examined and current QA procedures will be reviewed. Finally, real-time source identification by means of different detection modalities will be unpacked and reviewed.

2.1 Prostate Anatomy

The prostate is an exocrine gland of the male reproductive system [6]. It's location is directly inferior to the bladder and anterior to the rectum, which can be seen in Figure 2.1.1 The urethra passes through the prostate gland from the bladder to the penis.

The primary function of the prostate is to secrete fluid from the seminal vesicle to protect

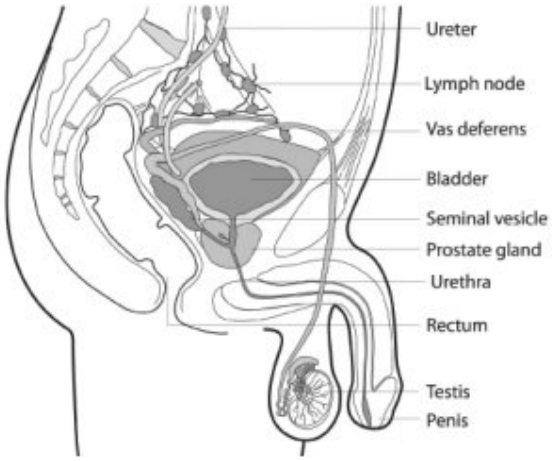

Figure 2.1.1: Sagittal view of the prostate gland within its local anatomy [6].

and enrich the volume of sperm.

2.1.1 Prostate Cancer

Prostate cancer is a form of malignancy in the prostate in which the development of atypical cells grow to form a tumour volume. These atypical cells may uncontrollably multiply and ultimately result metastasis; the growth of secondary malignant sites which occur in a different location from the primary cancer site via the lymphatic or circulatory systems.

The prevalence of prostate cancer can be seen on the world scale, with the most recent data showing an estimated 1 276 000 new cases and 359 000 deaths in 2018 [7]. Furthermore, as a result of growth and ageing of the population by 2040 the worldwide cancer burden will see an expected 2.3 million new cases and over 740 000 fatalities [7].

2.2 Comparison of treatment options for prostate cancer

A study conducted by the Prostate Cancer Results Study Group [8] provides an evaluation of the prostate specific antigen free survival outcomes of low, intermediate and high risk subjects. The study compares the effectiveness of different treatment options which include surgery (radical prostatectomy), external beam radiotherapy (EBRT) and brachytherapy (both low-dose rate and high-dose rate). In order to reach a comparative conclusion, the study involved the analysis of retrospective studies conducted from 2000-2010 which critically evaluated the treatment of localised prostate cancer.

The study found that data from over 52000 patients showed that brachytherapy proved to be more effective in stopping low-risk prostate cancers compared to other modalities. For the intermediate risk patients it was found that brachytherapy alone showed similar effectives compared to the combination of external beam radiotherapy and brachytherapy regimes. Brachytherapy also proved to be more effective compared to surgery or external beam radiotherapy alone. For high risk patients, a combination of brachytherapy and external beam radiation treatments proved to be more effective compared to single modality treatments [8].

2.3 High dose rate (HDR) brachytherapy

Brachytherapy (short range therapy) is a form of radiotherapy which involves the use of an internal radiation source to allow dose delivery. A therapeutic radionuclide, usually Iridium-192 (^{192}Ir) is placed within/close to the treatment volume delivering a small dose directly to the targeted area. The precise positioning of the source allows clinicians to achieve high level of dose conformity and accuracy, minimising exposure to healthy tissues with results similar to those obtained with surgery [9].

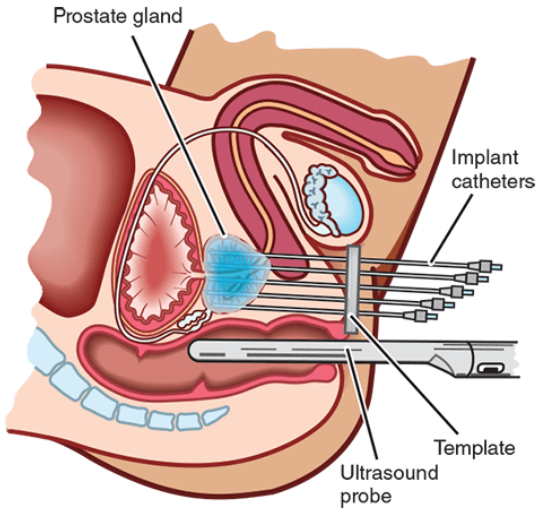

Figure 2.3.1: HDR Brachytherapy Treatment [5].

Brachytherapy generally is delivered using two distinct methods, low dose rate (LDR) and high dose rate (HDR):

Low Dose Brachytherapy (LDR) involves the implantation of low dose rate radiation seeds into the treatment volume. The seeds remain permanently implanted in the volume while de-

livering dose over an extended period of time. After the treatment is finished, the seeds often remain within the treatment volume [4]. The permanent implantation of the radiation seeds have an inherent degree of uncertainty. Manual insertion of the seeds into the soft tissue, which is prone to deformation, results in localising the final position and dose distribution to the volume being difficult and unpredictable [9]. Once inserted, there is no way to alter the seed's position which also means that there may exists differences between the planned treatment and the one delivered.

High Dose Rate Brachytherapy (HDR) employs hollow catheters which are temporarily inserted directly into the target volume. The positioning of these catheters are accurately verified using CT images and a treatment plan is generated based on these positions. Using the catheters, high dose rate radiation pellets (192-Ir) are inserted. The positioning of the pellets within the catheter and the time in which they are in position are all controlled by computer guidance systems and a fixed grid template to accurately deliver precise dose treatment volumes to within 1mm [4]. During the procedure, the computer guided system positions the radioactive seed at pre-determined dwell positions inside of the catheter for a designated amount of time before moving onto the next position. The times at each dwell position are determined based on tumour dose requirements and normal tissue dose constraints [9]. This allows a controlled dose distribution.

Due to its ability to deliver a large biological effective dose whilst minimising dose to the surrounding organs, high dose rate (HDR) brachytherapy (BT) has provided an efficient treatment to prostate cancer [10]. The report produced by *Kumo et all. 1997* of the AAPM Radiation Therapy Committee qualitatively outlines the benefits associated with

HDR Brachytherapy treatment. These include:

- A higher dose conformity to the treatment volume
- The time efficiency of the procedure
- Lower patient movement effect
- Lower dose to surrounding tissue.

The article fails to mention the low time benefits associated with the treatment [11]; there is an increase in risk of healthy tissue dose with treatment time.

An eight year study was conducted by Demanes *et al.* which evaluates toxicity and tumour control for patients which have low- and intermediate-risk prostate cancer. Between 1996 and 2005, the data from 298 patients with localised prostate cancer who were treated with HDR brachytherapy was analysed [9]. Each patient received one of two hyper-fractionated delivery protocols, both with biological equivalence. One protocol saw a delivery of 42 Gy in six fractions using a computed tomography (CT) based treatment plan while the other protocol delivered 38 Gy in four fractions based on transrectal ultrasound (TRUS) planning. The dose delivered to radiosensitive organs (bladder, urethra and rectum) were similar across all the procedures. It was found that after 8-year follow up, there was a 97% biochemical tumour control, 99% local control, 99% distant metastasis-free survival and 99% cause specific survival. It was also found that there was an overall 95% survival [9]. Based on these results, there is a demonstrated low morbidity which indicates an affective overall treatment option for prostate cancer. Despite the studies supporting evidence for effective means of tumour control, the study fails to evaluate the long term survival trends to give a long term evaluation.

2.3.1 HDR Radiation Source

A majority of clinical brachytherapy environments sees the employment of ^{192}Ir as the primary source of radioactive isotope. The production of the radioisotope is achieved through neutron bombardment of stable ^{191}Ir. This allows minimal wastage of unwanted isotopes during production.

According to the National Nuclear Data Centre [12], ^{192}Ir has a half life of 73.827 days, which relates to approximately a 1% daily correction. It's long half life, coupled with its high air strength kerma (41mGy·m^2·m^{-1}), is a primary reason for its widespread use for brachytherapy treatments.

^{192}Ir decays via (95.13%) β^- transitions to excited levels of ^{192}Pt or (4.87%) electron capture to ^{192}Os [13, 5]. There is on average 2.2 photons with energy of 0.354 MeV produced by both decay processes.

Data analysed by Strohmaier *et al.* [14] showed that the distance to the source in water has a direct influence on photon energy; A maximum local dose difference of -14% was observed at a 5cm depth from the ^{192}Ir source in water.

2.4 Uncertainties associated with high dose rate brachytherapy

Although HDR BT for prostate lesions provides an effective treatment, the technique still hasn't reached it's full potential. According to Petereit*et al*, one reason that prostate brachytherapy has low utilisation rates is due to the uncertainties associated with the procedure [15].

There exists a degree of uncertainty with the overall procedure of HDR brachytherapy. One such uncertainty is associated with catheter localisation. Traditionally, BDR brachytherapy utilised post-operative computed tomography (CT) imaging to generate treatment plans. In order to obtain a CT image, the patient positioning is altered from dorsal lithotomy [16]. This movement can result in catheter shift in the inferior direction. To reduce the uncertainties associated with the use of CT scanning for treatment planning, Trans Rectal Ultra Sound (TRUS) probes have been implemented for catheter localisation and treatment planning. By using TRUS, the patient can remain in the same position for the entirety of the treatment which reduces the chances of catheter movement. One problem associated with real-time brachytherapy is the difficulty associated with locating the catheters using the TRUS probe. There is an inherent distortion when the catheters are reconstructed on the US image, which in turn can result in an overestimation of the prescribed dose to the prostate and/or dose delivery to healthy tissue (urethra, bladder, rectal wall) [17]. Furthermore, localising the catheters on the TRUS image can be time consuming and are subjective and operator de-

pendant due to shadowing effects and calcifications [18].

As part of investigating the impact of catheter reconstruction using ultrasound image study, 20 patients with cancer classification of intermediate- or high-risk were treated with a single fractionation 15 Gy boost. Three treatment planners with a history of experience in catheter localisation were chosen to manually reconstruct catheter paths using 3D static transrectal ultrasound images. Using these updated positions, new treatment plans were generated and compared to the original patient study reference plan [17]. The difference between the two plans, which subsequently result in a difference in dosimetric effect, was evaluated. Nicolae *et al.* found that there was <3 mm variation for >98.9% of catheter localisation using TRUS based images[17]. Furthermore, there was a significant decrease in planning target volume which subsequently results in an increase in urethral dose maximum values. The study found that there was a significant change in brachytherapy plan quality based on observer variability. As a result, there may be an inadequate treatment volume coverage which subsequently translates to excessive urethral or rectal dose.

Furthermore, literature from the International Commission on Radiological Protection (ICRP) which evaluates HDR brachytherapy notes that there are a significant number of cases in which human error and mechanical failure has played a role in uncertainties. These include incorrect data input into treatment planning systems, incorrect catheter placement and organ movement/applicator movement from the treatment and imaging sequence. The consequences for such errors have profound effects for the patient, with small deviations in dose positioning and time resulting in significant errors in patient dose.

2.5 Task Group 43 Protocol

In 1995, based on findings of the Interstitial Collaborative Working Group (ICWG), the American Association of Physicists in Medicine (AAPM) formed Task Group No. 43 (and its subsequent update TG43-U1) which devised new formalism for dose calculation [19, 20]. Prior to this document, previous dose calculations did not account for source-to-source differences of internal construction or encapsulations. TG-43 is able to account for these shortcomings by employing dose-rate constants and specific source design parameters which are derived directly from measurements or calculation for each HDR/LDR source.

Overall, the formation and introduction of the TG-43 findings has lead to significant improvements in clinical implication of brachytherapy with the standardisation of dose-calculation methodologies alongside dose rate distributions.

2.5.1 General 2D formalism

In all point dose calculations in brachytherapy, the geometry seen in Figure 2.5.1 is used.

The dose rate equation used to determine the dose at some point P is described as

$$\dot{D}(r,\theta) = S_{\mathrm{K}} \cdot \Lambda \cdot \frac{G_{\mathrm{L}}(r_0,\theta)}{G_{\mathrm{L}}(r_0,\theta_0)} \cdot g_{\mathrm{L}}(r) \cdot F(r,\theta) \tag{2.1}$$

where r is the distance in cm from the point of interest to the centre of the active source; r_0 is the reference distance (1cm); θ is the polar angle specifying the point of interest; P(r,θ) is the point of interest and θ_0 defines the source transverse plane, specified to be 90^0. In a

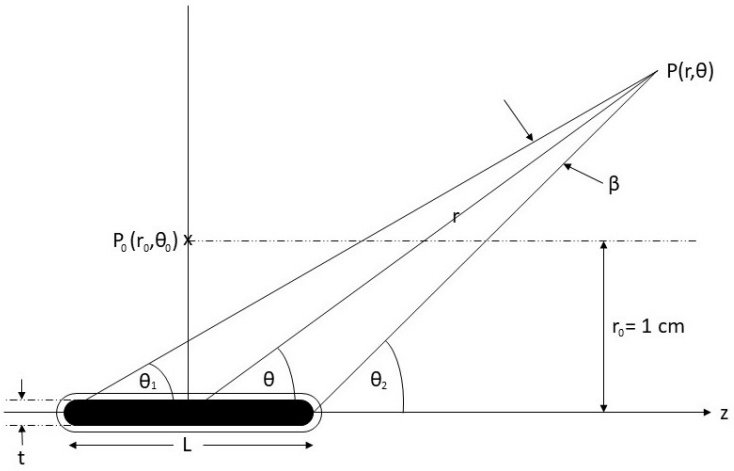

Figure 2.5.1: Brachytherapy dosimetric coordinate system used for calculations[19]

clinical setting, radio-opaque markers are used to define source position and orientation.

2.5.2 Air Kerma Strength, (S_K)

TG-43U1 further revises the definition of Air Kerma Strength to allow low-energy cutoff [20]:

$$S_{\mathrm{K}} = \dot{K}_{\delta}(d) \cdot d_2 \tag{2.2}$$

where $\dot{K}_{\delta}$(d) defines the air-kerma rate in vacuum due to photons of energy which is greater than δ at some distance d. The distance d is described as some distance from the source centre to $\dot{K}_{\delta}$(d) located on the transverse plane of the source. Typically, d is taken on the order of 1 metre such that d is much larger relative to the source size to ensure that S_K is independent of d·$\dot{K}_{\delta}$(d). The unit for Air Strength Kerma is μGy·m^2·h^{-1}.

The energy cutoff δ is introduced to eliminate low energy/contamination photons which arise from photon interaction with surrounding media.

2.5.3 Dose Rate Constant, (Λ)

The Dose Rate Constant (Λ) is defined as the ratio of the dose rate at the P(r_0,θ_0) and the air kerma strength (S_K) in water:

$$\Lambda = \frac{\dot{D}(r_0, \theta_0)}{S_K} \tag{2.3}$$

The value depends on both the radionuclide and the source model (internal design and experimental methodology) and has units of cGy·h^{-1}·U^{-1} which equates to cm^{-2}.

2.5.4 Geometry Function, G(r,θ)

The geometry function allows an improvement to the accuracy of dose rate estimation by means of interpolation from data tabulated at discrete points. The function provides a correction which follows an inverse squared law based upon an approximate model of source radioactivity distribution.

For point source model approximations, the geometry factor is

$$G_P(r, \theta) = r^{-2} \tag{2.4}$$

For line source model approximations, the geometry factor is calculated in conjunction with the following conditions

$$G_L(r, \theta) = \begin{cases} \frac{\beta}{Lr sin\theta} & \text{if} \quad \theta \neq 0^0 \\ (r^2 - \frac{L^2}{4})^{-1} & \text{if} \quad \theta = 0^0 \end{cases} \tag{2.5}$$

where β is the subtended angle between both ends of the line source with respect to the point of calculation P(r,θ); L is the length of the line source and θ is the angle of the source from the point of calculation.

2.5.5 Radial Dose Function, $g_X(r)$

The radial dose function, $g_X(r)$, allows for the dose fall-off on the transverse plane which arises from scattering and attenuation to be accounted for. The function is calculated by

$$g_{\mathrm{X}}(r) = \frac{\dot{D}(r_0, \theta_0)}{\dot{D}(r_0, \theta_0)} \frac{G_{\mathrm{X}}(r_0\theta_0)}{G_{\mathrm{X}}(r_0, \theta_0)} \tag{2.6}$$

The subscript X allows the radial dose function to be determined for both a point source "P" or a line source "L".

2.5.6 2D Anisotropy Function, F(r,θ)

The 2D Anisotropy Function(F(r,θ)) is defined as

$$F(r, \theta) = \frac{\dot{D}(r_0, \theta_0)}{\dot{D}(r_0, \theta_0)} \frac{G_{\mathrm{L}}(r_0\theta_0)}{G_{\mathrm{L}}(r_0, \theta_0)} \tag{2.7}$$

The function describes the variation in dose with respect to the polar angle with the transverse plane. The function returns a value of 1 along the transverse plane of the source.

2.6 Task Group 186

In 2012, the AAPM formed Task Group 186 (TG-186) [21] in order to establish practice uniformities by addressing the shortcomings of early model based calculation algorithms. The accuracy of brachytherapy dose calculations is highly dependent on photon interaction. Model based calculation algorithm dose values are correlated to the dose specific medium which in turn results in energy-dependent differences between TG-43 calculations (water geometry based) and dose calculated in heterogeneous mediums. TG-43 calculation formalism saw the introduction of pre-calculated dose distributions for a single source in a water environment and superimposing it on patient plans. Despite being fast for clinical applications, it fails to take into account tissue heterogeneities and patient dimensions or the influence of scatter-dose. This is significant when using TG-43 formalism when calculating dose values in mediums which are not the prostate, ie. rectum or detectors.

In order to account for the above shortcomings, TG-186 recommends to perform radiation transport in the heterogeneous medium alongside TG-43 calculated doses. To achieve this, a number of standardised materials should be used across institutions to maintain uniformity.

2.7 Task Group 59

The American Association of Physicists in Medicine (AAPM) Radiation Therapy Committee Task Group no. 59 was established in December 1997 to examine the HDR delivery protocols and to manifest a document to standardise safe HDR delivery practices [10]. The document

provides extensive quality assurance procedures whilst also outlining training and emergency procedures.

The main ideology behind the development of a standardised quality assurance document was to minimise treatment delivery errors and other potential hazards. They believed that this would be achieved through a carefully designed treatment delivery process with contributing factors such as treatment accuracy, patient safety, physician convenience and cost effectiveness kept in mind [10]. The AAPM group outlines the treatment delivery process as the applicator selection and insertion, the planning of the implantation and dose evaluation. Special emphasis is placed on the quality assurance being implemented throughout the process of HDR procedure as opposed to a set of checks and activities which are separate.

The document outlines essential patient specific documentation, procedural check-lists and forms and the recommendations to ensure that the chance for misinterpretation or incorrect data input is minimised. The main purpose the documentation is to minimise miscommunication of verbal transfer. The key information that the documentation should outline as a minimum are as follows[10]:

1. Detailed cross section diagram which documents catheter positions with appropriate numbering with respect to the local anatomy should be provided. Any information which will be used to compute procedural parameters shall be included.

2. Catheter-by-catheter information such as insertion depth, dwell position, dwell times and distance between surrounding catheters shall be included for all implants. The insertion depth is HDR afterloader specific, so this information is crucial in cases of cross-department procedures.

3. Information regarding *active* dwell positions and localisation of sources along the catheter track. This information is manually obtained using radiographic means.

4. Isodose (Dose information at differing dose levels across the treatment volume) plots for graphical representation of treatment plan.

5. Calculations of dose and strength of the source to verify computer-based calculations.

The document further outlines staff training such that potential errors in the treatment may be noticed and avoided. There exists a balance between an appropriate number of staff and the reduction of error risk; this is dependant on the complexity of the patient case and the training and experience of the staff [10]. Furthermore, credentials and recommended training for each member of staff are outlined.

The treatment specific quality assurance that Task Group no. 59 outlines involve appropriate applicator preparation and insertion as well as implant localisation. One such area which the document places considerate emphasis on is the evaluation of the implant location. Most of these involve properties of the afterloader whilst additional information is obtained from radiographs. Due to the heavy reliance on the afterloader, there is an importance placed on a daily quality assurance protocol [10]. One such method is the use of a sequence of radiographic distinct dummy seeds loaded inside the applicator. These dummy seeds are cross referenced using orthogonal radiographs and the implant diagram to determine dwell positions and time. This process in itself is prone to a certain degree of uncertainty. If the process is performed incorrectly, the sequence of dwell positions and time will be incorrect. It is recommended that at least two persons should be working in unison to cross check each

step in the process.

One such problem with the AAPM Radiation Therapy Committee Task Group no. 59's document, despite it being over two decades old, is the focus of quality assurance for HDR brachytherapy equipment. The document focuses heavily on the daily execution of QA protocol for the remote afterloader in order to accurately determine source dwell positions and time. **One such problem for a system which relies heavily on device-centric quality assurance is that it fails to give assurance for the entirety of the procedure.**

2.8 Task Group 100

In 2016, Task Group no.100 of the AAPM was established. Traditional methods of quality assurance have primarily focused on the monitoring of the functional performance of the radiotherapy equipment. These traditional QA measures fail to recognise that many errors which occur in radiation oncology stem from complications in work flow and process rather than devices and software. The no.100 task group's document outlines a structured methodology which allows analysis of clinical process and to develop clinic and site specific QA measurement programs which will take into account workflow parameters [22].

The document examines two main shortcomings of traditional approaches to quality control management:

A lacking in addressing the treatment process comprehensively. The device-specific

quality assurance approach will result in errors associated with information flow and poor training. An overall understanding in the interactions between all aspects of a procedure including human users and devices is paramount and will see an overall improvement in efficiency and reduction of error.

Delays in establishing accepted quality control procedures for changing technology. The increase in the rate of radiation technology development has seen a challenge to traditional quality assurance protocols. Device-centric quality assurance coupled with a rapidly changing industry will inevitably lead to a time lag between the development of quality control measures and the implementation of new technologies.

Overall, the report finds that the only way to mitigate the risk of error associated with radiotherapy is by careful consideration of all aspects of the planning and treatment; **end-to-end testing**. The process-orientated quality assurance includes integrated dosimetric and quantitative testing.

2.9 Current clinical quality assurance methods for high dose rate brachytherapy procedures

The implementation of quality assurance (QA) programs in clinical brachytherapy environments is to ensure a level of consistency across all treatments whilst also maintaining a high

level of safety to the patient and other individuals who may be exposed to radiation as a result of the treatment. There are a series of performance checks carried out at fixed intervals, documentation standards, measurements and training standards which form a typical QA program [23].

In 2011, the Australasian College for Physical Scientists and Engineers in Medicine (ACPSEM) Radiation Oncology Speciality Group (ROSG) formalised a series of QA recommendation papers to provide a guidance foundation for Australasian radiation oncology medical physics practices. The proceedings are based upon the AAPM's Task Group no.56 (Code of practice for brachytherapy physics) [24] as well as other QA practices used in other countries [25]. The document serves more as a guideline for the frequency in which to perform the QA tests, rather than providing in depth procedure. Each QA test is grouped based on the frequency to which it must be conducted; tests frequencies are classified into daily, quarterly (or at source replacement) or annual frequencies.

2.9.1 Real-Time source localisation

The known location of HDR sources during clinical procedure compared to planned positions is paramount in ensuring correct dose delivery. ACPSEM's Task Group no.56 [24] as well as ESTRO Booklet 8 [26] recommends that the source position accuracy test is to be performed daily. In order to determine the source position accuracy, the source can be exposed on radiographic film and compared to external markings.

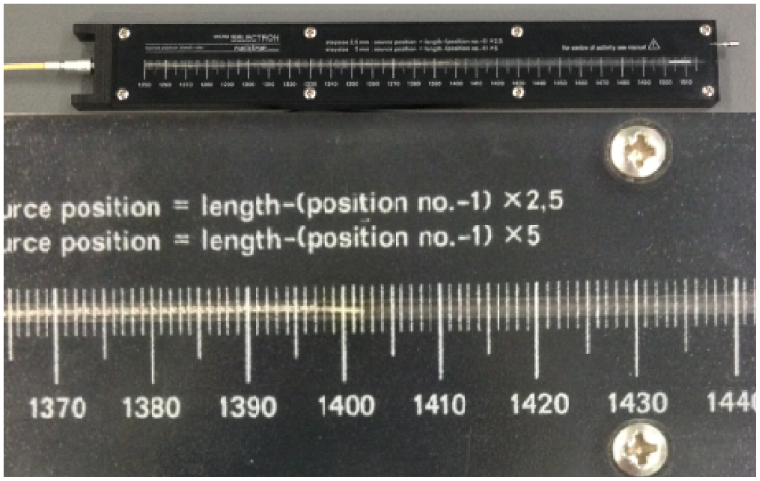

Figure 2.9.1: Source accuracy check ruler which is used daily [27]

.

The typical tolerance for for most quality assurance protocols, as provided by the ACPSEM recommendations, is 1mm with action to be taken after 2mm differences [23].

2.9.2 Dwell-Time

In order to determine the dwell time accuracy, the time in which the source is in its planned position is compared to the designated time specified by the treatment planning system. The typical tolerance range as specified by ACPSEM recommendations is 1% with action to be taken with differences of over 2% [23].

2.10 *In-vivo* Dosimetry and Treatment Delivery Verification

In vivo treatment verification (IVTV) is a mechanism through which the minimisation of risks associated with the incorrect delivery of HDR PBT can be achieved. It allows verification of treatment delivery by means of quantifying patient dose directly as well as determining source dwell times and localising source positions; *in-vivo* dosimetry and *in-vivo* source tracking.

2.10.1 Different detector based *in-vivo* systems

In HDR brachytherapy, the use of IVD does not see typical clinical use due to its invasive nature [28]. The typical organs surrounding the prostate, such as the rectum, urethra and bladder, are often chosen as sites to monitor dose as non-invasive sites such as skin levels are not a priority. Reaching these monitor sites often requires insertion of a probe or additional interstitial catheters [28, 29].

Furthermore, the high dose gradient creates additional challenges. For a typical linear source, at a distance of 4mm the dose gradient is ≈50% mm^{-1}. At a distance of 20mm, the gradient is ≈6% mm^{-1} [29]. The significance of the differences in dose gradients will consequently result in small errors of detector positioning causing a large degree of dose error. A study conducted by Waldhausl *et al* outlined the importance of these geometric considerations in HDR brachytherapy. 55 patients with cervix carcinomas were evaluated; dose in the rectum and bladder were measured using diodes and compared to the calculated values. If there

was a difference of at least 10% between the two values, the diode's position was moved and evaluated. It was shown that shifts in patient detector probe position of 2.5mm for a rectal probe and 3.5mm in a bladder probe resulted in dose differences exceeding 10% [29].

There are many studies in the literature which explore the use of different detector systems for *in-vivo* dosimetry. The following review is based on different detector types.

Thermoluminescent dosimeter (TLD)

The thermoluminescent dosimeter's (TLDs) ability to be shaped and manufactured by an array of different materials have seen clinical studies of TLDs for HDR BT. Lithium fluoride (LiF) TLD rods are able to fit easily within treatment catheters and so, are the most common form used. However, due to the invasive nature of the TLDs, fading correction factors needed and due to the TLDs not being real time dosimeters, their use for daily clinical QA is limited.

Anagnostopoulos *et al* [30] evaluated the potential use of TLDs to measure dose delivery accuracy in vivo for HDR BT. 50 LiF TLD-100 were used for 18 fractions in 5 different patients and compared to commercial TPS based on CT images. Fourteen individual dosimeters were loaded into a 4F catheter for each treatment fraction and were placed either close to the urethra or around the median posterior wall of the prostate. A maximum discrepancy between the planned and observed dose values was 8.56%±2.61% with the average difference being 6.88%±4.93% across all patients. The findings provided a good correspondence to the expected values within uncertainties.

By means of a similar method, Jaselske *et al* [31] proposed in vivo dose verification using TLD-100 dosimeters compared to theoretical dose values. A pre-implanted dosimetry catheter filled with 6mm long TLD 100-H rods, adjusted using reconstructed CT scans, was used for three head and neck and one breast patient during randomly selected treatment fractions. For the head and neck patients, it was found that the average dose difference varied from 4.02% to 12.93% and 7.17% to 8.63% for breast patients. These values fall below the 20% recommended margin from the AAPM. One problem associated with the author's methodology was catheter reconstruction was only performed for the first treatment which resulted in incorrect dosimeter positions due to organ moment. This different accounted for an estimated 2-3% dose error.

Radiophotoluminescence glass dosimeter (RPLGD)

RPLGDs and TLDs operate under similar reading processes, with the main difference being ultraviolet light is used to stimulate the detector rather than heat [32]. This leads to a direct benefit over TLDs; RPLGDs can be annealed and reused.

The rational behind RPLGD IVD is explored by Takayuki Nose *et al* [33], where the largest sample of patients for an interstitial brachytherapy in-vivo dosimetry was analysed to study the limits of current treatment planning software. Sixty-six patients were treated with HDR interstitial brachytherapy, twenty-six of which were prostate cases. A total of 1004 points were measured by **radiophotoluminescence glass dosimeter (RPLGD)** and compared with treatment planning software. The study concluded that there was a greater than 20%

deviation in measured and calculated doses. This can be attributed to movements of organs and the associated detector position uncertainty.

The accuracy of glass dosimeters was further explored by Moon *et al* [34]. A pelvic phantom which mirrored typical patient anatomy was created and used in conjunction with an applicator which housed the dosimeters to evaluate the accuracy of the dwell positions and time. The arrangement of the dosimeter and the source was optimised for three different conditions using doses of 10, 50, and 100 cGy. Once the optimal arrangement was found, phantoms of solid water with different thicknesses were placed between the source and the dosimeter; effectively changing the distance between the source and the centre of the glass dosimeters. The measured values for each distance were compared to the TPS. The errors found between the TPS and the obtained values were -6.25%, -2.1%, -4.18%, 6.31% and -0.39%, with a mean of 3.85%. The author remarks that this error was acceptable when considering the innate error of the glass dosimeter itself, being 3%, and that with further error calibration this method could be clinically used.

Radiophotoluminescent glass dosimeter's use to validate dose in prostate HDR-BT was also examined by Shih-Ming *et al* [35]. The group set out to compare the accuracy of dose measurements using RPLGDs to a typical clinical TPS and as a result, potentially identify factors which hindered the accuracy of the measurements. The group used TLDs as a further comparison. Phantom in-vivo dose measurements were performed using both the RPLGDs and TLDs with both single source dwell positions and multiple source dwell positions. Overall, the difference between the measured dose and the TPS dose was less than 5%, which was seen as a clinically acceptable accuracy.

Optically stimulated luminescence dosimeters (OSLDs)

Optically stimulated luminescence dosimeters (OSLDs) are gradually replacing TLDs due to their instantaneous readout and the permanent record of their irradiation signal. The OSLS can be operated in both post irradiation readout using an external optical stimulation (typically a LASER) or live readout during irradiation. The quality, as well as their small size of sub millimetre, is appealing for IVD [28].

In 2009, Claus E. Anderson *et al* [36] developed a prototype which was to facilitate dose delivery error identification in remote afterloading brachytherapy. The system was constructed of an OSLD made from aluminium oxide crystals which was coupled to optical fibre cables which transported the light signals to the readout system. The detector system was able to be placed inside of treatment catheters which allowed for direct online in vivo dosimetry inside of the tumour volume. Using a water phantom and a Varian GammaMed Plus ^{192}Ir afterloader, the system was tested in the range of 0Gy to 4Gy. It was found that the calibrated system was linear within the tested dose range. Monte Carlo code was used calculate the theoretical expectations for depth dose, which returned profiles which the author quoted as 'agreeing well' with the measured data. For source-to-probe distances of 2-50mm, the energy dependence for the dosimeter probes (compared to water) was less than 6%. Despite it feasibility, it was noted that the generated radioluminescent online signal could be greatly affected from light generated in the optical fibre being irradiated. It was concluded that OSLD were an adequate option for IVD.

Gustaco Kertzsher *et al* conducted a feasibility study for fibre-coupled carbon doped alu-

minium oxide OSLDs [37]. The main goals of the study was to quantify the sensitivity of the detector under clinically relevant imposed treatment errors while concurrently testing a new statistical error decision criterion. Two gynecological and one prostate cancer phantom studies were conducted which saw imposed treatment errors including source displacement from 2mm to 20m being monitored by real-time OSLDs in the tumour region. The detection of error capability was qualified based on dwell positions, source channel and faction. The statistical error criterion allowed the incorporation of correlated source position uncertainties as well as other sources of error. Out of 20 imposed errors, the system identified 17 based on time-resolved analysis while 2 errors were found from a fraction level analysis. It was also found that the minimum displacement that dwell position dose rate comparisons could identify was 5mm. The study showed the capability of carbon-doped aluminium OSLD in detection of clinical relevant errors as well as outlining the need for statistical error criterion as opposed to constant error criterion.

Plastic scintillation detectors (PSD)

Another promising detector system for IVD is plastic scintillation detectors (PSD). Light is emitted proportionally to incident dose upon the organic scintillation material. The crystals are coupled to fibre-optics and are then incident upon a detector. PSDs are linear with dose, have a high spatial resolution and are water (tissue) equivalent. The detectors can be cut into specific sizes are shapes easily, making them desirable for catheter insertion. However, at certain energy levels the detectors are prone to Cherenkov radiation which needs to be accounted for [28].

In 2011, Therriault-Proulx *et al* [38] evaluated the accuracy of a plastic scintillation detector (PSD) for HDR brachytherapy IVD. To detect scintillation light, a red-green-blue photodiode was built. A prostate brachytherapy treatment plan with clinical relevance was developed using the TPS and performed in a water phantom. Two out of the thirteen catheters used for the procedure were used for PSD dose measurements at the urethra and rectal wall; the remaining catheters were used for dose delivery using a ^{192}Ir source. Furthermore, the removal of Cherenkov radiation effects was evaluated. The ratio of detected dose compared to dose calculated by the TPS was found to be 1.003±0.004 in the urethra and 1.043±0.003 for the rectal dose. It was also shown that a 5mm positioning error of the source were able to be detected, depending on the acceptable range chosen, from 78% to 100% of the time. The study also showed the importance of the remove of Cherenkov radiation by showing the reduction in false-error-detections. From the obtained results, the author emphasises the potential for PSD for online dose verification during treatment delivery as well as the importance in the removal of Cherenkov radiation effects. However, the main limitation of the study was the inability to measure dwell times greater than 5 seconds and more than 10Hz measurements.

Metal oxide semiconductor field effect transistors (MOSFET)

It is desired for IVD to have immediate readout of dose information. Metal oxide semiconductor field effect transistors (MOSFET) are an alternative to TLD detectors for IVD. The

detectors can be produced as micro-MOSFETs which are suited for external and sensitive volume BT applications. The small volume also allows steep dose gradient dosimetry as well as the option of placement within treatment catheters. However, there are two disadvantages associated with MOSFETs: (1) they have a limited lifetime and (2) they are not tissue equivalent, which has implications on dose response based on radiation quality [28].

The feasibility of MOSFET dosimetry systems for IVD verification was investigated by Zhen-Yu Qi *et al* [39]. The paper proposed to implement a new miniature MOSFET design which allows pretreatment QA by means of insertion into a treatment catheter. Among others, key MOSFET characteristics such as the energy dependence were measured. The dosimetric accuracy of HDR brachytherapy treatments were then verified. It was found that the detector has a good dose linearity up until the threshold voltage. When comparing the detector to the TPS for CT based HDR BT for dose calculations, it was shown that the mean relative deviation for dose points 1cm from the source was 2.2±0.1 % and 2.0±0.1 % for 2 cm away. Overall, there was a percentage deviation for all measurements of less than 5%.

2.10.2 Current modalities for HDR source tracking

IVTV can also be attained through in-vivo source tracking, which verifies source position and dwell times accurately track the position of the HDR source in three-dimensions.

Point Detectors

One method of determining source position is derived from TG43 calculations using a measured dose rate at multiple positions and triangulation algorithms [19, 20]. Such methods of source localisation can be seen within the literature [40, 41, 42, 43]. Wang *et al*'s 2014 study demonstrated the use of GaN dosimetric probes for HDR seed position verification [43]. Optical fibre connected to a photodetection module was used to detect any radioluminescences from the GaN transducer. The dose rate readout from one transducer can be used to determine the distance and angle to the source. By incorporating a second transducer at some distance d from the first, the seed detection range is increased. The study returned a mean 1% deviation from the expected source locations, although the contribution of Cerenkov radiation needs to be further investigated.

Pinhole Collimator

The principle of pinhole collimation in order to localise HDR source can be seen in past studies [44, 45, 46]. Watanabe *et al* investigated the use of a charge-coupled device camera integrated with a scintillator and a dual-pinhole collimator [44]. By using template matching from successive images of scintillation light from, the system was able to detect source positions every two seconds. The system was used in conjunction with a water phantom to test its ability to source track within the context of cervical cancer. It was found that the difference between the average measured source position compared to the reference values was 1.5±0.7mm. One limiting factor of this study, as outlined by the author, is the timing

resolution of 2 seconds; the current operating parameters limit it's application in real-time detection in a clinical setting.

The integration of collimator based source localisation and the TRUS Probe is investigated further in section 2.12.2.

Electromagnetic Tracking

Electromagnetic tracking (EMT) is a system in which accurate positions within space can be determined by means of an induced inhomogeneous magnetic field and sensors. The use of EMT in the field of HDR tracking can be seen in the literature [47, 48, 49, 50]. Particularly, EMT has had promising results when applied to catheter and applicator localisation, as outlined by Poulin *et al*'s 2015 study [50]. The study used ten catheters within a tissue equivalent gel phantom, using EMT to reconstruct their locations and compared directly to CT. The mean distance error in 3D space for the EMT measurements was found to be 0.66±0.33mm, compared to 1.08±0.72mm for CT. EMT tracking also has proven its ability with some aspects of error detection. Bert *et al* outlines EMT's role in successfully being able in error detection in interstitial BT; the system can be used in afterloader source positioning and dwell time pretreatment verification, intra- and interfraction organ/applicator movement and any afterloader malfunctioning [47]. However, the one significant limitation of EMT is it's inability to be used for dose assessment.

Flat Panel Detectors

The development of a EPID system which can be placed under the patient during treatment has been driven in recent years by publications from RL Smith [51, 52, 53, 54, 55] and GP Fonseca [56, 57, 58]. Foneseca *et al*'s 2017 study aimed to provide real-time treatment verification using a silicon electronic portal imaging device (EPID) and gynaecological applicator which was verified using CT [57]. The systems performance in pre-treatment verification was further demonstrated by introducing errors (such as catheter shift, incorrect dwell times and changing afterloader connections). The overall source position standard deviation was 0.2mm with an error of 0.2s for dwell time measurements. The system was also able to identify all imposed errors.

Smith *et al*'s latest study shows a clinical application of their treatment verification system using a flat panel detector embedded directly into the BT treatment couch [55]. Monitoring of the source position was performed throughout each treatment delivery and verified directly against the treatment plan. The study returned a mean deviation for the planned dwell positions of 1.9mm with a maximum of 4.9mm from 280 positions. The integrated system proved its feasibility, with it currently in routine clinical use.

2.11 Magic Plate Detector System

The emergence of 2D electronic arrays used for measuring dose at multiple locations started gaining traction in the clinical environment [55]. The 2D detector arrays allowed the ability

to perform planar/fluence dose comparison as well as real time dose information feedback. The Magic Plate (MP) detector system is a 2D array of 11 x 11 silicon epitaxial diodes embedded in a 0.5mm Kapton substrate using "drop-in" mounting technology which was developed at the Centre of Medical Radiation Physics (CMRP) as a dosimetric tool for IMRT quality assurance. Radiation source position is determined from the generated signal from a source by the interaction of photons and secondary electrons in the 2D array. Using a proprietary algorithm, the 3D source location can be calculated as well as the dose deposited. There have been several studies in the literature which show the development of the MP detector system; from general characterisation to applications in quality assurance [59, 60, 61, 62, 63]. The following review is chronologically arranged except when related studies are discussed and only considers BT studies.

2.11.1 General Characterisation

Prior to clinical application of the magic plate, a general characterisation to determine its clinical suitability needed to be conducted. The test parameters which were investigated by Wong *et al* were similar to that of tests carried out for previous clinical dosimeters; percentage depth dose, energy dependence, field size and angular dependence, radiation damage effect, beam perturbation effect and dose per pulse dependence [62].

Percentage Depth Dose and Dose Linearity

In order to measure the percentage depth dose, a 6 MV photon beam was measured in a solid water phantom at selected depths. For dose linearity, the plate was set at 100cm SSD and measured with a dose range of 5 cGy to 1000 cGy.

When comparing the depth dose curve of the MP to a CC13 ion chamber, it was shown that the MP exhibits a degree of over-responding for depths beyond d_{max}(1.74% maximum at depth 10cm). This was determined to be a direct consequence of the dose rate response. Once corrected for, the depth dose curve closely agreed with the CC13 curve within 0.7%.

The dose linearity, when measured for the dose range of 5-1000 cGy showed a high degree of linearity.

Energy Dependence

Using both an orthovoltage machine and a linear accelerator, the energy response of the MP was measured for energy ranges of 75-250 kV and 6/10MV respectively. Measurements were normalised to 1 at the energy of 6MV and evaluated at 4 different geometries: face up - in phantom, face down - in phantom, face up - in free air geometry and face down - in free air geometry.

For the in phantom - face down configuration, the study showed that at 6MV there was an enhanced response at lower energies up to 7.5 times and a maximum dose response at 75kV photon energy. This is primarily due to increased photo electric effect in the silicon at lower energies. The study also demonstrated the effect of backscatter electron contribution

to signal response, with the free air geometry showing a lower signal response. Further more silicon is not tissue equivalent and thus, is sensitive to energy spectrum changes. The response of the detector was also found to be heavily dependant on the orientation of the MP; the face-up configuration yielded a lower response compared to the face-down configuration. This result shows the impact of the 0.375 mm silicon substrate coupled with if the detector is in free air or phantom geometry.

Radiation Damage Effect

The silicon lattice structure is sensitive to ionising radiation; point defects (gamma irradiation) or cluster defects (fast neutron) become recombination sites for minority charge carriers which in turn reduces their lifetime.

The plate was irradiated with 41.5kGy, delivered using 6MV photons from a LINAC and a high dose rate cobolt-60 source.

After a dose of 41.5 kGy, the accumulated radiation in the Si-SiO_2 layer results in a positive charge build up which resulted in the increase of the detector by a factor of two. It was also found that there was a 2.1% coefficient of variation for the detectors within the central 20%-80% region. As a result, it was shown that the diodes are suitable within reasonable uncertainty for detector response comparisons. It was further shown that there was no radiation damage observed in the kapton board.

Angular Dependence

A fixed number of MU was delivered to the MP which was sandwiched between solid water pieces at 100cm SDD. Gantry angles of 0° to 180 ° in 15° intervals were used with the MP in the face up configuration. Couch attenuation was taken into account when measuring angles 120° to 180°. EBT2 film was used as a comparison dosimeter. The angular coefficient (ka_i) of the diodes is evaluated by the signal ratio of the MP over the EBT2 film for some ith column. Thus, the angular response for any arbitrary angle θ is taken as the ratio of the MP angular coefficient ($ka_{\theta i}$) to the angular coefficient at 0°.

For gantry angles of 0° to 60°, the angular response of the MP diodes was <2.7% and 4.5% for 75° (or 285°). For angles 90° to 270°, the mean angular response was 10.5%±0.7% and 10.8%±0.7% at an angle of 180°.

This indicated that due to the anisotropy of the silicon diodes the MP showed angular dependency; the sensitive volume (50 μm) is surrounded by a non symmetrical passive silicon volume (365μm).

Through the conduction of this study, Wong *et al* were able to determine the MPs general characteristics and demonstrate its dosimetric potential.

2.11.2 Pretreatment quality assurance feasibility

In order to prove useful for quality assurance in BT, an ideal system needs to be able to measure dwell and transit times, provide dose localisation information and compare these parameters to the TPS. A preliminary study by A Espinoza *et al* explores the characterisa-

tion of the MP with an emphasis on pretreatment QA [61]. Two solid water slabs of 1.5 cm thickness are used to sandwich the MP with two rows of 10 catheter holes. In order to be feasible in determining source location, the source to distance dose measurement as well as the angular response of the detector needed to be characterised.

A subsequent 2015 study by Espinoza *et al* [60] saw the extension of prior work to include the possibility of complete HDR pretreatment and afterloader verification. To do this, a Magic Plate Phantom was developed - three slabs of PMMMA plastic of 1cm thickness with the MP sandwiched inside with 13.5cm of water equivalent material surrounding the setup. The layers directly above and below have ten channels each which allow the insertion of up to 20 HDR treatment catheters at a distance of 6mm from the detectors. To further test the capabilities of the system, errors - including differing dwell times and positions and shifted locations - were introduced to the treatment plans.

Dose measurements

The **source-to-detector distance dose measurements** are fundamental due to ^{192}Ir's large dose gradient. In order to achieve accurate source localisation using a triangulation method, the SSD dose response of the MP was determined. Espinoza *et al*'s feasibility study [61] included a stationary HDR source placed at the directly over the middle detector was used with varying SSDs from 6 to 71mm in order to measure the response. At 15mm SDD the diode was normalised to 100% and the radial dose function was calculated and compared

to values obtained from the AAPM TG-43 protocol.

For source-to-detector distances over 15mm, there are deviations in detector response. For measurements up to 30mm, the radial dose function followed the TG-43 calculations within 8% and 40% for measurements up to 70mm. One main source of differing response from the MP is the contribution of low energy scattering.

In order to test the prescribed and measured doses, Espinoza *et al*'s 2015 study saw the MP software using TG-43U1 formalism to perform dose calculations [60]. In order to verify the doses calculated by the MP software and the TPS, Gafchromic EBT3 film was used. Dose maps were generated from the TPS and measured data. The EBT3 film was used to measure the original treatment plan and generate another dose map - it was cut to match the MP dimensions and was placed within the MP phantom. Further, an estimation of the transit dose for the source positions was measured.

The MP software dose calculations compared to the TPS saw an agreement within ±0.76%. The transit dose calculations saw a maximum value of 18cGy, which equates to a 4.8±2.3% dose increase compared to only dwell measurements. A 95% pass rate was achieved when considering a dose difference of 4% and a 3mm distance-to-agreement value. When taking into account the transit dose, this pass rate reduced to 90%. The study quantitatively demonstrated the MP's ability to be an effective means of dose calculation by using dwell position and time values.

HDR Source Tracking

When measuring energy deposited, each detector element is measuring the energy deposited by primary and secondary electrons emitted from a source without any information of source direction. In order to gain some **locational information**, the radial SSD which can be determined from the diode response. By using a minimum of 3 detectors, a triangulation method can be used to determine the location of the source based on estimation and iteration. In order to minimise uncertainty as a result of lower signals, the study only considered the detector with the highest response and its immediate neighbours. The central diode of the MP array was used for measuring a known activity ^{192}Ir source at a distance of 10mm. Once the diode with the highest response is found (D1), the inverse function of $r_i = f^{-1}(R_i)$ can be used to calculate the distance from the source to some detector i. Based on at least 3 detector derived distances r_i, the first source location can be estimated S'(x'$_S$,y'$_S$,z'$_S$). A series of iterations based on this first location estimate is computed using the sum of the squares and varying each respective x, y and z distance by ±5mm. A further correction is applied as the relative angle of each detector to the source is calculated, followed by another series of iterations.

In order to experimentally validate the MPs ability to determine the source position, the feasibility study [61] used an afterloader to move the source at 2.5mm step sizes with dwell time of 2s in the direction of the catheter, which was positioned directly above the central column within a water equivalent phantom. This was carried out with a SSD of 10mm below

the stepping plane. Once positions were determined for each step, they were compared to the TPS input positions.

It was determined that approximately 75% of the measurements fell within 0.5mm of the prescribed positions. Larger differences between measurements and prescribed positions were determined to be a product of source in transit measurements. As a result, Espinoza *et al* determined the validity of using the MP to accurately track a HDR source in **real time**.

The subsequent 2015 study conducted by A Espinoza *et al* saw the delivery of a 20 catheter treatment plan to the Magic Plate Phantom [60]. Source position and dwell time for each catheter was collected and a position-frequency histogram was generated. From this histogram, dwell position and uncertainty was determined and the dwell time was calculated from the counts for each peak as the count timing was dependent on the sampling frequency. These values were compared to the treatment plan data.

The source position and dwell time which was determined using the algorithm shows a strong agreement for positions larger than 5mm with the pre-defined source locations on the treatment plan. It was also shown that six dwell positions were less than 0.8mm differences with the average difference being 0 ± 0.63mm (2SD).For source locations close to the tip of the catheter and edge of the MP FOV, there was a difference in true location compared to calculated. This is directly correlated to less neighbouring detectors close to the edge of the plate being used to determine the source location.

2.11.3 In-vivo source position verification

Prior to 2018, MP detector studies have focused on performing measurements on homogeneous media. In this state, the studies returned source localisation accuracy of less than 1mm [59, 61, 60, 62] and a 1ms temporal resolution. Subsequently, the MP has proven its ability in real-time source localisation. However, the complications of patient heterogeneity as well as the implications of ultrasound based treatments to the MP's accuracy had not been investigated.

Patient heterogeneities

Poder *et al*'s 2018 study presents an initial assessment of the MP in its source position verification with the influence of patient heterogeneities [63]. The study also further tests clinical suitability by positioning the detector plate within the carbon fiber patient couch.

Monte Carlo simulations were performed using Geant4 - a Flexisource Ir-192 simulated inside a heterogeneous voxelized patient geometry with the dose deposited within each detector's sensitive volume being evaluated. As a result, the distance from the simulated source position to the detector elements was determined. Subsequently using an iterative procedure, the source position was determined.

Before source positioning verification simulations, the Flexisource model used was verified using TG-43 simulation. Once validated, the source was simulated within the patient model. The model is based upon a patient HDR BT treatment CT study, with the DICOM converted into a native form for Geant4. The plans chosen for the study included 4 catheters,

which each spanned the entire geometry of the prostate with 3mm step sizes. By doing so, maximum and minimum clinical HDR treatment distances would be verified. For each source position 20 simulations were conducted, each with 10^9 primary photons. Once these 20 simulations were completed, each of the voxel was replaced with water density and the simulations were re-run to quantify the influence of inhomogeneities.

The study found between the MP source positions compared to the actual source positions was found to be 2.1±0.8mm. It was also shown that the Z positioning showed a consistent over estimation with an error of 1.9mm. When comparing to the water only environment, it can be seen that source positioning improved to within 1mm. The introduction of inhomogeneities had significant influence on the Z direction location estimate, as its Z position is determined using the absolute dose deposited. It was further concluded that the introduction of a correction factor may increase the accuracy of the source locations.

Overall, the study emphasises the importance of the consideration of patient-related inhomogeneities in future *in-vivo* MP studies.

Ultrasound based HDR BT

The next progression in the goal of achieving clinical application of the MP detector system is to determine the influence of the TRUS probe in source localisation for HDR prostate BT. Poder *et al*'s 2019 study investigated the *in-vivo* accuracy of the MP900 detector system during TRUS based HDR prostate BT using Monte Carlo simulations [64].

Similarly to the 2018 study[63], Poder *et al*'s study performs Monte Carlo simulations using the Geant4 toolkit im order to simulate a Flexisource Ir-192 inside a heterogeneous voxelized

patient geometry with the dose deposited within each detector's sensitive volume being evaluated. This was then used to evaluate each simulated source position to the MP900. The location information was then compared to the source positions in the TPS. The simulations were then performed with the presence of the TRUS probe and compared. Three individual voxelised patients which were simulated and used in the study.

The study found that with the TRUS probe present, the average 3D error across all three patients was 11.9±2.4mm compared to 1.5±0.3mm without the probe. In order to reduce the effect of the TRUS probe on source tracking, a thresholding technique was applied to the tracking algorithm; By doing so, the effect of the shadowed diodes can be reduced. It was found that a 70% threshold was optimal, with an average source tracking error of 1.8±0.4mm inside the rectum.

As a result of this study, it was concluded that the presence of the TRUS probe would introduce incorrect source tracking data. Although, by introducing a post-correction factor, this error could be reduced.

2.12 TRUS Based Measurements

Alongside the development of 2D electronic arrays for dose determination, there has been an increase in research into the combination of *in-vivo* dosimetry with the trans-rectal ultrasound probe. The coupling of the two different systems would see a single device which could provide both a tool for imaging and for source tracking/dosimetry.

The following review will chronologically look at the development of a TRUS based detector

system in the literature.

2.12.1 MO*Skin* integration for rectal wall dose

Mo*Skin* detectors, developed by CMRP, are a type of MOSFET characterised by their ability to operate effectively in steep dose gradient areas and skin dosimetry; The packaging used to seal the sensitive volume incorporates a kapton layer which is sealed using with a water equivalent thin film, providing a build-up layer and an effective depth of 70μm in tissue [65]. Tenconi *et al*'s 2014 paper investigated the integration of MO*Skin* detectors with TRUS probe in order to simultaneously performing imaging and dosimetry [66]. Two MO*Skin* detectors were placed with their sensitive volume facing the target along the longitudinal axis on the surface of a clinical TRUS probe. In order to quantify the systems ability to determine rectal dose, a cylindrical gel phantom simulating the rectum was used. A template and six interstitial needles were used to replicate treatment conditions. US images were acquired and a plan was generated. The phantom was irradiated using an afterloader and the measured doses were compared to the TPS expected values.The study showed excellent dose agreement; The average discrepancy was -0.6% $\pm$2.6%.

Building upon the work of Tenconi *et al*, Carrara *et al*'s 2016 study uses the TRUS probe with the two MOS*kins* directly for on-line treatment planning [67]. A total of 12 patients across 18 treatment sessions were chosen for the study. By using a known reference structure inside the prostate, the z position of the probe system was defined such that the longitudinal position of each detector was known to within 1mm. *In-vivo* dose measurements were taken

by the probe and compared directly to both the pre and post treatment image calculated doses. When comparing the measured dose to the pre-treatment dose calculation, the difference was found to be -2.1%±8.3% while compared to the post-treatment measurement the difference was found to be -0.6%±4.1%. This shows a close agreement with results obtained in previous phantom measurements [66]. It was further shown that at higher delivered doses, there exist a higher discrepancy between post and measured dose measurements as well as the calibration of the detector systems was conducted in a different temperature environment. Overall, the paper demonstrated the effectiveness of dose determination for the rectal wall using the MO*Skin* TRUS system; The results showed closer agreement with the reconstructed compared to the planned doses.

A subsequent 2017 study from Carrara *et al* further demonstrated the capabilities of TRUS-coupled detector systems. The catheter positions within prostate geometry are susceptible to movement from the time of implant, to image acquisition and finally to dose delivery. The shift in these positions, particularly in the anterior-posterior direction towards the rectum, results in a modification of dose to the surrounding organs. Fourteen HDR Prostate BT patients were considered, with two MO*Skin* detectors placed longitudinally along the TRUS probe used in the study [68]. Implant displacement was measured using barycenters of each needle location on the pre-treatment images compared to post delivery. The TRUS-MO*Skins* coupled detector system was able to determine the change in dose between measured and calculated dose discrepancies, which ranged from -19.5% to a maximum of 15.8%. Ultimately, the study was able to quantify the relationship between an increase in rectal wall dose and any implant migration, further highlighting the prospect of TRUS based IVD.

The next iteration for the MO*Skin* detector system undertaken by Poder *et al*'s 2020 paper [69]which sees the examination of the feasibility of catheter-by-catheter analysis for IVD of the rectal wall as well as reproducing the results found previously [67, 68], within a different clinical setting. The study utilised thirteen patients receiving a HDR pBT boost [in conjunction with EBRT] in two fractions, with rectal IVD analysed retrospectively. Similar MO*Skin* configuration to prior studies [67, 68, 66] with four dosimeters place along the longitudinal axis of the TRUS probe was used. MO*Skin* rectal dose was compared to the TPS predicted doses and a comparison was drawn based on their relative differences. $\Delta_{\mathrm{DDPvsTPS}} = (D_{\mathrm{DPP}} - D_{\mathrm{TPS}}/D_{\mathrm{TPS}})$. Furthermore, the comparison of these two doses was investigated on a catheter-by-catheter basis. The MO*Skin* dose deposition was determined by the transit time of the source through the catheters. Overall, the study found the average difference in rectal wall dose between the measured and the TPS predicted dose to be 0.3% ±11.6%, which agrees with previous results [68]. The catheter-to-catheter measurements yielded promising results, with the average dose difference being 1.0%±15.7% when excluding small dose contributing catheters. Due to the high dose nature of some modern HDR BT regimes, it is important to monitor the delivery of this dose.

2.12.2 Internal source tracking

Brachy *View*

In 2013, Petasecca *et al* investigated the feasibility of real-time *in-vivo* seed identification for LDR pBT using a novel in-body imaging system consisting of a TRUS probe and gamma

camera[45]. The design of the probe saw three Medipix2 detectors in conjunction with a multipinhole lead collimator design. The collimator consists of 400μm lead plate which allows the attenuation of 22-35 keV emitted photons from the ^{125}I seeds with truncated-cone shaped apertures with an angle of $\pm 50.5^{o}$ at 10mm distance. By using the centre of mass of the Medipix2 detector image of the seeds and tracing lines to the pinhole, stereoscopic back-projection can be used to determine the three-dimensional position of the seeds. A PMMA prostate phantom with parallel horizontal channels(pitch of 10mm) which mirrored the standard HDR brachytherapy grid to house the seeds was used. Four $_{124}$I seeds were positioned within the phantom at different source-to-collimator distances SCD. Data was acquired for 3s at 50 frames/s. The longitudinal accuracy of the system was determined to be SCD dependent; 10mm SCD accuracy was $\pm$0.2mm and $\pm$6mm at 60mm SCD. It was further shown that the 3D source localisation also decreased with SCD, with localisation achievable within 3mm at 60mm SCD. Overall, the study demonstrated the feasibility of the BrachyView system in determining seed positioning within 1mm for SCD of 20mm.

Alnaghy *et al*'s 2017 study saw the application of BrachyView to LDR brachytherapy to allow real-time source reconstruction within the prostate. Using a tissue equivalent prostate phantom, a thirty seed LDR treatment plan was performed and imaged using both TRUS and CT [46]. The BrachyView probe follows a similar design to prior generations [45], utilising three cone pinholes and high-resolution silicon Timepix detectors. The study showed that 75% of the thirty seed positions imaged were reconstructed using BrachyView to within 1mm. The maximum discrepancy of seed position found using CT was 1.78mm. Visualisation of seed position within prostate anatomy was further demonstrated, fusing TRUS images with

the reconstructed source positions.

Although proving its ability, there are some inherent shortcomings with the Brachy*View* system. These include the difficulty in achieving the high degree of accuracy required for the machined holes in the tungsten housing, the low flux of photons reaching the PCB, orientation dependency and the small FOV.

Although the primary focus of Brachyview is LDR BT, its principals can be used concurrently with HDR BT.

Summary

The need for a means of clinically accurate dose localisation and verification which can be used as through the entire HDR prostate brachytherapy procedure under TRUS guidance has become apparent.

An in-vivo source tracking system which is non-invasive, novel and practical is desired for routine clinical use. The system must be easily integrated into clinical use; a compatibility with US based treatment planning is necessary.

Chapter 3

Development of an anthropomorphic prostate insert and a feasibility study for end-to-end testing

This chapter serves as a preliminary study to establish the feasibility of the End-to-End phantom and Gel Prostate insert to be used in conjunction in future end-to-end studies. Prior to the application of clinically relevant HDR pBT plans on the E2E system, the following suitability tests will be undertaken:

1. Gel Prostate insert behaviour when imaged under US image will be evaluated
2. Volumetric study to evaluate Gel Prostate insert characteristics as an anthropomorphic phantom

3. Gel Prostate insert will be validated using clinically relevant treatment plans

4. Validation of catheter reconstruction to establish uncertainties through the employment of CT

Through the successful completion of the above steps, the Gel Prostate inserts potential in clinically relevant end-to-end quality assurance will be verified. The anthropomorphic characteristics of the phantom will be established and it's response to clinically relevant conditions will be noted. Ultimately by doing so, proceeding E2E system experiments can be carried out with confidence.

3.1 Proposed Instrumentation

3.1.1 Gel Prostate Insert

In order to create an efficient end-to-end quality assurance based system which allows clinicians a similar clinical environment, an anatomically accurate and tissue equivalent prostate phantom was developed. 3D CAD software was employed to develop an anatomically accurate prostate, which included a urethra and ejaculatory duct. This detail can be seen in Figure 3.1.1. The size of the human prostate varies, with the average range of size being from 23.8 - 143 cc [70]. And so, three gel prostates were constructed with sizes of 28cc, 60cc and 100cc. The varying prostate size also allows the possibility of multiple treatment catheter number studies.

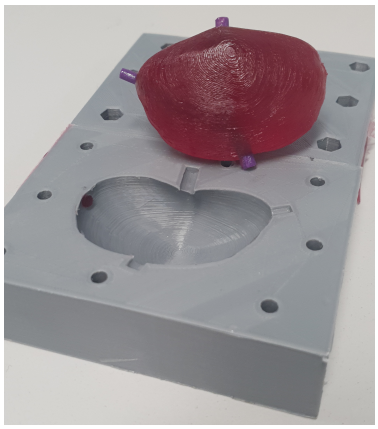

(a) 28cc Gel Prostate insert. Note the urethra and ejactulatory duct running from the base to the apex.

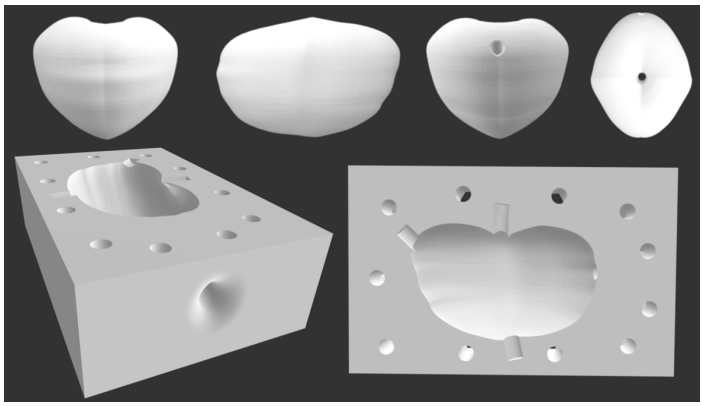

(b) The raw .STL prostate file of mould.

Figure 3.1.1: The Gel Prostate insert and the raw CAD files showing the mould and prostate

In order to match the same radiobiological effectiveness as human tissue, as well as having the ability to be imaged using ultrasound imaging techniques, the following method based on a study published by RO Bude *et al* was used [71]. 80g of food-grade gelatin was added to 250ml of boiling water and mixed thoroughly to ensure complete absorption. The solution was filtered through a strainer to remove any undissolved gelatin and air bubbles to avoid any potential US artefacts. A red food dye was added to the mixture to aid in localising the prostate when in a gel environment. The mixture was injected into the mould using a syringe and left to set in the refrigerator for a minimum of 2 hours. The finished phantom can be seen in Figure 3.1.1.

3.1.2 The 'End-to-End Phantom'

The End-to-end phantom is a clear perspex cube constructed with dimensions of 20cm x 20cm x 20cm with a 2.5cm diameter cylinder running the length of the cube. The phantom allows for a tissue equivalent environment as well as the potential for TRUS probe integration with the use of the rectum analogous. In one of the walls of the phantom there is an opening which allows for insertion of treatment catheters.

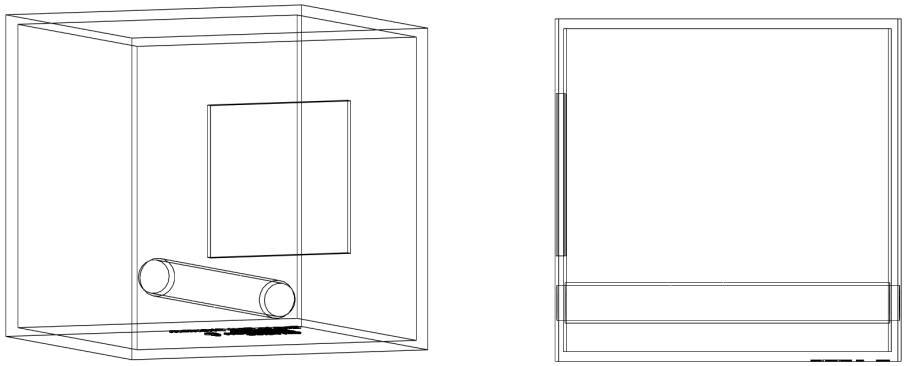

Figure 3.1.2: The End-to-End Phantom schematics. Note the template window on the front face and the rectal cylinder which runs across the phantom.

3.2 Initial proof of concept

Before proceeding to volumetric and clinical relevant HDR BT plans, an initial proof of concept was completed to establish the relationship between US imaging and the Gel Prostate insert. This will elucidate if and how the US imaging will show the Gel Prostate insert under conditions which emulate further E2E Phantom testing.

Methods

To validate the use of US imaging for the Gel Prostate insert, the E2E phantom was used in conjunction with a B&K Medical US system. Two Gel Prostate insert of sizes 60cc and 100cc were used. The E2E phantom was filled with water and the prostate was placed with correct anatomical positioning on a platform within close proximity to the rectal cylinder. The TRUS probe was placed in the stepper mount and inserted into the E2E phantom. A series of images were acquired from the base of the prostate to the apex in 5mm steps. The clarity of the image was qualified by the presence of a clear outline of the prostate.

The behaviour of the US image when interacting with an interface of two different gel densities was also investigated. A single 28cc Gel Prostate insert was made and placed in a container and surrounded by gelatin of different consistency. A cylinder of diameter equal to that of the TRUS probe was inserted into the container to allow a channel for US imaging. The stepper mount was used to image the prostate. The US's ability to differentiate the two different gel densities was evaluated by the system's ability to clearly define the prostate at the interface between the prostate and the surrounding gel.

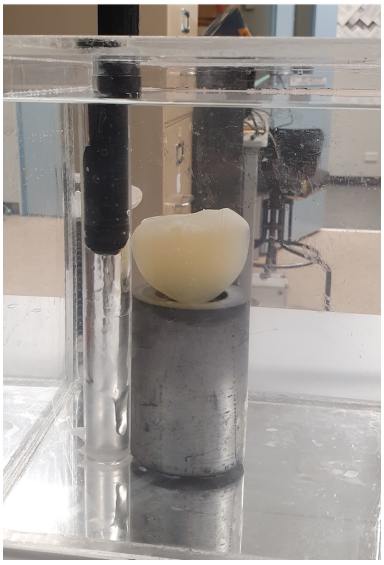

(a) Preliminary US testing. The Gel Prostate insert can be clearly seen in the E2E phantom surrounded by water.

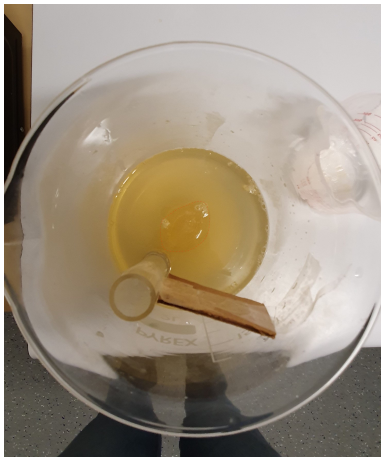

(b) Gel interface US testing. The Gel Prostate insert can be seen surrounded by a different density gel.

Results

In order to evaluate the Gel Prostate inserts future use in TRUS guided studies, a B-KMedical FlexFocus400 US system and a TRUS probe coupled with a stepper mount was employed to image the phantom. The images collect in 5mm increments were printed and analysed. From figures 3.2.0, it can be conclusively noted that the Gel Prostate insert can be seen in all images. A distinct outline of the prostate at each step, with the general shape in agreement with anatomy. It was also noted that the urethra and the ejaculatory duct were also present in the images. The presence of these two anatomical landmarks further demonstrates the Gel Prostate inserts feasibility to be used as an anthropomorphic phantom.

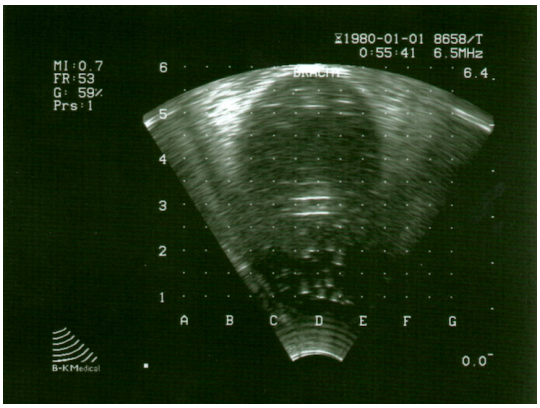

(a) 60cc Gel Prostate insert Base

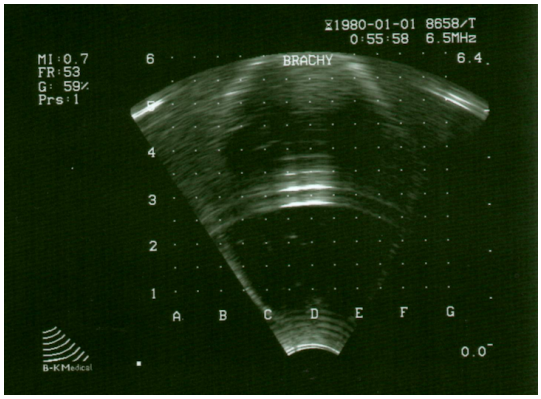

(b) 60cc Gel Prostate insert Base +5mm

To further evaluate the Gel Prostate inserts use in E2E studies, the phantom was set within a different density gel environment to investigate the behaviour of the US image with a gel-gel interface. A similar method using the stepper mount was used to obtain a single image, acquired midway through the prostate.

The images acquired shows a clear prostate outline, with the urethra present also. The interface between the prostate and the surrounding gel is present and defined so as to have the ability to volume the prostate.

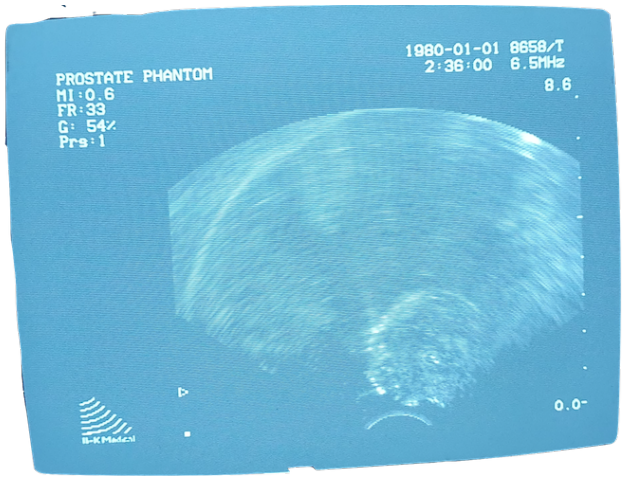

Figure 3.2.1: Gel interface US acquired image. The outline of the Gel Prostate insert can be clearly seen surrounded by a different density gel.

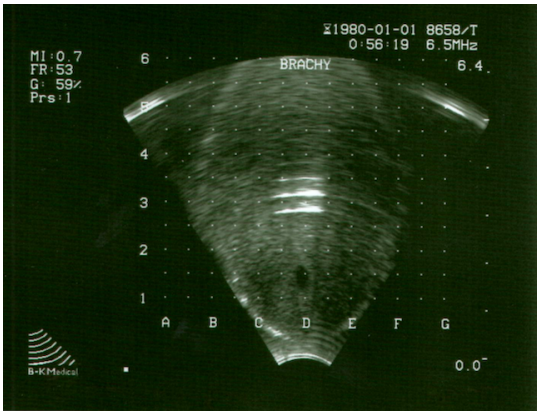

(c) 60cc Gel Prostate insert Base +10mm

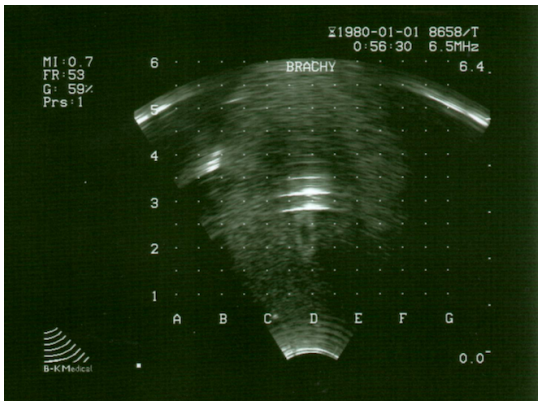

(d) 60cc Gel Prostate insert Base +15mm

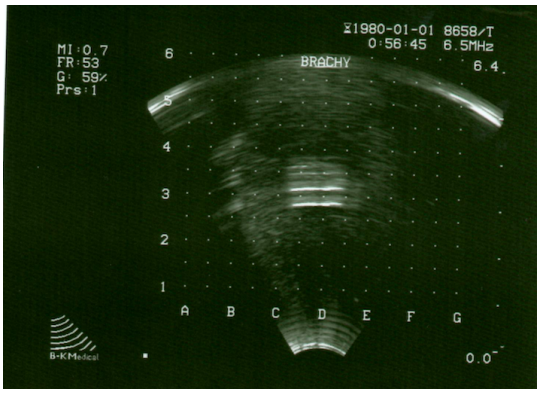

(e) 60cc Gel Prostate insert Base +20mm

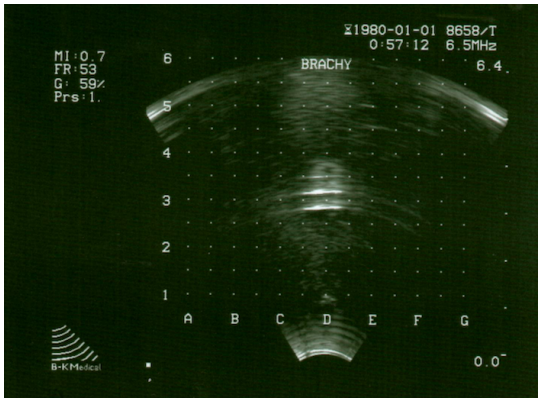

(f) 60cc Gel Prostate insert Base +25mm

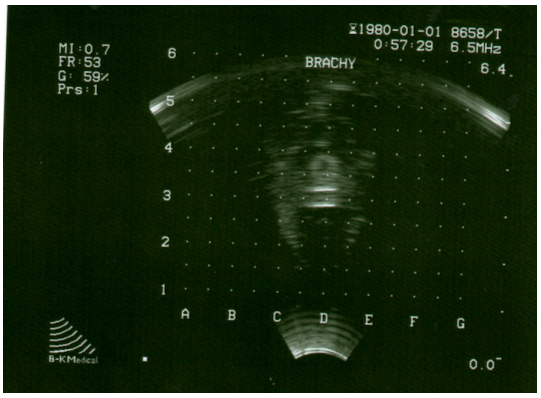

(g) 60cc Gel Prostate insert Base 30mm

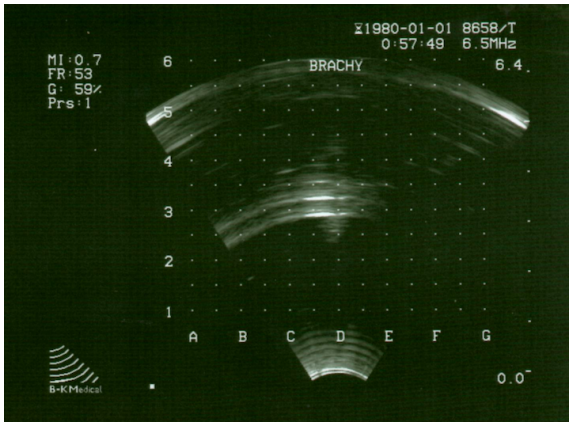

(h) 60cc Gel Prostate insert Base +32.3mm (Apex)

Figure 3.2.0: US images of 60cc Gel Prostate insert from base to apex. Note the urethra and ejaculatory duct in images c) through g).

3.3 Ultrasound Volumetric Study

In order for the Gel Prostate insert to be validated as an anthropomorphic phantom, a volumetric study of the system needs to be conducted. By doing so, the use of the phantom will be verified as suitable for future TRUS guided analysis of clinical pBT treatments.

Methods

The E2E Phantom was used in conjunction with a 28cc, 60cc and 100cc Gel Prostate insert to create a system in which the TRUS probe could be used in a clinically similar manner to scan and measure the volume of the prostates. The Gel Prostate insert were placed in the E2E Phantom in clinically relevant proximity to the rectal cylinder and surrounded by tissue equivalent gel with a gelatin concentration of 40g to 500ml of water.

The prepared phantom setup was secured on the patient couch in the same dorsal lithotomic position as brachytherapy patients. The TRUS probe was placed in the stepper mount and the US system was set up as per treatment protocol. The TRUS probe was inserted into the E2E phantom using US transmission gel, ensuring a close contact to the perspex cylinder to allow the best visibility. Each prostate was located on the US system and a radial scan of 120° was acquired. Each prostate was contoured on the Nucletron Treatment Planning System by outlining the prostate for each slice. Once a final prostate volume was defined, the geometric volume was calculated.

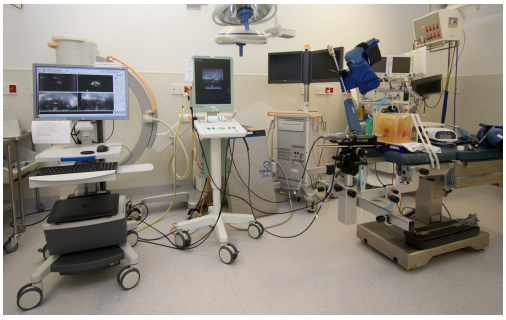

(a) Setup for volumetric study. From left to right; TPS, US system, and TRUS Probe and stepper mount with the E2E phantom secured on the patient couch.

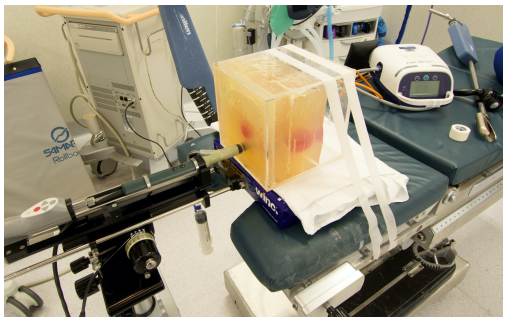

(b) TRUS probe coupled with stepper mount inserted in E2E phantom.

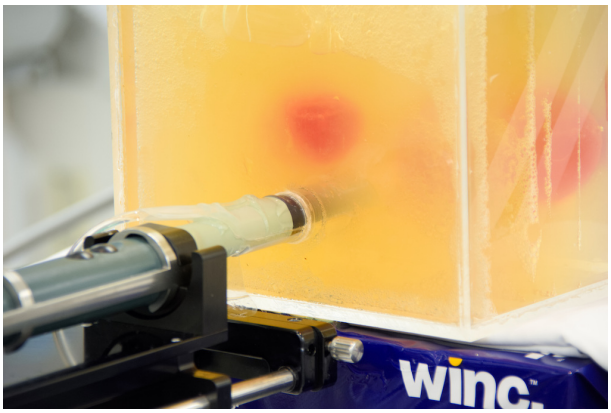

(c) Close up of TRUS Probe inserted inside the E2E Phantom. Note the presence of the prostates in red.

Figure 3.3.1: The experimental setup for the volumetric study of the 3 Gel Prostate insert.

Results

The 120° US acquisitions, after contouring, returned a geometric volume for each Gel Prostate insert. This volume was compared to the volume determined from the original prostate mould files, considering these values as the true volume.

The true volume from the 28cc .STL file was found to be 28.003ccs. The geometric volume which was calculated from the TPS for the 28cc prostate mould was (33.89±3.4)ccs. This is shown in figure 3.3.2.

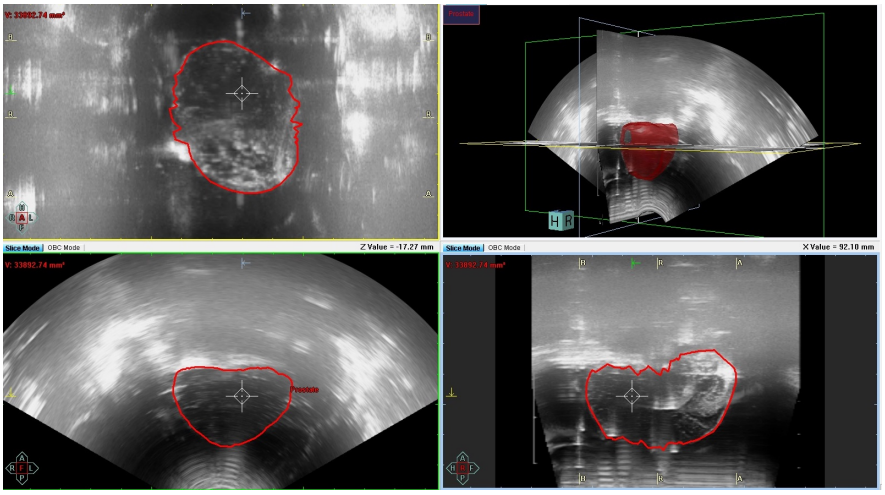

Figure 3.3.2: TPS output for the contoured 28cc Gel Prostate Mould. The axial, coronal and sagittal planes with the outlined prostate can be seen.

The 60cc prostate .STL file returned a true volume of 59.99cc. The geometric volume found from the TPS was calculated to be (66.65±6.7)ccs which can be seen in figure 3.3.3.

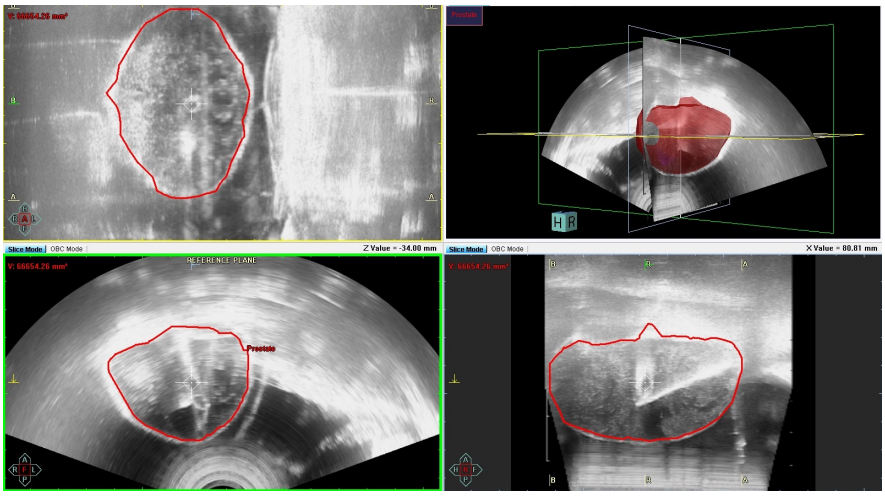

Figure 3.3.3: TPS output for the contoured 60cc Gel Prostate Mould. The axial, coronal and sagittal planes with the outlined prostate can be seen.

Finally, the 100cc prostate .STL file returned a true volume of 100.01ccs. The TPS calculated

geometric volume was shown to be (84.8±8.5)ccs. This is shown in figure 3.3.4.

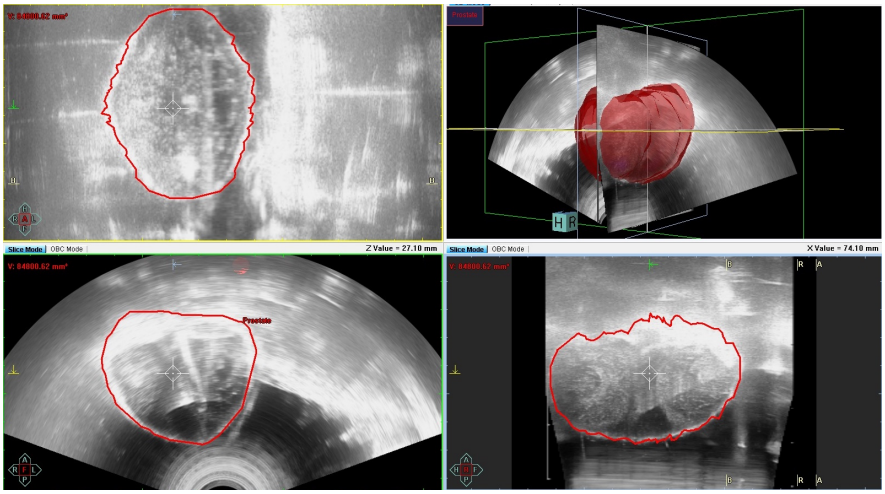

Figure 3.3.4: TPS output for the contoured 100cc Gel Prostate Mould. The axial, coronal and sagittal planes with the outlined prostate can be seen.

3.4 Insertion and ultrasound localisation of treatment catheters

To further qualify the Gel Prostate insert and E2E Phantom systems use with clinically relevant HDR pBT treatment plans, the systems behaviour when inserted with treatment catheters needs to be evaluated.

Method

A 60cc Gel Prostate insert was used with the E2E Phantom. The prostate was surrounded by a tissue equivalent mixture of 40g to 500ml of water. The prostate was then placed within close proximity to the rectal cylinder to replicate human anatomy.

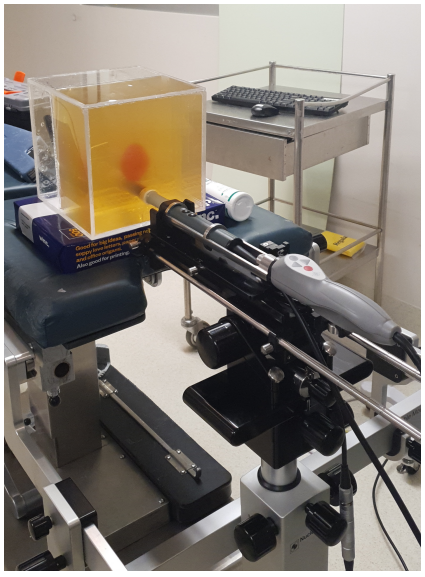

(a) The E2E Phantom with a single 60cc Gel Prostate insert. The TRUS probe and stepper mount can be seen inserted into the phantom.

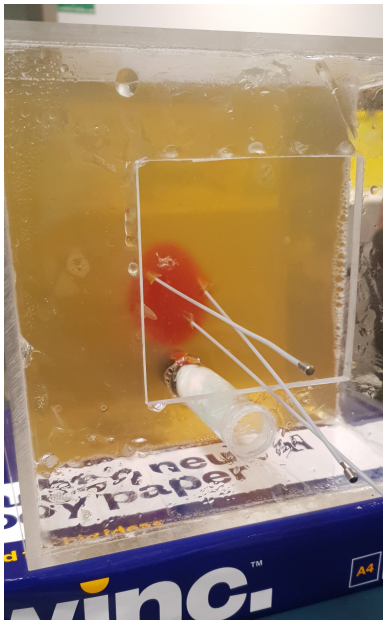

(b) The three treatment catheters inserted into the Gel Prostate insert.

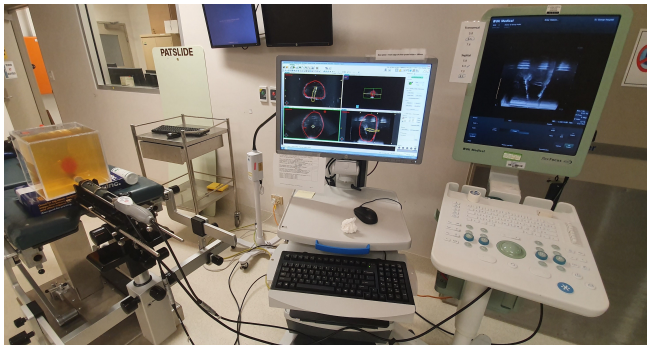

(c) The experimental setup showing from left to right the E2E phantom with Gel Prostate insert, TRUS Probe and stepper mount, the Nucletron TPS and the US system.

Figure 3.4.1: The insertion and US localisation of treatment catheters in the E2E Phantom.

The system was secured on the treatment couch in the same dorsal lithotomic position as

in previous studies. The TRUS probe from the BkMedical FlecFocus400 was placed in the stepper mount and the Nucletron TPS was connected to the US system. To retain clinical relevance, the standardised prostate HDR procedure was adopted. A pre-implant scan was obtained with typical QA conducted. Firstly, the grid array for the TPS and US were tested to ensure an overlay in agreement within error. The rotation and zero point of the stepper mount were also tested by rotating through 180° and stepping the mount to a set distance and then back.

Once certain that the setup was correct and did not display any signs of error, a pre-implant scan following clinical protocol was obtained. The superior aspect (base) of the prostate was located using the TRUS probe. Once found, this position was set as the zero point on the stepper mount and DICOM. A sagittal acquisition was selected and the TRUS probe was stepped through until the whole prostate was visible. A 120° scan was then obtained.

Using a technique similar to the section 3.2, the scan was contoured on the TPS and a geometrical volume for the prostate was found.

Once the pre-implant scan was acquired and a volume was found, 3 treatment catheters (Proguide 240mm) were manually inserted into the treatment volume in three different locations. The positions of the catheters were located on the TPS and another 120° radial scan was acquired.

Results

Three Proguide 240mm treatment catheters were manually inserted into a 60cc Gel Prostate insert within a tissue equivalent gel environment inside the E2E phantom. A post-implant radial acquisition was obtained using the TRUS probe and analyses on the TPS.

The three catheters were located on the US image which corresponds to the midpoint of the prostate. The distances between each treatment catheter was then quantified.

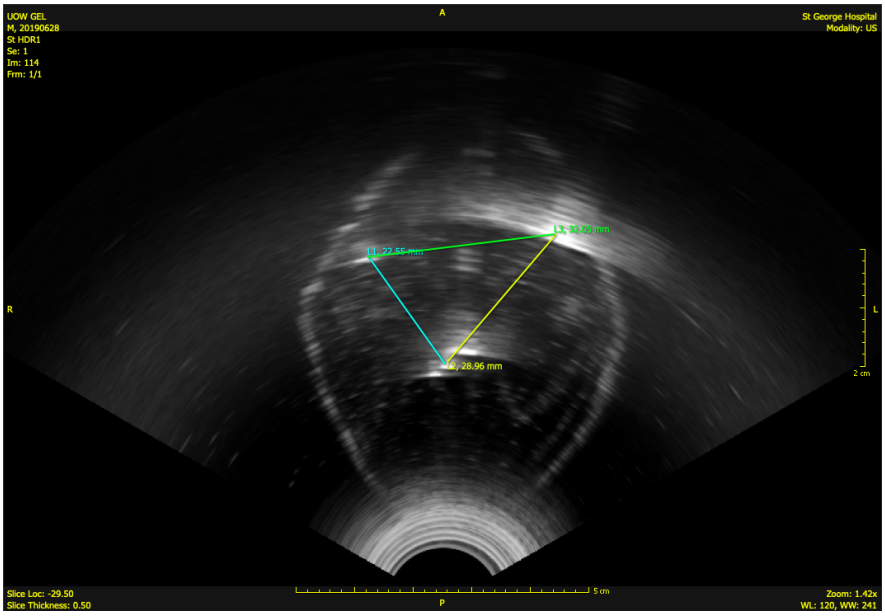

Figure 3.4.2: US image of the E2E phantom with a 60cc Gel Prostate insert with 3 treatment catheters inserted. A large degree of artefact can be seen around each catheter making localising difficult.

Starting at the left side of the US image (referring to Figure 3.4.2) and moving in a clockwise direction, the distance between catheter 1 and catheter 2 was found to be (32.05±5)mm, the distance between catheter 2 and catheter 3 was found to be (28.96±5)mm and the distance

between catheter 3 and catheter 1 was (22.50±5)mm.

3.5 CT verification of reconstructed catheters

For HDR Prostate Brachytherapy treatment, CT localisation of the catherers are considered the gold standard. A CT acquisition of the phantom setup, as seen in Section 3.3 with inserted treatment catheters, is used in order to quantify the uncertainties of the catheter locations found on the US image.

Method

The E2E phantom with the inserted catheters was placed on the imaging bed and the inbuilt lasers were used to align the setup at isocentre.

Due to CT's inability to register the outline of the Gel Prostate insert, CT markers were placed on the outside of the E2E Phantom at the midpoint of the prostate. Copper wires were placed inside of the treatment catheters to allow ease of CT localisation. A 271.0mm FOV image was acquired using prostate protocol 2mm iDose(4) at 120kV with 161mAs/slice. The DICOM images were exported and analysed.

The distance between each catheter was calculated and noted. The diameter of the rectum cylinder was also measured to ensure the accuracy of the results.

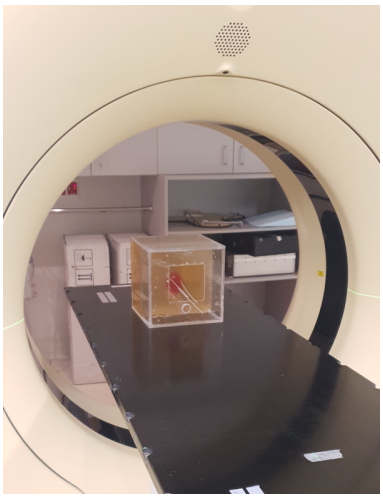

Figure 3.5.1: Catheter localisation in the E2E phantom.

Results

The slice corresponding to the midpoint of the prostate was used to obtain the distance between treatment catheters. This can be seen in figure 3.5.2.

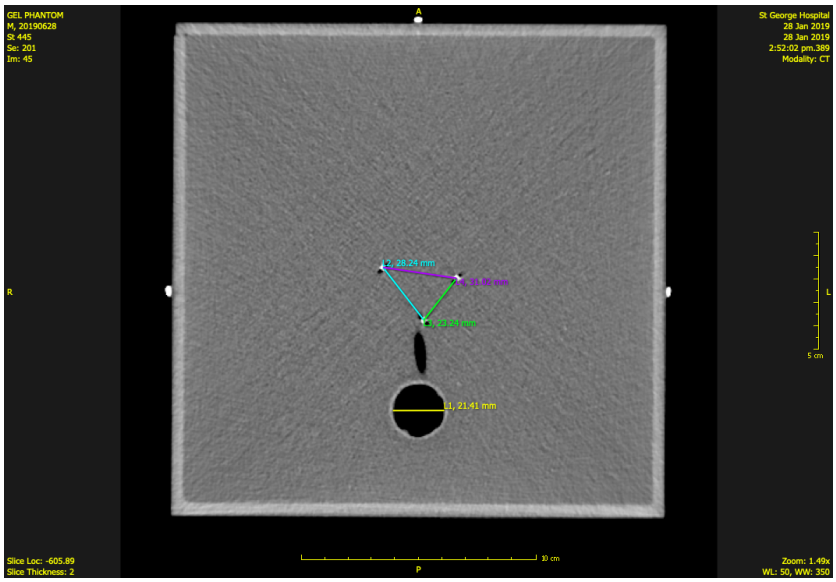

Figure 3.5.2: CT image of the E2E phantom with a 60cc Gel Prostate insert with 3 treatment catheters inserted. The CT markers can be seen on the outside of the E2E phantom indicating the midpoint of the prostate. The urethra can also be seen anteriorly to the rectum cylinder.

Using the defined catheter numbers as in Section 3.4, the distance between catheter 1 and catheter 2 was found to be (31.02±2)mm, the distance between catheter 2 and catheter 3 (23.24±2)mm and between catheter 3 and catheter 1 to be (28.24±2)mm.

3.6 Discussion and Conclusion

This chapter provided a preliminary overview of clinical aspects of the E2E phantom and Gel Prostate insert system. By doing so, the foundation of the system's use in further HDR studies was developed.

It was initially proven that the Gel Prostate insert could be imaged under US, with the overall prostate outline as well as the presence of the urethra and ejaculatory ducts being visible. By surrounding the Gel Prostate insert with tissue equivalent gel, it was further demonstrated that US imaging could distinguish the prostate from the surrounding gel environment. Despite being trivial, the experiments proved the possibility of further E2E testing.

TRUS guided analysis of the Gel Prostate insert was proven to be plausible through obtaining the geometrical volumes from the TPS and comparing them to the actual volumes. The geometrical volumes from the 28cc, 60cc and 100cc Gel Prostate insert were found to be (33.89±3.4)cc, (66.65±6.7)cc and (84.80±8.5)cc respectively. For the 28cc prostate, the difference between measured and actual volume is (5.89±3.4)cc, the 60cc prostate has a

difference of (6.6±6.7)cc and the 100cc prostate has a difference of (15.21±8.5)cc.

The differences between measured volume and the actual volumes may be a result of both inaccurate prostate contouring and US distortions. Contouring of the prostates on the TPS will be different for different operators due to the user specificity of the task; each individual will have different interpretations of the prostate ROI based on prior experience. In order to account for this source of inaccuracy, the contouring of the prostate should be conducted by 3 separate clinicians.

Furthermore, the images obtained exhibit a degree of US distortions. The echo effect which produces a halo around the outline of the prostate may be a result of the high density of gelatin used in the prostate phantom. This can be accounted for by constructing the ROI such that the halo is avoided.

The combination of TRUS guided, clinically relevant treatment plans and treatment catheters with the Gel Prostate insert and E2E system was proven by measuring the distance between three Proguide 240mm treatment catheters. The distance between catheter 1 and catheter 2 was (32.05±5)mm, between catheter 2 and catheter 3 was (28.96±5)mm and between catheter 3 and catheter 1 was (22.5±5)mm.

The acquired US image displayed visible artefacts which hinders the ability to clearly define the position of each catheter. The origins of these artefacts come from the existence of air gaps which occurred during the insertion of the catheters; a lateral motion was used in order for visualisation. This can be easily avoided.

To further improve the obtained results, the distances between each catheter should be known prior to insertion. This can be achieved using the TRUS template. By inserting the

catheters into known grid locations which are also mirrored on the TPS, accurate distances can be determined and verified.

Finally, to improve the usability of the results with further studies, the midpoint of the prostate should be marked prior to image acquisition. By doing so, accurate comparisons between the CT localisation and US values can be made.

The uncertainties associated with US localisation of the treatment catheters in the End-to-End phantom was obtained through the employment of CT imaging. The distances between each treatment catheter was measured at the midpoint of the prostate and compared to the measurements obtained in the US study. A comparison can be seen in the table below.

	Distance (mm)		Difference
	US	CT	(mm)
Catheter 1 to Catheter 2	32.05±5	31.02±2	1.03±0.2
Catheter 2 to Catheter 3	28.96±5	23.24±2	5.72±1.5
Catheter 3 to Catheter 1	22.5±5	28.24±2	5.74±1.7

Table 3.6.1: A comparison of the distances between three Proguide treatment catheters using both US and CT based measurements.

The differences between the CT and US catheter distances stems from the inherent uncertainties associated with the US based measurement.

Ultimately, the results obtained demonstrate the TRUS' suitability for localisation of treatment catheters within the E2E phantom and Gel Prostate insert system with the existence of a small error.

Chapter 4

Characterisation of the End-to-End phantom and the Magic Plate 987 using clinically relevant treatment plans

As shown in the previous study, the feasibility of combining the Gel Prostate insert with the End-to-end phantom to be used in end-to-end studies was proven; The foundation of the combined systems use in further clinically relevant studies was developed.

The next step in the development of a holistic quality assurance tool for HDR brachytherapy is the use of the Magic Plate detector system combined with the End-to-end and Gel Prostate insert to measure clinically relevant treatment plans. The following steps need to

be undertaken in order to quantify the systems *in-vivo* treatment verification (IVTV) ability:

1. Calibration and Initial set up of MP987
2. Clinically relevant treatment plans carried out on E2E phantom with the MP987
    - Comparison of treatment plan dwell positions and time to measured values
3. Introduction of a clinically relevant error to test the response of the setup.

4.1 Proposed Instrumentation

4.1.1 MP987

The MP987 is a 2D *p-type* monolithic detector array with dimensions of 29 by 31 pixels designed by Owen Brace and Marco Petasecca (CMRP). There are 987 diodes mounted to a kapton substrate using edgeless drop-in technology developed by the Centre of Medical and Radiation Physics (CMPR). There is a 13cm by 13cm central section of the plate which has a pitch of 5mm, with the rest of the plate having a pitch of 7.5mm. 16 AFE (analogue front-end) chips situated around the board provide a charge-proportional differential analogue output from accumulated charge in a capacitor during some defined time frame. Each of the AFE chips are coupled to an ADC (analogue-to-digital converter) and the output signal is synchronised by the FPGA (field programmable gate array). From the FPGA, the data is transferred via USB to the computer, where the signal is processed using the Magic Suite software. The software allows different acquisition parameters and visualise a integral

detector response in real-time.

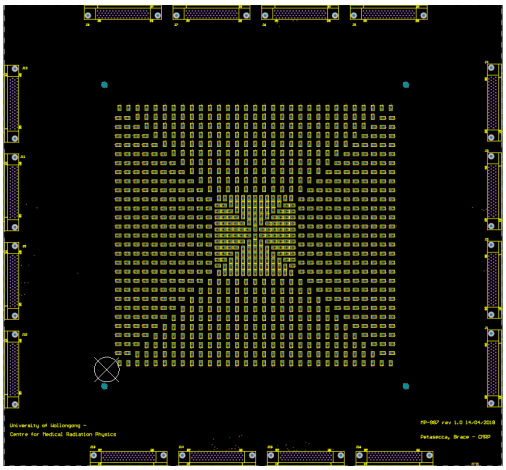

(a) PCB design of the MP987.

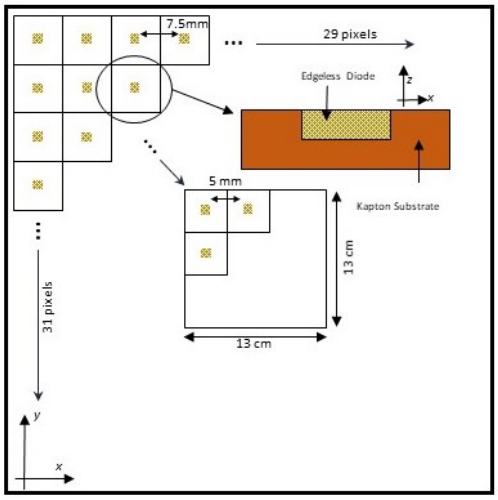

(b) A schematic showing the design of the MP987.

Figure 4.1.1: The E2E phantom used in conjunction with the MP987.

4.1.2 MP Tracking software

In order to obtain coordinate data from the MP987 readings, a tracking software was developed by Yashiv Dookie (CMRP). The program allows coordinate data to be returned from the acquired data in the following process:

- The raw data from the MP987 is decoded, an equalisation factor is applied and a baseline is removed. The equalisation factor is obtained from LINAC normalisation and the baseline is determined from 5s of data collected at the beginning of the acquisition when the source is still inside of the afterloader.

- In order to remove a level of noise from the data and reduce computational time, every

10 frames are averaged into one.

- The averaged data is mapped into a 2D matrix, which represents each diodes position on the MP.
- The difference in pitch (discussed in Section 4.1.1) in accounted for through the process of 2D radial interpolation. The new mapped data has a uniform 2mm pitch for each detector.
- The tracking component is then initiated for each frame and for the x and y axis separately.
    - The centre of mass is calculated for the top 30% of pixel responses using the following equation:

$$COM_{x,y} = \frac{\sum_{i=1}^{N} m_i x_i}{M} \tag{4.1}$$

    - The centre of mass for each frame is multiplied by 0.25 in order to return a position, not a diode number.
- The Z position for each frame is calculated using the top 90% of the pixel responses. This process is explored further in Section 4.2.

4.2 Calibration and initial set up of Magic Plate 987

Before commencing clinically relevant E2E testing, the general properties of the MP987 coupled with the tracking software needed to be established. There are three main attributes

of the system which need to be quantified in order to proceed with future measurements:

1. The repeatability (**r**) of the system between measurements need to be measured.
2. The variance of the system (σ) for measurements at difference SDD and dwell times needs to be investigated
3. Establishing a z calibration factor based on TG-43 calculations.

By quantifying these parameters by means of source positions, the subsequent studies will have defined properties which will propagate through each study.

Method

Repeatability

The definition of repeatability is the measure of closeness in agreement between two sets of results which are themselves mutually-independent, obtained within a short difference in time using the same equipment and experimental setup [72]. The value obtained for repeatability is **r**, which defines the an upper value for which the absolute difference obtained for 95% of measured cases (under repeatable conditions) will be below. This can be calculated using the following equation:

$$r = 2.8 S_{\mathrm{r}} \tag{4.2}$$

where S_r is:

$$S_{\mathrm{r}} = \sqrt{\frac{\sum_{i=1}^{q} {w_{\mathrm{i}}}^2}{2p}} \tag{4.3}$$

and:

- p = the total number of measurements for each run
- w_i = absolute difference between each measurement.

In order to determine the repeatability of MP987 and source tracking software system, data needs to be compared between subsequent acquisitions. The source will be delivered to a predetermined position for a set amount of time. This will be conducted twice in two separate treatments with the data acquired compared between measurements. The repeatability will be evaluated at two different dwell positions which are located at different SDD.

Standard deviation of acquired data (σ)

The measure of standard deviation (σ) defines the spread of some set of variables from the mean. It is important to define σ for the MP987 and tracking software system as this standard deviation will propagate throughout each measurement acquired. σ can be determined using the following equation:

$$\sigma = \sqrt{\overline{R^2} - \overline{R}^2} \tag{4.4}$$

The effect of dwell time and SDD on σ needs to be investigated before a singular value is determined. To investigate the impact of time on the calculation of σ, two dwell positions with times 5.7s and 33.1s will be used. The effect of SDD on σ will further be investigated by using the same dwell positions with varying SDD.

Z-calibration

Unlike the x and y positions, the z coordinate positions need to be obtained in accordance to TG-43 radial distance calculations (Equation 2.1). In order to utilise this function, the dose rate needs to be obtained from the pixel responses. This is achieved by a calibration factor, which when obtained can be used to convert any pixel response to a dose. In order to obtain a calibration factor, the pixel response from varying known SDD can be used and compared.

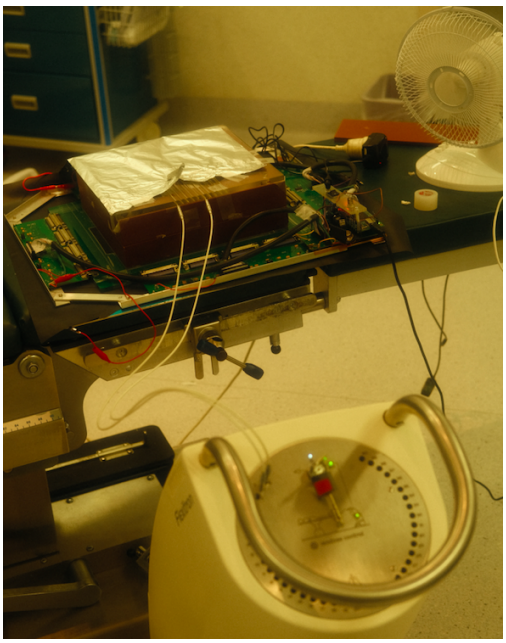

(a) The E2E phantom with a 60cc Gel Prostate insert inside. 20 treatment catheters have been inserted.

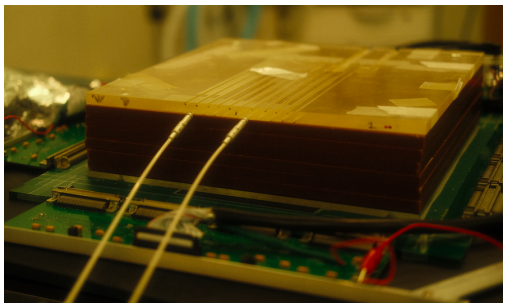

(b) A closeup of the treatment catheters inside of the phantom.

Figure 4.2.1: The experimental setup used in initial calibration studies

The same treatment plan which steps the source across the plate will be used for varying thickness of solid water: 4.5cm, 6.5cm, 7.5cm, 8.5cm, 9.5cm and 10.5cm. A calibration factor

will be calculated at each of the SDD values and applied to the tracking algorithm to quantify their robustness with varying SDD calculations.

Results

Repeatability

Two separate acquisitions were taken for the same dwell position and time. The data collected was compared and computed, according to Equation 4.1 and 4.2. The values for repeatability can be seen in Table 4.2.1. Note: Dwell position 1 has an SDD of 70mm and dwell position 2 has an SDD of 127mm.

Table 4.2.1: Repeatability values for two different dwell positions.

	r (mm)
Dwell Position 1	2.6
Dwell Position 2	1.2

Standard deviation of acquired data (σ)

A value for standard deviation was calculated in two different instances to investigate their effect on σ; at two different dwell positions of differing dwell times and at varying SDD for the same dwell time.

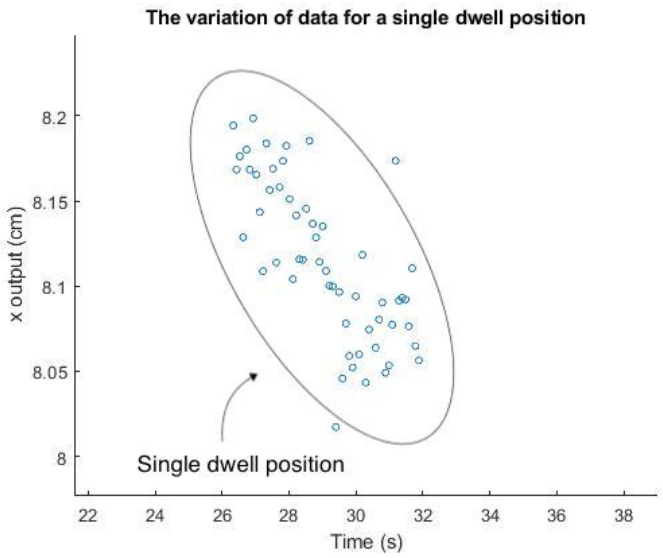

Figure 4.2.2: The tracking data returned for a single dwell position. The standard deviation over the dwell position can be seen.

Using Equation 4.4, the standard deviation was calculated for two different dwell positions with different dwell times. The first dwell position had a dwell time of 5.7s while the second had a dwell time of 33.1s. Each dwell position was measured three times and the average sigma was calculated. The results can be seen in Table 4.2.2

Table 4.2.2: Relative differences in timing of maximum dose rates.

	σ_1 (mm)	σ_2 (mm)	σ_3 (mm)	$\overline{\sigma}$ (mm)
Dwell position 1 (5.7s)	0.41	0.29	0.50	0.40
Dwell position 2 (33.1s)	0.18	0.16	0.16	0.17

Using Equation 4.4, the standard deviation was then calculated for various SDDs. Each calculation was made for data above the same area of the MP987 for each SDD. The obtained

values for σ can be seen in Figure 4.2.3

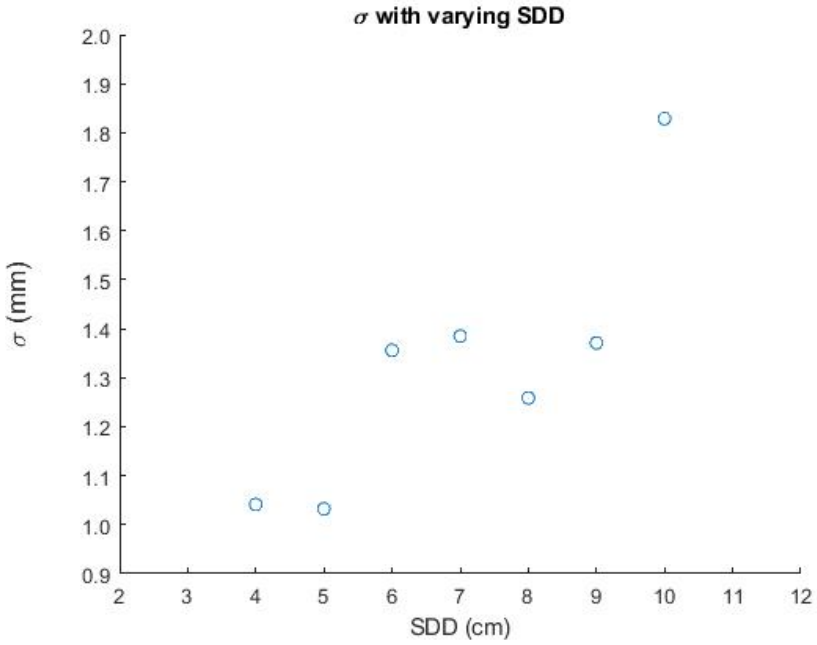

Figure 4.2.3: A value of σ calculated at different SDDs.

The maximum and minimum value for σ was 1.83mm for an SDD of 10cm and 1.04mm for an SDD of 4cm respectively.

Z-calibration

Measurements were taken for SDDs of 4.5cm, 6.5cm, 7.5cm, 8.5cm, 9.5cm and 10.5cm. The same dwell position across these measurements was used to obtain a mean pixel response. From this, a calibration factor for each SDD's data set was determined. This calibration factor was used in the TG-43 radial distance calculation.

In order to verify the effect of the choice of SDD calibration factor on the accuracy of z position output, each calibration factor was used in order to return a z position for an array

of measurements, which are outlined in Table 4.2.3. The z position output using the 4.5cm calibration factor for varying SDD measurements can be seen in Figure 4.2.4.

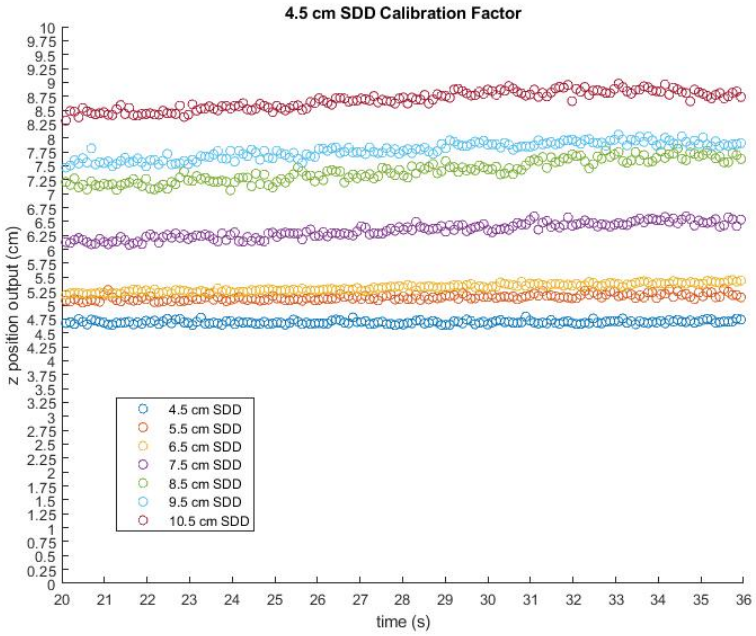

Figure 4.2.4: The z position outputs using the 4.5cm calibration factor. Note the difference in obtained value from the expected distances as SDD increases from 4.5cm.

Table 4.2.3: Relative difference (%) between the expected depth and the obtained depth for each calibration factor at each depth. The minimum difference is highlighted for each calibration factor.

		Depth of Calibration						
		4.5	5.5	6.5	7.5	8.5	9.5	10.5
Measurement Depth (cm)	4.5	4.5	7.6	9.4	24.6	32.9	36.4	45.1
	5.5	14.5	1.2	0.8	17.4	26.5	30.3	39.9
	6.5	18.9	5.1	3.1	14.2	23.6	27.6	37.6
	7.5	41.3	24.9	22.5	2.0	9.3	14.0	25.7
	8.5	64.8	45.7	42.7	18.8	5.7	0.2	13.5
	9.5	73.0	52.9	49.9	24.8	11.1	5.3	9.3
	10.5	92.8	70.5	67.1	39.2	23.7	17.4	1.1

Discussion

Before the MP987 and tracking software were to be used in conjunction with clinically relevant treatment plans, some general parameters of the system needed to be established. These included the repeatability (**r**) of the system, the standard deviation (σ) of measurements and the z calibration factor.

When quantifying the repeatability of the system, two measurements were taken for different SDDs to note its affect. The repeatability (**r**) for an SDD of 70mm was 2.6mm and 1.2mm for an SDD of 1277mm. This means that 95% of the measured cases between two data sets will have a difference of less than **r**. A known value of **r** is paramount as it defines the precision

of the systems spatial and temporal resolution in successive measurements.

The value obtained indicates the system has a strong level of repeatability for initial feasibility studies. However, for clinical applications there needs to be an improvement in **r**. The repeatability of the system needs to be sub mm to ensure its purpose of accurate source localisation can be obtained for each repeated application.

To determine the standard deviation of measurements taken with the system, a value of σ was obtained for varying dwell times and SDD. By doing so, the effect of these parameters on the standard deviation could be investigated. σ for a dwell time of 5.7 seconds was found to be 0.4mm while for a dwell time of 33.1s, σ was found to be 0.17mm. The increase in dwell time saw a decrease in standard deviation. One possible explanation for this observation is due to the detectors stabilising after a change in dose rate for longer dwell times. When calculating σ for different SDD, there was a correlation between an in increase in SDD and standard deviation; The minimum σ was found for a SDD of 4cm while the maximum σ was found for a SDD of 10cmm. The spread of the detected signal has a $1/r^2$ dependence. This will cause the standard deviation for each dwell position to be larger at larger values of r.

When comparing the two separate studies, the value of σ should be relatively similar however they vary by $\approx$1mm. This difference can be attributed to a large degree the time over which the SDD measurements were taken. The susceptibility of the MP's AFE system in picking up interference is also a factor which may have contributed to differences. The conditions between measurements may have changed which may have caused the MP to exhibit a degree of noise. This phenomena will be explored more in Section 4.3.

Finally, the calibration factor in determining z coordinates was investigated. Calibration

factors determined from SDD measurements of 4.5cm, 5.5cm, 6.5cm, 7.5cm, 8.5cm, 9.5cm and 10.5cm were calculated and used in the tracking software which utilises the TG-43 radial distance calculation. The returned z coordinate from the 4.5cm calibration factor can be seen in Figure 4.2.4. As the SDD deviates from the original calibration SDD, the deviation in determined and true z coordinate increases. For SDD values which are within 1cm of the calibration SDD, the returned z coordinate varies by 7% to 18.8%. This increases to 18.9% to 24.9% for an increase in 20mm from the calibration SDD. This pattern holds true for all calibration SDDs, and can be seen in Table 4.2.3. The z coordinate output from the tracking software is dependent on the z calibration SDD.

It is expected that the calibration factor calculated at any SDD would return accurate z coordinate results when used with the TG-43 calculation. This did not hold true for the MP system. The main reason behind this inaccuracy is the process of equalisation. Each diode, before any equalisation, will yield different responses for the same source. To equalise variation in diode response, the MP is subjected to a flat field from a LINAC and a correction factor is determined for each diode. Ideally, this correction factor would hold true for all future measurements but this is not the case. Furthermore, the size of the plate itself is too big for a flat field, and so equalisation is computed in sections. A more appropriate equalisation protocol would be one that is more frequent and robust. An alternate approach for equalisation would be to compute diode correction by adopting a diode by diode approach in which a HDR source is sent directly above each diode at the same hight.

4.3 Testing the source tracking capabilities of the Magic Plate 987 by means of clinically relevant treatment plans.

In order to test the feasibility of the MP987s use in HDR pBT *in vivo* treatment verification, the E2E phantom will be used to carry out a complete clinical procedure. The use of the MP in source tacking studies have seen localisation accuracies of less than 1mm [63, 60, 59]. In order to quantify the MP and E2E phantom's ability to perform source tracking, it is hoped to achieve the following objective: Source position verification of sub mm accuracy under clinical procedures.

Method

A 60cc Gel Prostate insert was used in conjunction with the End-to-end phantom for this study. By doing so, an anthropomorphic representation of the clinical environment could be emulated. The Gel Prostate insert was constructed as outlined in 3.1.1 and the E2E phantom was filled with a tissue equivalent gel. The phantom was placed on the MP in the same dorsal lithotomic position used in Chapter 3. This can be seen in Figure 4.3.1. The TRUS Probe from the BkMedical FlecFocus400 on a stepper mount was inserted into the E2E phantom and kept in position throughout the duration of the treatment, as per clinical procedure. The superior aspect (base) of the prostate was located, to retain clinical relevance. Twenty

treatment catheters were then inserted into the target volume under US guidance. As a result of artefacts caused from the treatment catheters, a US based plan was not able to be generated. Instead, a 271.0mm FOV CT using prostate protocol 2mm iDose(4) at 120keV with 161mAs/slice was acquired. Based on the acquired image, the prostate was contoured and a 9Gy per fraction plan was generated [Figure 4.3.2]

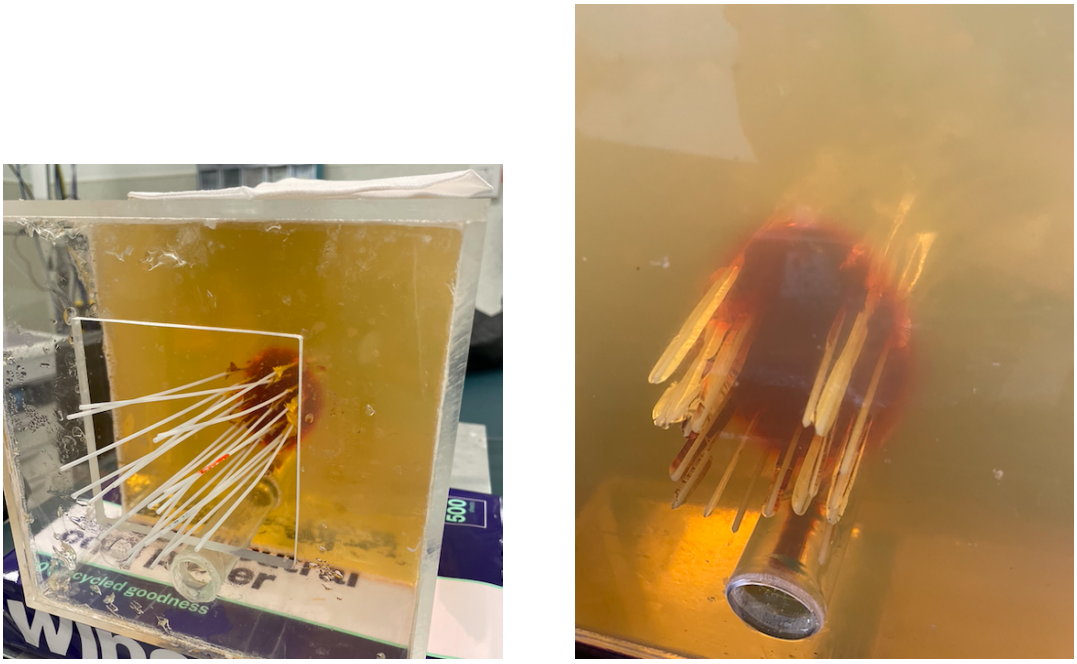

(a) The E2E phantom with a 60cc Gel Prostate insert inside. 20 treatment catheters have been inserted.

(b) A closeup of the treatment catheters inside of the phantom.

Figure 4.3.1: The experimental setup showing the anthropomorphic phantom.

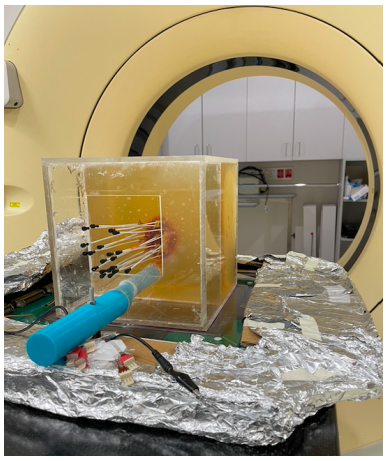

(a) The E2E phantom setup about to be CT scanned.

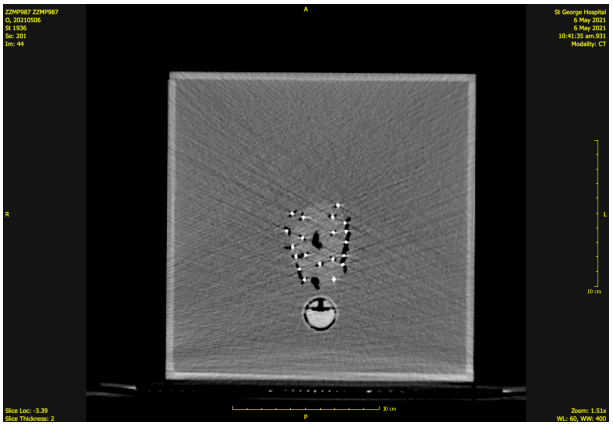

(b) A CT slice showing the treatment catheters inserted inside of the phantom. The MP can be seen below.

Figure 4.3.2: A CT based treatment plan was generated. Note the insertion of copper rods inside the treatment catheters to be registered.

Results

A total of three separate clinical procedures were carried out on the E2E phantom. Data from the MP987 was collected, decoded and interpolated as per Section 4.1.2. Each clinical procedure returned on average 8370 frames, with a large majority of the 987 pixels returning a response per frame. Figure 4.3.3 shows the response of the MP, once post interpolation has been applied.

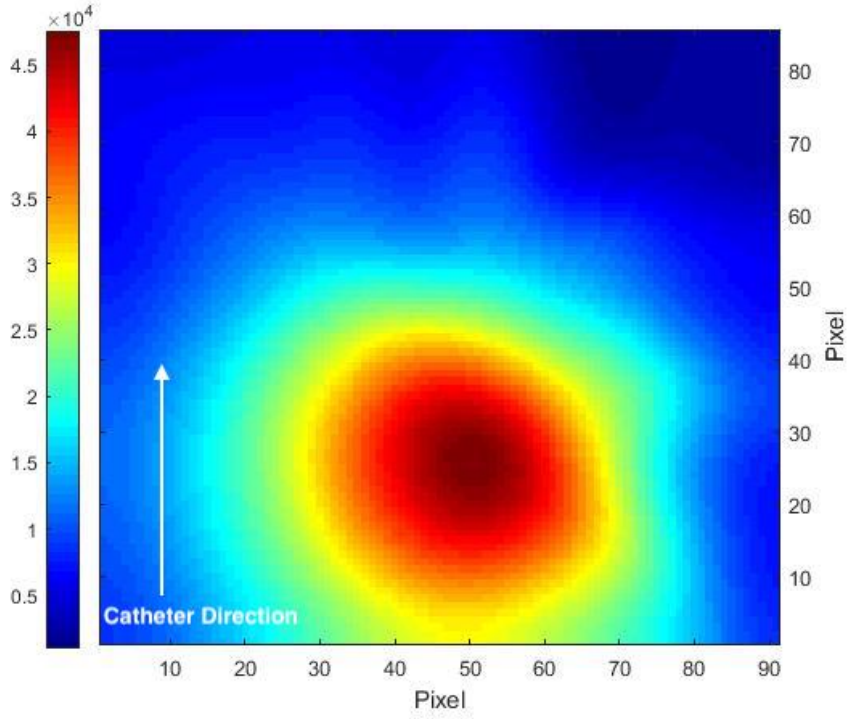

Figure 4.3.3: A colour map of the response of each pixel across the plate with a source directly above. The response is in counts.

Each of the three runs, once interpolated, was processed through the tracking algorithm. The x, y, and z coordinates with respect to time can be seen in Figure 4.3.4. Each individual catheter with its respective dwell positions can be seen.

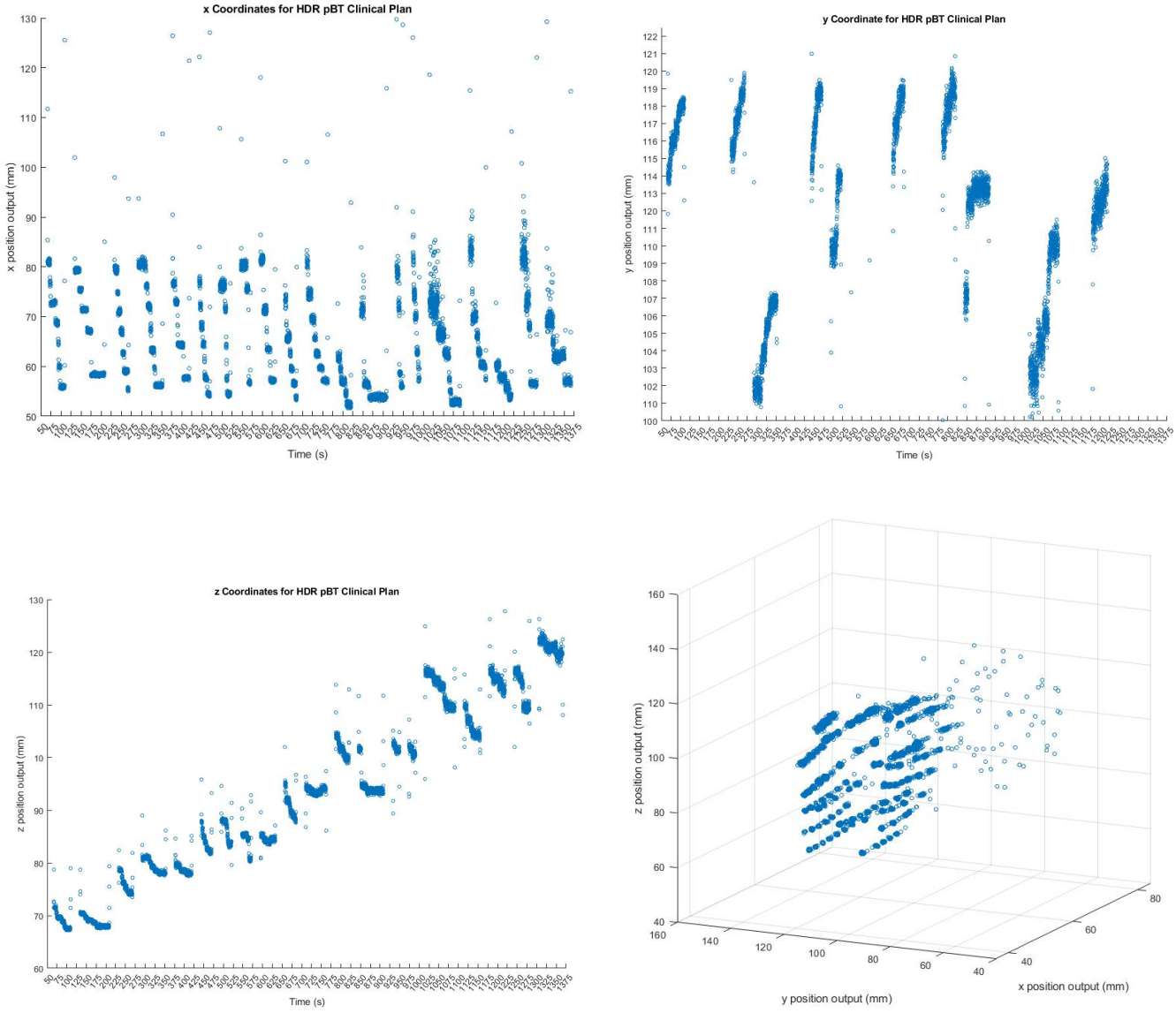

Figure 4.3.4: The tracking coordinates returned from the MP987 and tracking software. Each axis has been considered separately with respect to time.

In order to quantify the differences between measured dwell position and the TPS, the data collected for each catheter was sorted into a frequency histogram, with each cluster corresponding to an individual dwell position. Based on the width of these clusters, as well as the frequency of each cluster, position data is returned for the x, y and z coordinates. A defined

cut off frequency was established under which the counts would be disregarded. An example of an obtained histogram can be seen in Figure 4.3.5.

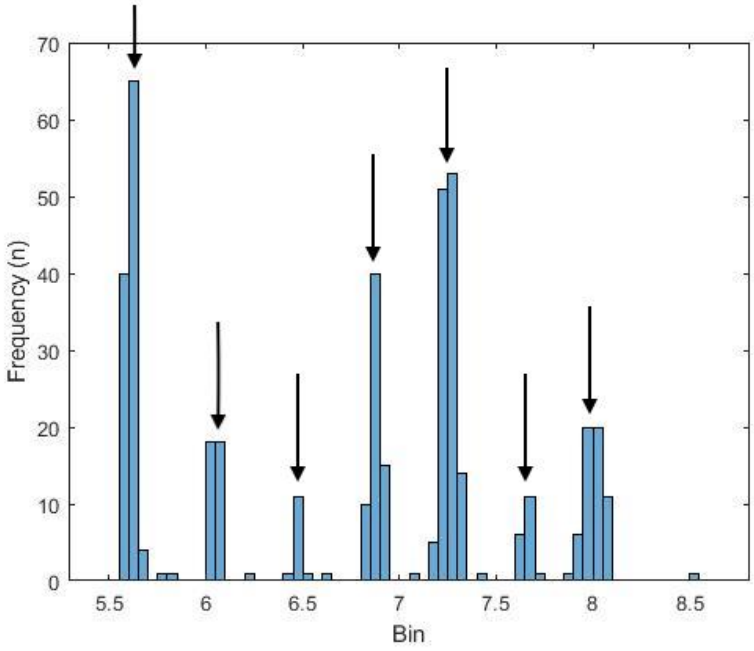

Figure 4.3.5: The histogram obtained from a single catheter. Note each dwell position is visible based on the clusters (indicated by the arrows).

Of the total 348 dwell positions across three runs, 21 returned zero counts for the frequency histogram. These points corresponded to dwell times of 0.2s or less.

Each of the coordinate positions across all catheters were compared to the TPS and a difference was obtained. These can be seen in Table 4.3.1. The average difference between TPS and measured coordinates for x, y, z and t were found to be (3.60±0.14)mm, (3.70±0.15)mm, (3.53±0.12)mm and (0.30±0.06)s respectively. The maximum difference for the x, y, z and t was found to be (11.42±0.4)mm, (18.02±0.4)mm, (10.07±0.4)mm and 15.3s respectively while the minimum difference for x, y, z and t was (0.02±0.4)mm, (0.03±0.4)mm,

(0.01±0.4)mm and 0s respectively.

Table 4.3.1: The average difference between TPS and MP measured dwell position.

	x (mm)	y (mm)	z (mm)	t (s)
Average Difference	3.60	3.70	3.53	0.30
Standard Error ±	0.14	0.15	0.12	0.06

Discussion

In this study, the feasibility of the MP987's use for source localisation in a clinical setting was proven. Typical dwell positions for real-time HDR procedures are 2mm-3mm. This was established to be the benchmark we hoped to attain. A complete clinical work flow was carried out on the E2E phantom with a 60cc Gel Prostate insert, from insertion of treatment catheters under US guidance to CT based treatment planning and afterloader delivery. Three separate treatment deliveries were carried out and the source position was evaluated at each dwell position and compared to the TPS plan. The overall average difference for the x, y, z and t components were (3.60±0.14)mm, (3.70±0.15)mm, (3.53±0.12)mm and (0.30±0.06)s respectively. The maximum difference for the x, y, z and t coordinates was found to be (11.42±0.4)mm, (18.02±0.4)mm, (10.07±0.4)mm and 15.3s respectively while the minimum difference for x, y, z and t was (0.02±0.4)mm, (0.03±0.4)mm, (0.01±0.4)mm and 0s respectively.

In previous MP tracking studies returned tracking capabilities of sum mm accuracy [64, 61, 60]. The accuracy obtained from these studies was not reproduced in the findings. However,

this is the first application of the MP system in phantom study in which the catheter placement is not well defined, which is also indicative of a clinical procedure. Furthermore, the accuracy of the system in measuring dwell times was (0.3±0.06)s, which indicate that the system is able to monitor the timing aspect of a typical clinical procedure with ease, as dwell timings range from 0.5s to 10s.

The positioning of the TRUS probe within the phantom was seen not to hinder any results. This is due to the large number of detectors.

One large contributing factor to the results obtained stem from the detector array itself. The tracking algorithm relies on a centre of mass calculation to determine x and y coordinates. The top 30% of the pixel responses are used in this calculation, utilising Equation 4.1. The accuracy of this calculation operates under the assumption that the detector has a uniform response directly under the source. If there are any irregularities in the pixel response, the distribution of the top 30% will not be uniform and so, the centre of mass calculation may not return a pixel from directly below the source, yielding inaccurate tracking. This was observed when the source was near any dead pixels; the response was not symmetric in shape, rather it was distorted around the location of the dead pixels. This can be seen in Figure 4.3.6.

This phenomena can also be observed when the source is located near the edge of the detector. To eliminate this issue, the tracking software must be further developed to eliminate/replace these dead pixels based on a relative response within a neighbourhood of pixels. As outlined in Section 4.2, each pixel could also be re-calibrated.

Another source of inaccuracy in source localisation using the MP987 system is the sensi-

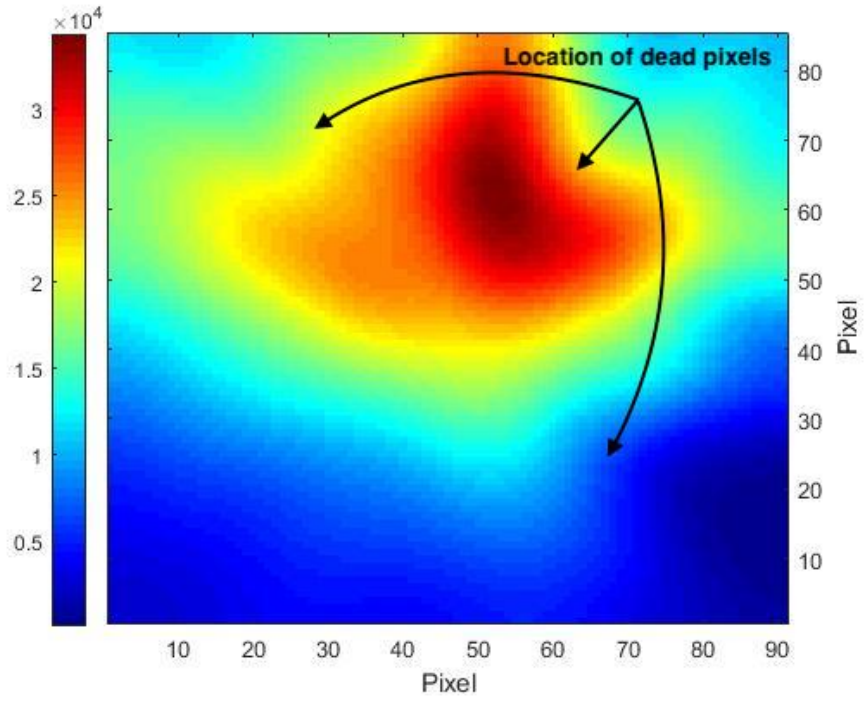

Figure 4.3.6: The colour map of the pixel responses highlighting the effect of dead pixels on the response.

tivity of the electronics to EMF and heat. It was found that any source of EM activity in the operating room caused there to be a significant degree of electronic noise which inhibited accurate localisation. Appropriate shielding in the form of aluminium plating was used which significantly reduced this noise, but a more permanent and robust solution is needed for future use.

4.4 Introduction of a clinically relevant error to test the capabilities of the Magic Plate 987.

In the previous study, the tracking capabilities of the MP987 system were quantified using a clinically relevant treatment plan. It was shown that the tracking system can achieve source localisation within 4mm for all coordinates. A clinically relevant error will be introduced and the systems ability to detect this error will be evaluated. By doing so, the feasibility of systems use as an *in-vivo* treatment verification tool can further be proven.

Method

The same experimental setup was used as in Section 4.3. The same 9 Gy treatment plan was also used. The clinically relevant error chosen to introduce to the system was a catheter swap: swapping of catheters 1 and 3. The reasoning behind this kind of error introduction was the clinical relevance associated with the user specificity of the task of connecting treatment catheters and transfer tubes.

Results

A single clinical procedure was carried out on the E2E phantom after catheter 1 and 3's transfer tubes were swapped. Like the previous study, the MP987 data was collected, decoded, interpolated and the tracking software was applied. The relative differences between

Table 4.4.1: The relative differences in MP measured positions with respect to TPS planned positions with the introduction of a catheter swap.

		Relative Difference (%)		
		x	y	z
Catheter 1	Dwell 7	16.5	-706.0	-8.8
	Dwell 6	45.6	47.1	-6.6
	Dwell 5	56.2	21.7	-6.2
	Dwell 4	61.2	12.7	-5.7
	Dwell 3	75.4	8.5	-3.2
	Dwell 2	82.2	6.4	-1.3
	Dwell 1	83.6	5.4	-1.1
Catheter 3	Dwell 7	-82.1	-69.4	5.9
	Dwell 6	-44.9	-103.1	6.6
	Dwell 5	-4.1	-319.8	7.9
	Dwell 4	16.8	241.6	8.6
	Dwell 3	32.7	59.7	9.4
	Dwell 2	40.0	22.8	9.8
	Dwell 1	39.3	6.8	10.1

the TPS and measured x, y, and z coordinates can be seen in Table 4.4.1.

The average difference in position for x, y and z coordinates for catheter 1 was (3.07±0.71)mm, (14.31±0.67)mm and (5.68±1.20)mm respectively. For catheter 3, the average difference in position for the x, y and z coordinate was (1.97±0.36)mm, (4.38±0.82)mm and (11.04±0.80)mm. The maximum difference in position for both catheters was 17.48mm with a minimum of 0.38mm.

Discussion

The purpose of this study was to verify if the MP987 and tracking software system was able to determine the introduction of a catheter swap. In order to successfully determine the existence of a catheter swap, the system should return a larger than normal difference in position compared to the TPS. When comparing catheter 1 and 3, which are they catheters

which were swapped prior to treatment, the differences in measured dwell position for each dwell position can be seen in Table 4.4.1.

No defined parameter was set in order to verify if a catheter swap was detected, however the average difference in each coordinate position does clearly indicate the misplacement of a catheter. There is a defined displacement for each dwell position with a corresponding dwell time. This data in itself can be used in the determination of a treatment error; a set difference in threshold could be defined before any intervention.

Further, the data collected from the misplaced catheter could be used retrospectively to determine which catheter it had been swapped with. The dwell position data can be cross-referenced with the TPS data to find a catheter which exhibits the smallest difference with it.

4.5 Conclusion

This chapter investigated the feasibility of the MP detector system for the use of HDR source localisation. The MP987 detector system coupled with the source tracking algorithm proved it's potential for use in HDR pBT source localisation. The E2E phantom, which is an anthropomorphic representation of prostate anatomy, allowed the detector system's abilities to be tested in a clinical setting.

Preliminary aspects of the MP system were evaluated for the plate, highlighting its design and software limitations. When conducting source localisation, the returned measured coordinates on average across all axis fell within 5mm. The introduction of a clinically relevant

error to the system highlighted the capabilities of the plate, with the catheter swap being evident. With some of the limitations of the current system addressed, further clinical testing will be rudimentary in the integration of the MP into a typical BT work flow.

Chapter 5

In-vivo treatment verification feasibility for the TRUSProbe Tracker combined with MO*Skin* dosimeters.

The need for a device which can perform accurate *in - vivo* treatment verification (IVTV) is apparent, as demonstrated in Chapter 2. Characteristics of HDR pBT, such as the high dose gradients as well as the ease of clinician error, exemplify the need of achieving accurate end-to-end IVTV [25, 5]. This chapter hopes to offer a novel means of both *in-vivo* dosimetry as well as source localisation within the one unit: the TRUSProbe Tracker. The End-to-end phantoms use as a tool for E2E studies was proven in Chapter 3 and so, will be used to provide a holistic QA tool in this study.

The development of an all-in-one system is built upon the work of earlier studies [69, 68, 46,

64] and hopes to incorporate the ability to both monitor rectal dose in real time as well provide accurate source localisation. The first half of the chapter hopes to perform preliminary source tracking tests to establish both the accuracy and characteristics of using dose rate information from MO*Skin* dosimeters inbuilt into the TRUSProbe Tracker. The second aim of this chapter is to achieve a high level of dosimetric accuracy. Similar rectal dose accuracies obtained by Carrara *et al* and Poder *et al* are hope to be replicated, as well as assessing the feasibility of real-time catheter-by-catheter dose monitoring and finally to test the ability of the system to detect a clinically relevant error.

5.1 Proposed Instrumentation

5.1.1 MO*Skin* Detectors

The MO*Skin* system developed by the Centre of Medical Radiation Physics (CMRP), University of Wollongong, Australia, is a MOSFET sensor packaged in a kapton strip with a gate oxide thickness of 0.55μm [65]. This can be seen in 5.1.1. Using 'drop in' technology, the system is hermetically sealed with a thin polyamide film. This film layer acts as a build-up layer for the MO*Skin* which equates to a water equivalent depth of 0.07mm in tissue [73]. This water equivalent depth can be varied based on this film layer. The measure of accumulated radiation dose involves the measurement of the voltage across the gate under a threshold voltage. Typically, the detector system is used for real-time *in-vivo* skin dose measurements.

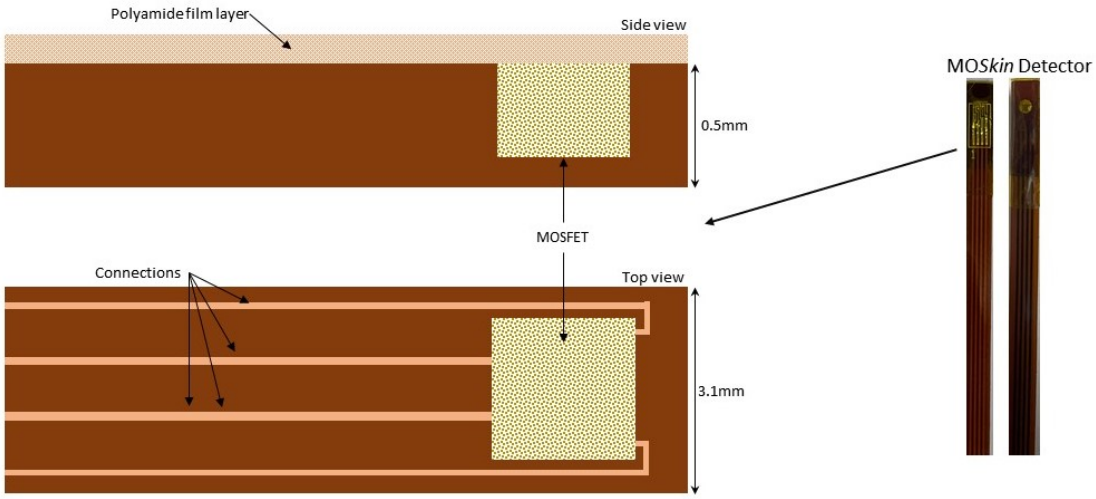

Figure 5.1.1: The schematics of a MO*Skin* dosimeter, with both the side view and the top view showing the polyamide build up layer as well as the connections on the kapton tail.

For the purpose of our experiments, the MO*Skin* dosimeters will be used to obtain a real-time readout of dose rate which will be used in an application of source tracking.

The dose data from each MO*Skin* dosimeter is managed using the OneTouch readout system. The system allows up to six dosimeters to be simultaneously read out in real-time and transferred wirelessly via bluetooth to a computer. The system also automatically compensates for any temperature variation in the output doses.

5.1.2 TRUSProbe Tracker

The TRUSProbe Tracker (TPT) is an original design which hopes to appease the need for *in-vivo* treatment verification by offering both verification of treatment delivered and quantifying patient dose. By using CAD software, a model of a BK-Medical trans-rectal ultrasound probe was created with 1:1 dimensions. This model can be seen in 5.1.2. In order

(a) The raw CAD drawings of the TRUSProbe Tracker and the three separate bodies that make up the probe.

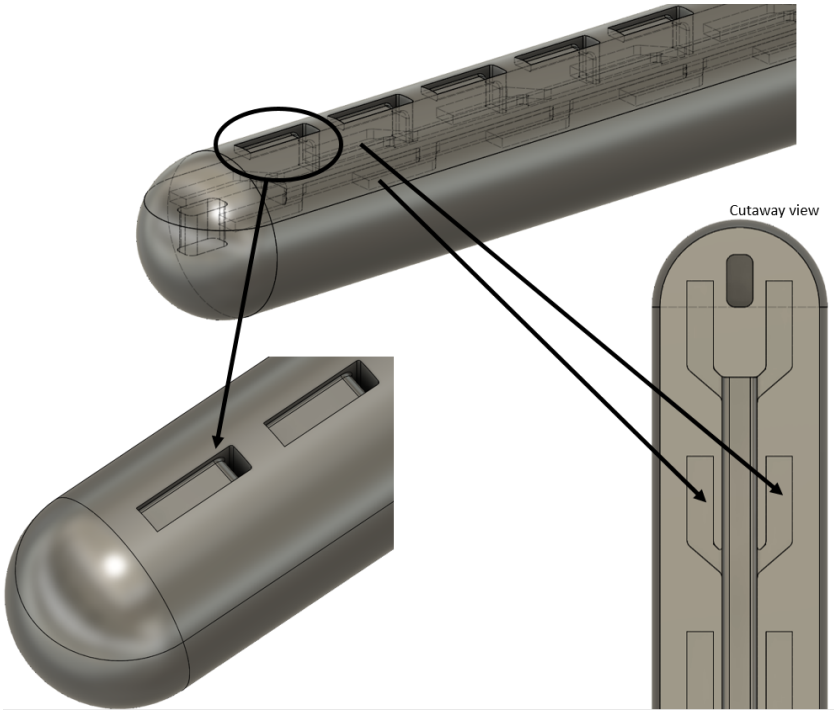

(b) A close up view of each of the slots for *in vivo* rectal dose measurements and slots for source tracking

Figure 5.1.2: Schematics of the TRUSProbe Tracker showing its design.

to facilitate *in-vivo* dose determination, there are five separate, embossed slots which run along the longitudinal direction of the TRUS probe designed specifically for MO*Skin* diodes. At the end of each slot is a channel which allows the kapton tail of the detector to feed into the central channel, which runs along the probe to the handle to allow cable connection. For treatment delivery verification, there are twelve slots in two rows, separated by 15mm. They are positioned on a plane 5mm below the top surface of the TRUS probe. The central channel, which runs the length of the probe, separates the rows.

5.1.3 Seed Position Algorithm

In order to obtain source coordinate data based on dose rate measurements, a source tracking algorithm was employed. The algorithm operates based on the method of simulated annealing which involves optimisation based on iterative improvement randomisation. Typically, an initial function is calculated at a random starting position. The function is then recalculated at a neighbouring position and compared to see if there is an improvement. If there is an improvement, that new position is then set. This iterative method is repeated until there is an optimisation in the solution [74].

The algorithm operates based on the following methodology:

- The locations of the virtual detectors were established. The activity of the source at the time of treatment is also input into the algorithm.
- The dose rate data for each detector is loaded into the algorithm.
- A virtual source is placed in the centre of the simulation. Based on this location, the

integral counts in each detector is calculated based on TG-43 formalism..

- An optimisation function is computed

$$F = \sum_{i=1}^{6} (I - V)^2 \tag{5.1}$$

Where I is the recorded integral counts, V is the virtual integral counts computed based on the virtual seed. The function is computed for all 6 detectors.

- The virtual seed is then repositioned systematically in three dimensions in 1mm step sizes. The integral counts based on this new position is then re-calculated in each dosimeter.

- Iteration is computed until F is minimised.

- 0.01mm steps are then used to further improve the accuracy of the seed positions.

Once computed, the locations of each source in each time iteration is known.

5.2 Initial source tracking feasibility for the use of MO*Skin* dosimeters coupled to the TRUSProbe Tracker

In order to proceed with further source delivery verification studies, it is first required to prove the feasibility of the TRUSProbe Tracker and MO*Skin* systems ability to perform *in-vivo* source position verification. To validate some level of source tracking ability, the system must be able to perform the following task; By using the dose rate data from each of the

individual MO*Skin* dosimeters, the source location along the axis of the TRUS probe can be quantified. At the successful completion of this task, further source tracking testing will performed using the tracking algorithm.

Method

The TRUSProbe Tracker is used in conjunction with MO*Skin* dosimeters to allow for preliminary tracking to be tested. Six dosimeters were arranged in an alternating fashion inside of the TRUSProbe Tracker, as shown in Figure 5.2.1.

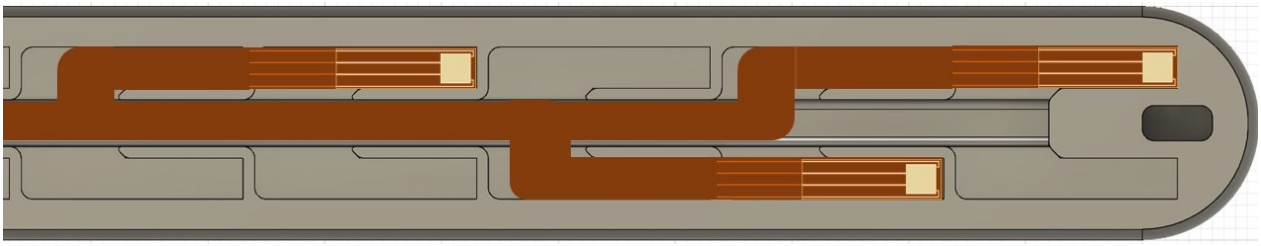

Figure 5.2.1: A schematic of the TRUSProbe Tracker with the individual MO*Skins* arranged in their alternating fashion.

The setup was placed in a specially designed holder, which accommodated the probe whilst also providing a surface for solid water to be placed. A slab of perspex with channels the size of treatment catheters was used to ensure consistency and to maintain a straight path for the source to traverse. Two treatment catheters were used; one directly above the centre of the probe and one offset 2cm to the right. The experimental setup can be seen in Figure 5.2.2. A QA plan with 5mm steps and a 5 second dwell time was chosen for both catheters. The SSD for the treatment was 17.15mm, and was kept constant throughout the treatment.

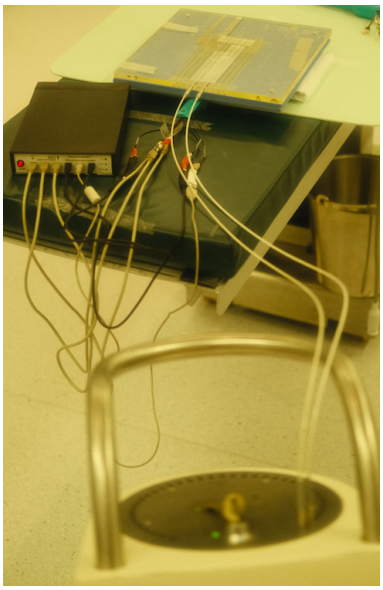

(a) The experimental setup, showing the afterloader in the foreground connected to the TRUSProbe Tracker. The OneTouch readout system can be seen connected.

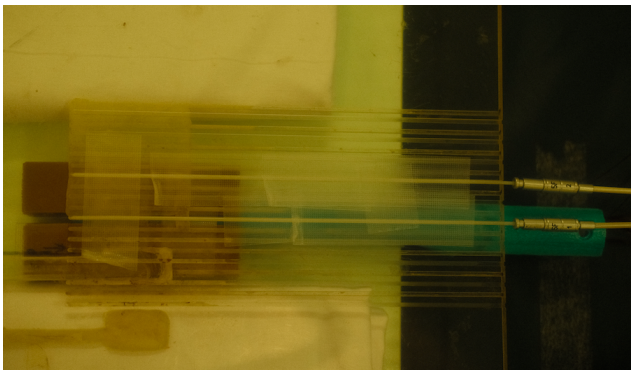

(b) A overhead view of the catheters above the TRUSProbe Tracker.

Figure 5.2.2: An overview of the initial tracking feasibility for the TRUSProbe Tracker.

The dose-rate delivered to each of the 6 MO*Skin* dosimeters was monitored in real-time using the OneTouch readout system.

In order to validate the systems ability to track a HDR source, the coordinate system of the probe needed to be established. In keeping with the convention of the source tracking code, the z axis is defined along the direct of the probe, the y axis pointing vertical and the x axis horizontal. The origin of the coordinate system is defined by the plane of the detectors.

Results

During the course of the study, all six MO*Skin* dosimeters returned usable dose rate values. A total of 357 data entries were taken for six separate dosimeters throughout the entire proce-

dure, with a maximum dose rate returning 3.58 $cGys^{-1}$ and a minimum value of -0.54$cGys^{-1}$. The average dosimeter response was 0.39$cGys^{-1}$ with a standard deviation of $\pm$0.58$cGys^{-1}$. The initial qualitative feasibility of the TRUSProbe Tracker's ability to perform source tracking was evaluated by comparing the dose rates for each dosimeter. It is expected that the dose rate will give a clear indication of the location of the HDR source along the z axis; an increase in dose rate corresponds to the source being located in close proximity. As the source travels towards the tip of the probe, each dosimeter's dose rate will increase momentarily, and then decrease when the source passes. The results comparing the dose rates for each dosimeter can be seen in Figure 5.2.3.

In order to quantify the feasibility of using dose rates to achieve source localisation, as well as to establish a baseline accuracy, the z positions of each dosimeter will be compared based on their known fixed differences. Using the assumption of the maximum dose rate being an indication of the source dwelling directly above the dosimeter, each time stamp corresponding to the maximum value was noted. Using these values, as well as the fact that each 5s dwell position is separated by 5mm, the difference between each dosimeter can be evaluated. These values can be seen in Table 5.2.1.

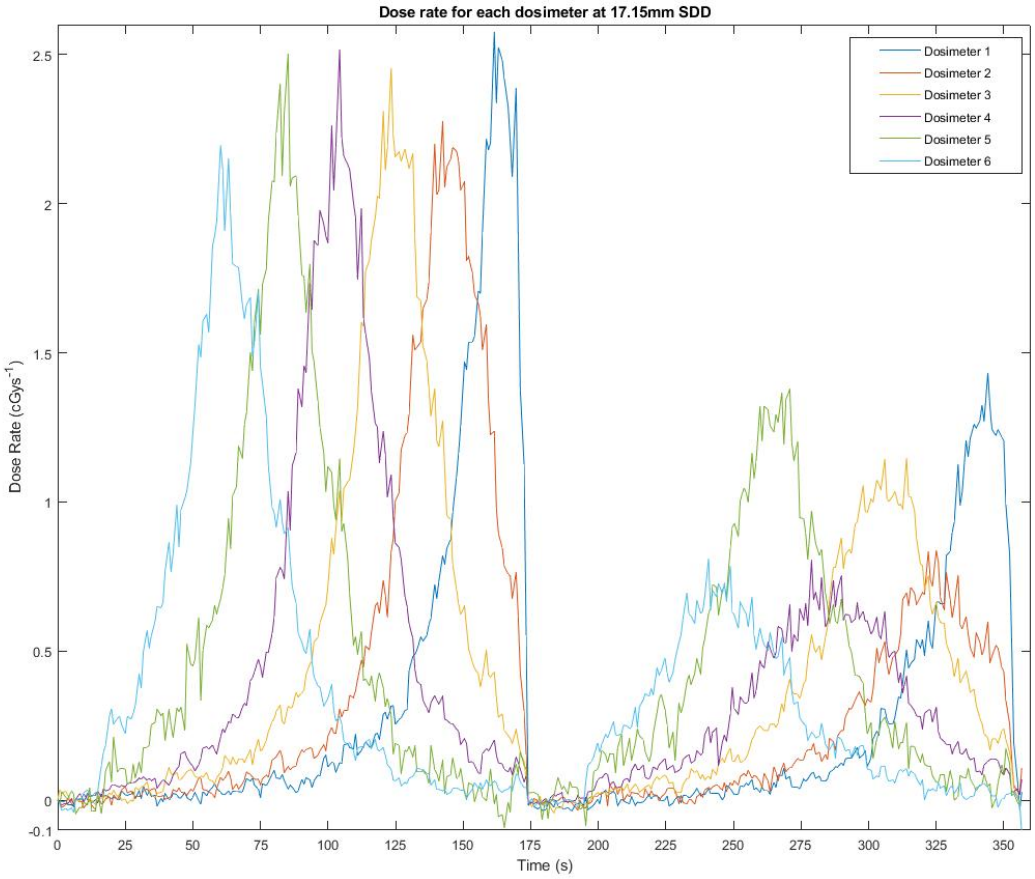

Figure 5.2.3: A comparison of the dose rate of each MO*Skin* dosimeter as the HDR source steps along the z axis of the probe. Note the two different catheters, the first directly above the probe and the second offset by 2cm.

Table 5.2.1: Relative differences in timing of maximum dose rates.

	D1	D2	D3	D4	D5	D6
Time of Maximum (s)	165.231	146.127	129.987	102.891	83.055	58.826
Time Between Successive Dosimeter (s)	-	19.104	16.14	27.096	19.836	24.229
Relative Difference (%)	-	-4.6	23.9	26.2	-0.83	17.4

The next step in investigating the source tracking feasibility of the TRUSProbe Tracker system is to evaluate source positions in space using the source tracking algorithm. The source strength at the time of treatment was used in the algorithm. The output of the x, y, and z positions with respect to time can be seen in Figures 5.2.4, 5.2.5 and 5.2.6 respectively.

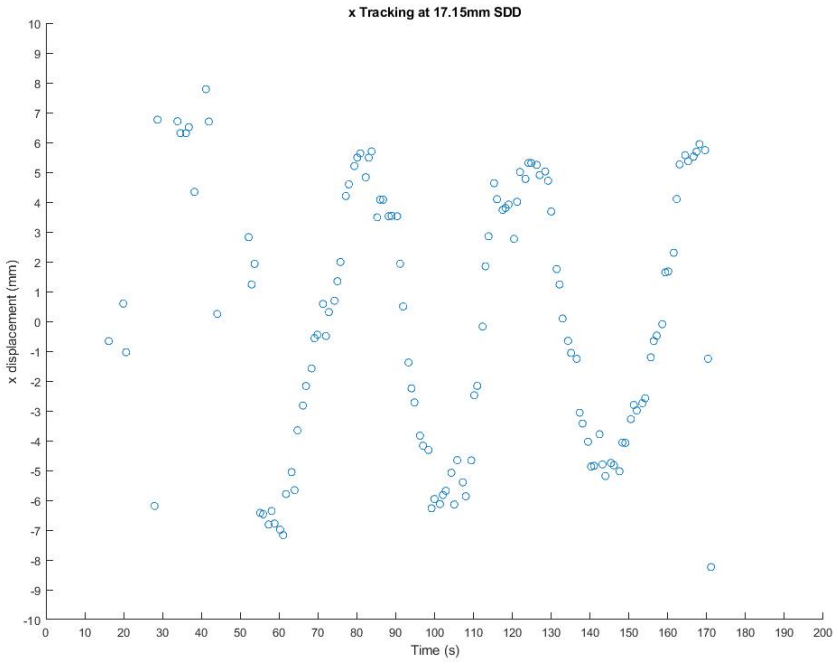

Figure 5.2.4: Source positioning algorithm returning x positions against time.

Starting with the x tracking, it can be seen from Figure 5.2.4 that there exists a regular oscillation in position either side of the mid line. The turning points of this oscillations were investigated in order to determine if they coincide with the positions of the dosimeters. Due to the 5mm step size and 5s dwell time of the treatment as well as the known (20mm) z separation of each dosimeter, the time between the source being at its closest point to a dosimeter (i.e above) is 20 seconds. The time at which each turning point occurs is shown in Table 5.2.2.

Table 5.2.2: x axis Turning points of the source tracking data.

Turning Point Number	1	2	3	4	5	6
Time of Turning Point (s)	58.8	80.9	101.4	124.9	143.9	168.2
Error (s)	±5					

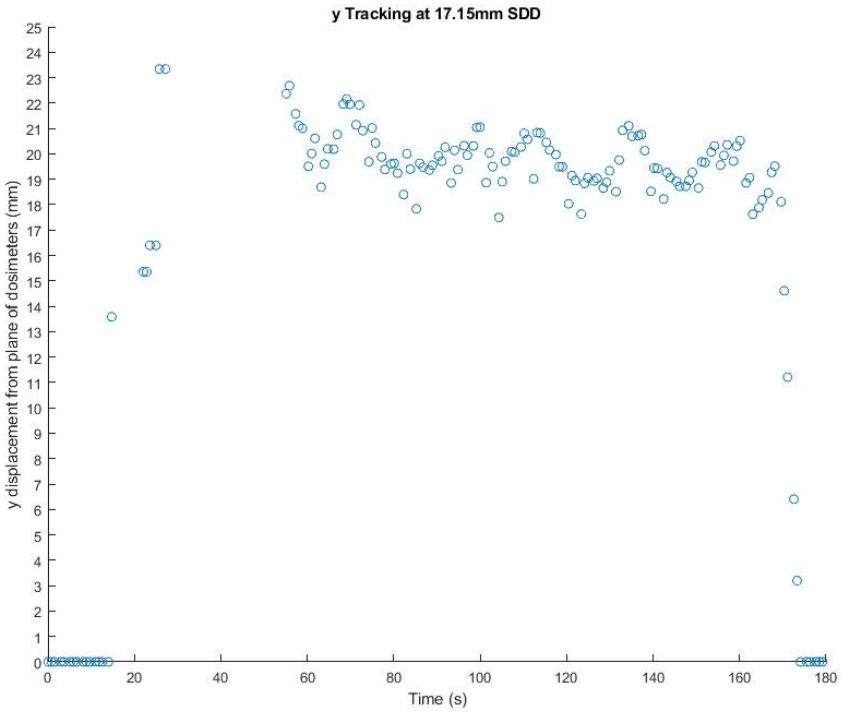

Figure 5.2.5: Source positioning algorithm returning y positions against time.

When investigating the y tracking data, as shown in Figure 5.2.5, the oscillating nature seen in the x tracking is observed. The y separation of the catheter and the plane of the dosimeters is 17.15mm. The average y separation from the tracking data was found to be (19.6±3.3)mm.

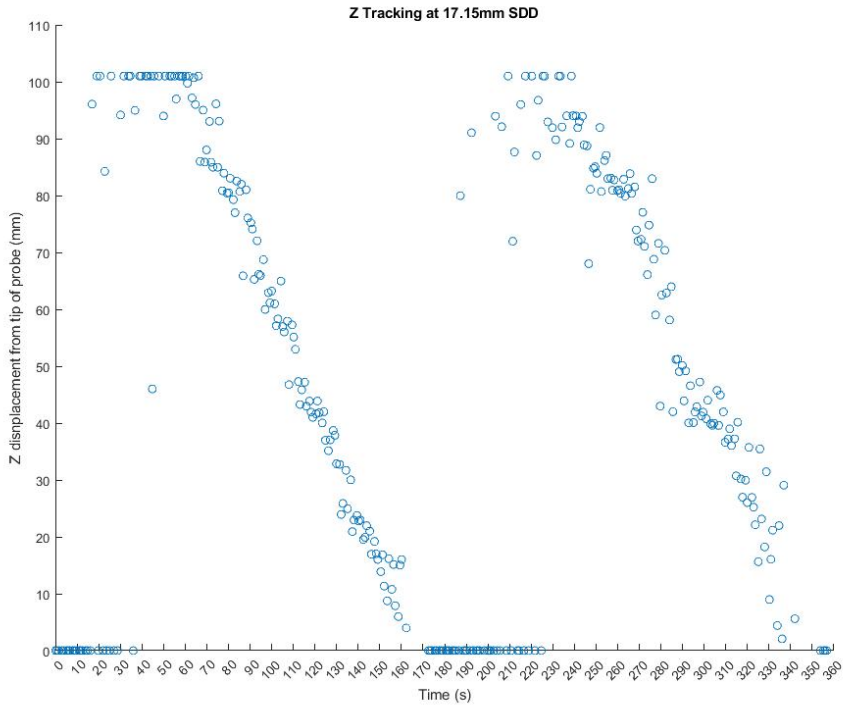

Figure 5.2.6: Source positioning algorithm returning z positions against time.

The z tracking data can be seen in Figure 5.2.6. As expected, the z tracking data returned a straight line. Individual dwell positions however cannot be distinguished. Based on the treatment parameters, it is expected that it would take twenty 5mm-steps to travel from the first dosimeter to the last. At 5 seconds per dwell position this equates to 100 seconds. From the tracking data, it can be seen that to travel the 10cm, it has calculated it to take (101.3±4)s.

Discussion

To validate the feasibility of using MO*Skin* dosimeters inside of the TRUSProbe tracker as a tool for source position verification, the dose rate from six dosimeters were recorded. It was hypothesised that the position of the HDR source along the z axis could be determined based on the dose rates of each dosimeter; a maximum dose rate in any dosimeter corresponds to a minimum in distance between it and the HDR source.

A single catheter was placed above the TRUSProbe and a QA plan of 5mm, 5s dwell times was carried out on the system. The dose rates obtained can be seen in Figure 5.2.3. Qualitatively, it can be seen that the dose rates for each successive dosimeter increase to a point, followed by a decrease back to a low baseline value. This is an indication showing when the source is directly above. Further, it is expected that dosimeter 6, which is located at the furthest point back from the tip, would see this peak first as the afterloader delivers the seed in steps toward the tip. By this logic dosimeter 1 which is closest to the tip, would also display this peak last. The dose rate curves for each dosimeter indicate this logic; dosimeter 6 shows the first peak at t≈60s and dosimeter shows its peak at t≈165s.

The dose rate data obtained clearly indicates that the premise behind source tracking along a single axis has merit. To quantitatively prove this relationship between dose rate peaks and z axis position, the timing between successive peaks was measured. The results can be seen in Table 5.2.1. The smallest relative difference between dosimeters was found to be -0.83%, with the largest being 26.2%. The differences in relative difference can be attributed to the temporal resolution of the MO*Skin* dosimeters; the OneTouch system allows direct

read out of dose data every 1 second. The peaks which are associated with the source being the closest to the dosimeter do not have a narrow peak; the maximum can be seen to spread over ≈10 seconds. Furthermore, taking into account the findings of Jong *et al*'s 2014 study, the angular dependence of surface dose deviates based on any oblique incidence [73]. Because the dosimeters are not directly below the source, there may be some introduced angle for which the value is not known.

Despite the obtained relative difference having a standard deviation of 17.57%, the obtained results still prove to be useful in the determination of the location of the HDR source along the z axis.

The next step in determining the feasibility of the systems source tracking ability is evaluating the performance of the source tracking software. The x, y and z location data with respect to time is seen in Figure 5.2.4, 5.2.5 and 5.2.6 respectively.

The obtained x position data can be seen to oscillate in a regular fashion. The turning points of these oscillations were investigated and the time of each turning point can be seen in Table 5.2.2. Each successive turning point can be seen to occur approximately every 20 seconds, which is the locations of the dosimeters based on QA plan used.

The y source position data also exhibits this oscillation. The y coordinates should have returned as a horizontal line, as there was no deviation in the y axis. When averaging the y points, the returned value was (19.6±3.3)mm, while the expected y was 17.15mm.

The oscillation observed in both the x and y axis can be attributed to the limitations of the MO*Skin* dosimeter; the angular dependence on the measurements is evident in the obtained data. The changing in angels between the source and each dosimeter based on its relative

position in space has a great influence on the dose measurements.

The z source position data returned considerably consistent data. The returned z positions are linear in nature, with a constant gradient. Individual dwell positions cannot be determined however. To quantify the source position data, the time taken to travel from the first dosimeter to the last was determined. To travel the 10cm, the algorithm values returned a timing of (101.3±4)s. This is consistent with the expected timing of 100s.

5.3 Evaluation of the Source Tracking limitations of the TRUSProbe Tracker system with varying SDD.

In the previous study, it was demonstrated that preliminary tracking can be achieved using the TRUSProbe Tracker and MO*Skin* dosimeters. The next step in the commissioning of the tracking system is to quantify the effect on its ability to track a source with varying SDD. At the completion of this study, it is hoped to quantify the relationship between SDD and tracking capabilities.

Method

Similarly to the previous study, the same configuration of MO*Skin* dosimeters used in an alternating fashion inside of the TRUSProbe Tracker was used. The probe was placed in the same holder with the catheter perspex holder above. The same QA plan of 5mm step sizes

and 5 second dwell times was used. MO*Skin* data was collected in real time. Solid water was added in between measurements to change the SDD. Data was collected at 17.15mm, 21.15mm, 26.15mm, 31.15mm, 36.15mm, 41.15mm and 51.15mm SDD.

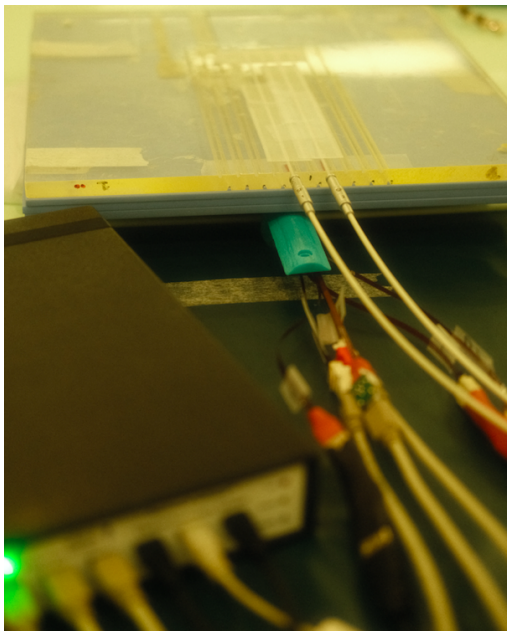

Figure 5.3.1: The TRUSProbe Tracker with solid water pieces on top. The two treatment catheters can be seen above.

Results

For each SDD, all of the six dosimeters returned usable dose rate values. These dose rate values were used in the tracking software to return source positions. Due to the findings in the previous study, x positions were neglected and not compared. In order to obtain a quantifiable effect of the SDD on tracking capability, both the z and y components were compared separately.

Similarly to the previous study, based on the treatment parameters the time taken for the source to travel the length of the probe can be compared at each SDD to quantify any vari-

ations for the z positions. Qualitatively, from Figure 5.3.2 it can be seen that as the SDD increases, the linearity of the output decreases. Quantitatively, the difference in time taken to travel the 10cm is compared in Table 5.3.1.

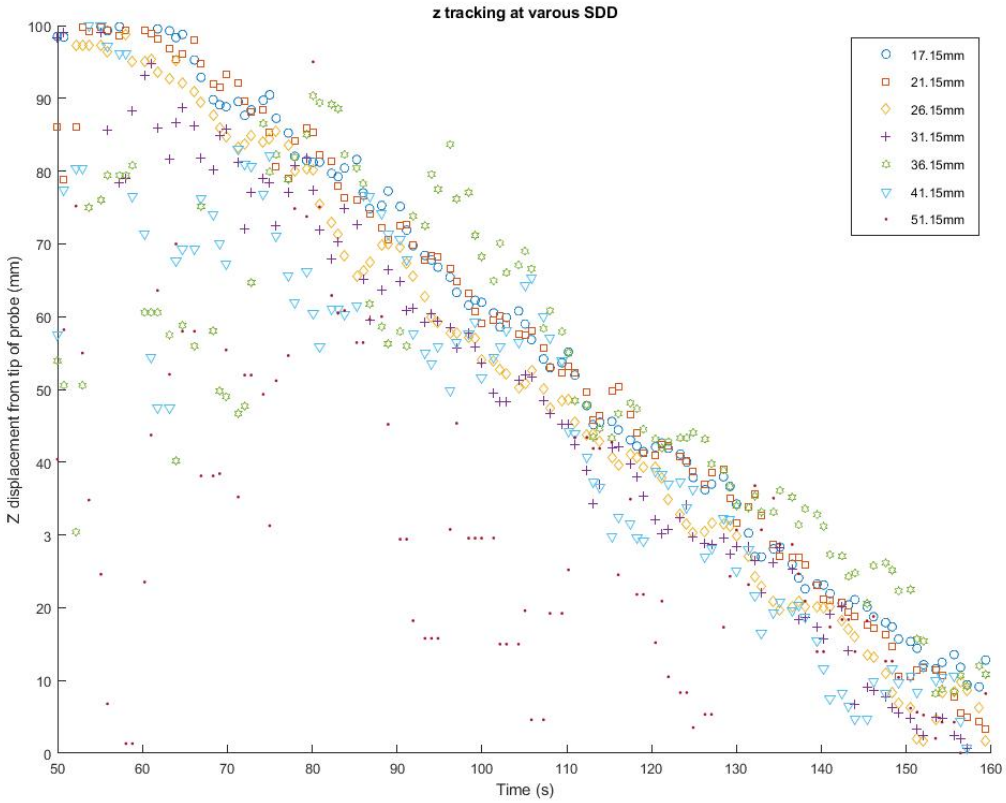

Figure 5.3.2: Source positioning algorithm returning y positions against time.

Table 5.3.1: A comparison of the time taken to travel 100mm across each SDD.

SDD(mm)	17.15	21.15	26.15	31.15	36.15	41.15	51.15
Time Taken (s)	101.28	100.5	102.0	110.1	113.7	121.8	130.6
Error (s)	4	5	9	13	15	19	22
Relative Difference (%)	1.3	0.5	1.9	9.1	12.1	17.9	23.5

Table 5.3.2: A comparison of the average y value for various SDD.

SDD (mm)	17.15	21.15	26.15	31.15	36.15	41.15	51.15
Average y (mm)	19.6	24.2	29.6	34.6	40.0	45.2	50.1
Error(mm)	3.4	1.9	2.8	4.7	9.0	8.8	12.1
Relative Difference(%)	12.6	12.5	11.8	10.0	11.5	9.0	0.8

For each SDD, the average y value was calculated with its associated error to quantify any relation to SDD. The results can be seen in Table 5.3.2. Qualitatively, Figure 5.3.3 shows clearly as SDD increases so too does the y coordinate, as expected.

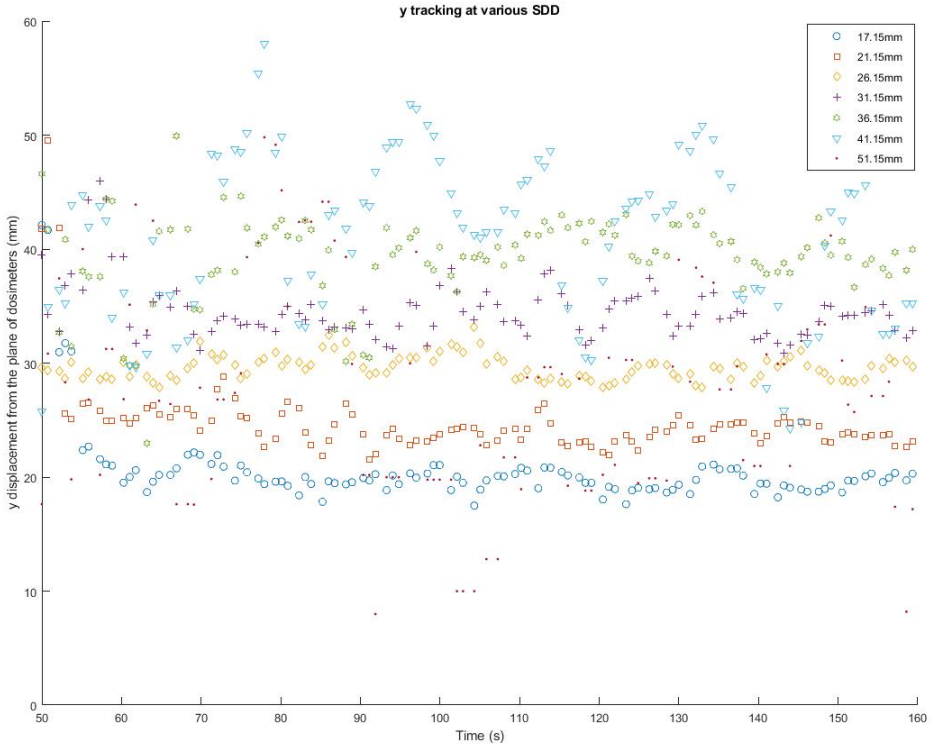

Figure 5.3.3: Source positioning algorithm returning y positions against time.

Discussion

Through the completion of this study, a relationship between the SDD and the tracking capabilities was hoped to be achieved. Measurements were taken for SDDs of 17.15mm, 21.15mm, 26.15mm, 31.15mm, 36.16mm, 41.15mm and 51.15mm. Due to the poor tracking ability in the x, only the y and z axis were considered.

By observing Figure 5.3.2, it can be seen that as SDD increases, the returned z coordinates loses it's linearity. For SDDs of 17.15mm, 21.15mm and 26.15mm, there exists a consistent linearity in z position which indicates accurate tracking due. At SDD of 31.15mm, the increase in deviation from this linear trend is started to be observed. This trend of declining linearity with increasing SDD continues, with SDD of 51.5mm showing little to no linear trend.

In order to quantify the relationship between each SDD and the z coordinates, the time taken for the source to travel the length of the probe was compared at each SDD. These values can be seen in Table 5.3.1. The relative difference was calculated for each SDD, with the smallest being 1.3% and the largest being 23.5%. The relative difference at each SDD can be seen to follow a trend; as SDD increases, so too does the relative difference.

This trend can be attributed to the dose rate detected at these depths. At a SDD of 51.15mm, the maximum dose rate across all dosimeters was 0.718cGys^{-1} while at SDD of 17.15mm the maximum dose rate was 3.58cGys^{-1}. The source tracking algorithm, as explained in section 5.1.3, calculates a radial distances based on the dose rate. A lower dose rate corresponds to a larger radial distance, in accordance to TG43 [20].

For the y coordinates, the effect from varying SDD can be seen in Figure 5.3.3. Similarly to the z tracking, there exists a consistent linearity for SDD values of 17.15mm, 21.15mm and 26.15mm. At SDD of 31.15mm and 36.15mm, this linear trend looses its consistency, with a larger variation in y values. At SDD of 41.15mm and 51.15mm, the linear trend is lost.

To quantify the accuracy of the y tracking at various SDDs, the average y value was calculated, along with its relative difference. These values can be seen in Table 5.3.2. The largest relative difference can be observed for SDD 17.15mm of 12.6% while the lowest relative difference was observed for SDD 51.15mm of 0.8%. Despite SDD 51.15mm having the lowest relative difference, it had the largest standard deviation of ±12.1mm. One possible explanation for this is the reduction in the occurrence of lower value dose rate fluctuations. This fluctuations in dose rate can provide incorrect radial dose calculations in the algorithm; the reduction of these calculations leave only the true radial distance values and hence, a more correct y value.

5.4 Determining the x-axis limitations of the MO*Skin* dosimeters for HDR tracking

In the assessment of the feasibility of the TRUSProbe Tracker's source tracking ability, it has been shown that for sources directly above the probe preliminary tracking can be achieved. However, the systems x axis limitations need to be evaluated. It is hoped that a FOV in the

x direction will be established as well as a quantitative evaluation of the effect of varying x.

Method

The same TRUSProbe and MO*Skin* configuration as previous studies was used. The 5mm step size and 5 second dwell time QA plan was also used. In order to evaluate the systems performance in the x axis, two experimental configurations were used: Two catheters running along the z axis of the probe, one directly above the probe and one 2cm to the right at 17.15mm SDD followed by two catheters with the same separation running perpendicularly (along the x axis) to the probe at 17.15mm SDD. This is shown in Figure 5.4.1.

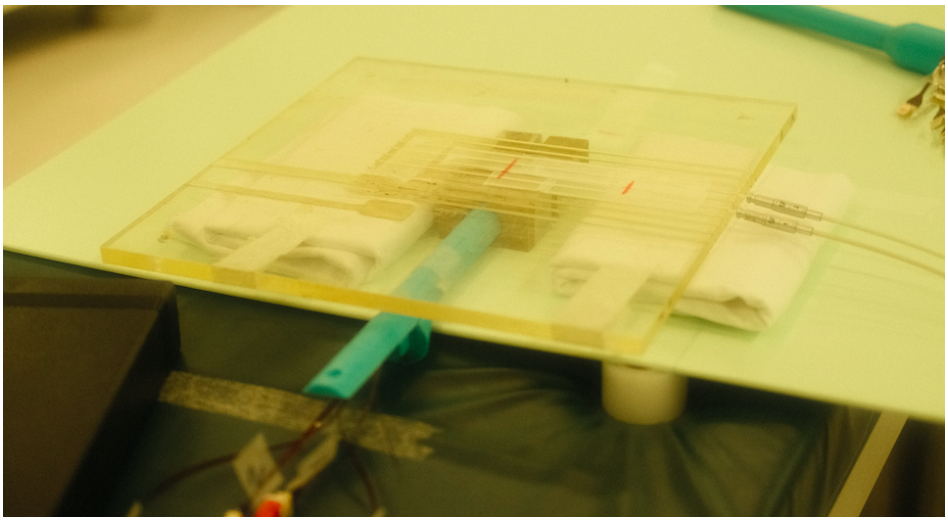

Figure 5.4.1: Source positioning algorithm returning x positions against time with catheters travelling across the TRUSProbe Tracker.

Results

The dose rate values at a SDD of 17.15mm, with two treatment catheters travelling along the z plane can be seen in Figure 5.2.3 from Section 5.2. Qualitatively, it can be seen that there exists a clear difference in dose rate values from the catheter above and the catheter to the right. Quantitatively, the average dose rate for the catheter above the probe was 0.513cGys^{-1} with a standard deviation of 0.721 cGys^{-1} and a maximum value of 3.585 cGys^{-1}. The catheter 2cm to the right returned an average of 0.319cGys^{-1} with a standard deviation of 0.387cGys^{-1} and a maximum value of 2.181cGys^{-1}.

Adopting the similar principal as in Section 5.2, the time of the maximum dose rate for each dosimeter was noted. The values as well as their relative differences to the expected timing can be seen in Table 5.4.1.

Table 5.4.1: Relative differences in timing of maximum dose rates for catheter 2 cm to the right of the central z axis.

	D1	D2	D3	D4	D5	D6
Time of Maximum (s)	342.71	330.92	315.55	280.40	271.60	238.61
Time Between Successive Dosimeter (s)	-	11.79	15.38	35.15	8.80	32.99
Relative Difference (%)	-	-69.6	-30.2	43.1	-127.2	39.4

The next step in evaluating the systems x axis tracking involved rotating the two treatment catheters 90^{o} such that they travelled across the TRUSProbe Tracker. The x, y and z tracking

coordinates can be seen for the two treatment catheters in Figures 5.4.2, 5.4.3 and 5.4.4.

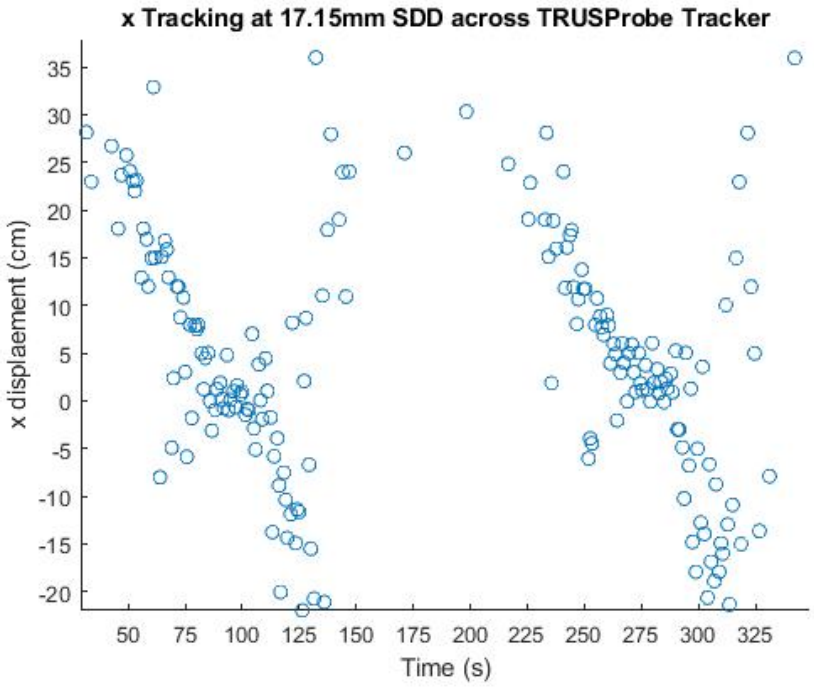

Figure 5.4.2: Source positioning algorithm returning x positions against time with catheters travelling across the TRUSProbe Tracker.

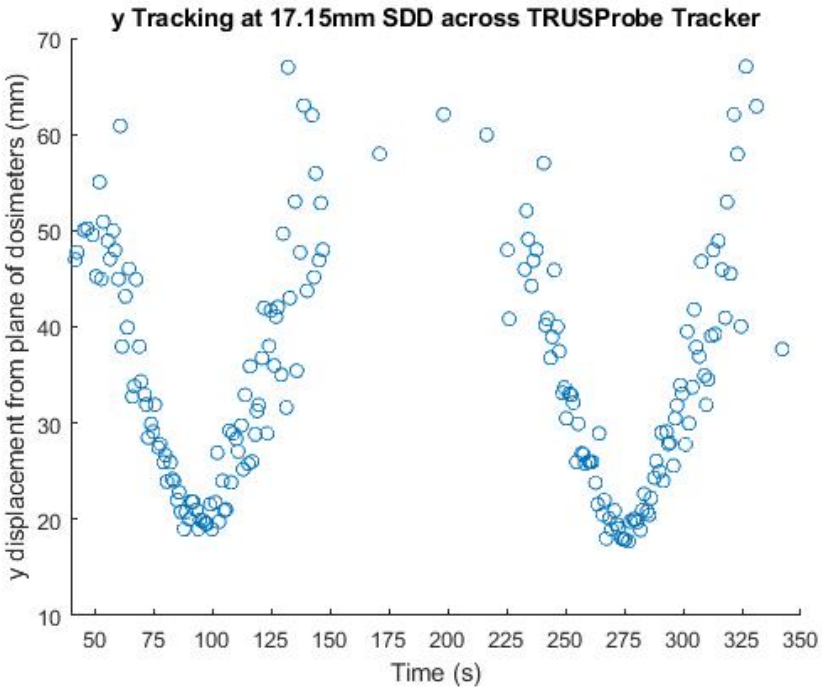

Figure 5.4.3: Source positioning algorithm returning y positions against time with catheters travelling across the TRUSProbe Tracker.

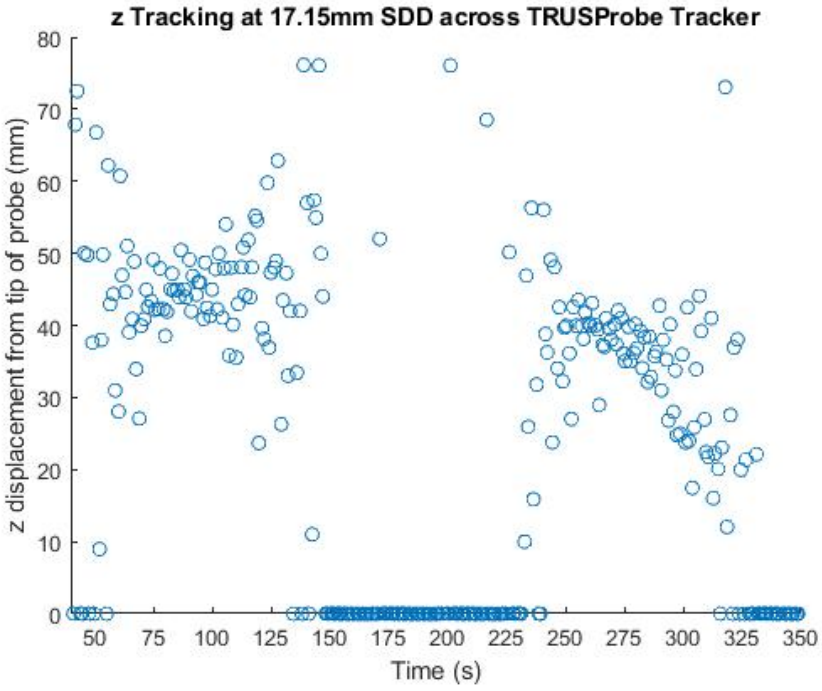

Figure 5.4.4: Source positioning algorithm returning z positions against time with catheters travelling across the TRUSProbe Tracker.

Discussion

The purpose of this study was to investigate the x axis limitations of the TRUSProbe Tracker system. Measurements were taken at 17.15mm SDD, both along the axis of the probe and perpendicularly.

The dose rates for the catheter directly above the dosimeters and the catheter 2cm to the right can be seen in Figure 5.2.3. The catheter which is directly above the probe is treated first, followed by the second catheter. From the dose rate comparison, it is clearly evident that there is a reduction in dose rate for the catheter off centre. The maximum dose rate observed for first catheter was 3.585 $cGys^{-1}$ compared to 2.181$cGys^{-1}$ for the second. Further, the overall average dose rate for the first catheter was 0.513$cGys^{-1}$ with a standard deviation of 0.721 $cGys^{-1}$ and 0.319$cGys^{-1}$ with a standard deviation of 0.387$cGys^{-1}$ for the second. Despite there only being a 2cm difference, this corresponded to a 55% reduction in dose rate. Further quantitative analysis was applied to the timing between each dosimeter, similarly to Section 5.2. The results are listed in Table 5.4.1. The maximum relative difference obtained was 43.1% with a minimum of -127.2%. This is significantly larger than those obtained for the catheter directly above (Table 5.2.1).

The catheters were rotated 90^{o} and the tracking algorithm was applied to the dose rate data. The x, y and z tracking coordinates can be seen in Figures 5.4.2, 5.4.3 and 5.4.4.

Across all three figures, there exists a high degree of over estimation. For the y, there was no variation across the treatment however it can be seen that there is a parabola-type response, with the vertex corresponding to directly over the probe. The z coordinates returned similar

results, with somewhat expected results for a small region above the probe and then a high degree of misrepresentation.

The presence of these over estimation data points may have been the result of the way in which the algorithm obtains radial distance; a lower dose rate corresponds to a large radial distance. This explains why we have the parabola-type response for the y coordinates.

The limitations of the MO*Skin* dosimeters also contribute to the results obtained. As a result of the large angles associated with the measurements, the angular dependence of the dosimeters may have also caused incorrect dose rate measurements for those points laterally further from the probe. Furthermore, the spacing between the dosimeters has an effect on the accuracy performance; by using a probe with detectors further apart it is expected that the accuracy would increase

5.5 Testing the limitations of the TRUSProbe Tracker with varying step sizes

The final test in investigating the feasibility of the TRUSProbe Tracker and MO*Skin* system for HDR source tracking is determining if the system can distinguish between different step sizes. In order for the system to be used in clinical applications, the system must be able to differentiate between different step sizes.

Method

The same experimental configuration as previous tests was used, which can be seen in Figure 5.2.2. SDDs of 17.15mm and 37.15mm were chosen. A QA plan of 5s dwell time was used. In order to test the systems ability to distinguish between dwell steps of different sizes, the dwell step sizes were chosen to be 2mm, 5mm and 10mm in a repeating pattern.

Results

The varying step size QA plan was delivered at both 17.15mm and 37.15mm. Dose rate data was collected for all six dosimeters and was used in the tracking software. The y coordinates were neglected due to their independence from varying step size and the x coordinates were neglected due to the limit accuracy of these values as found in the previous study.

The z coordinates for each SDD can be seen in Figure 5.5.1. It can be observed that there exists regular ≈10mm steps across the 17.15mm z coordinate data. However, these same steps cannot be resolved in the 37.15mm SDD. The 2mm and 5mm step sizes were not observed.

Discussion

A qualitative study investigating various step sizes was conducted at two different SDDs. The z coordinates were only taken into consideration. Qualitatively, from Figure 5.5.1 the 10mm step size can be seen. From the plan, these steps occur every 15 seconds. This corresponds to

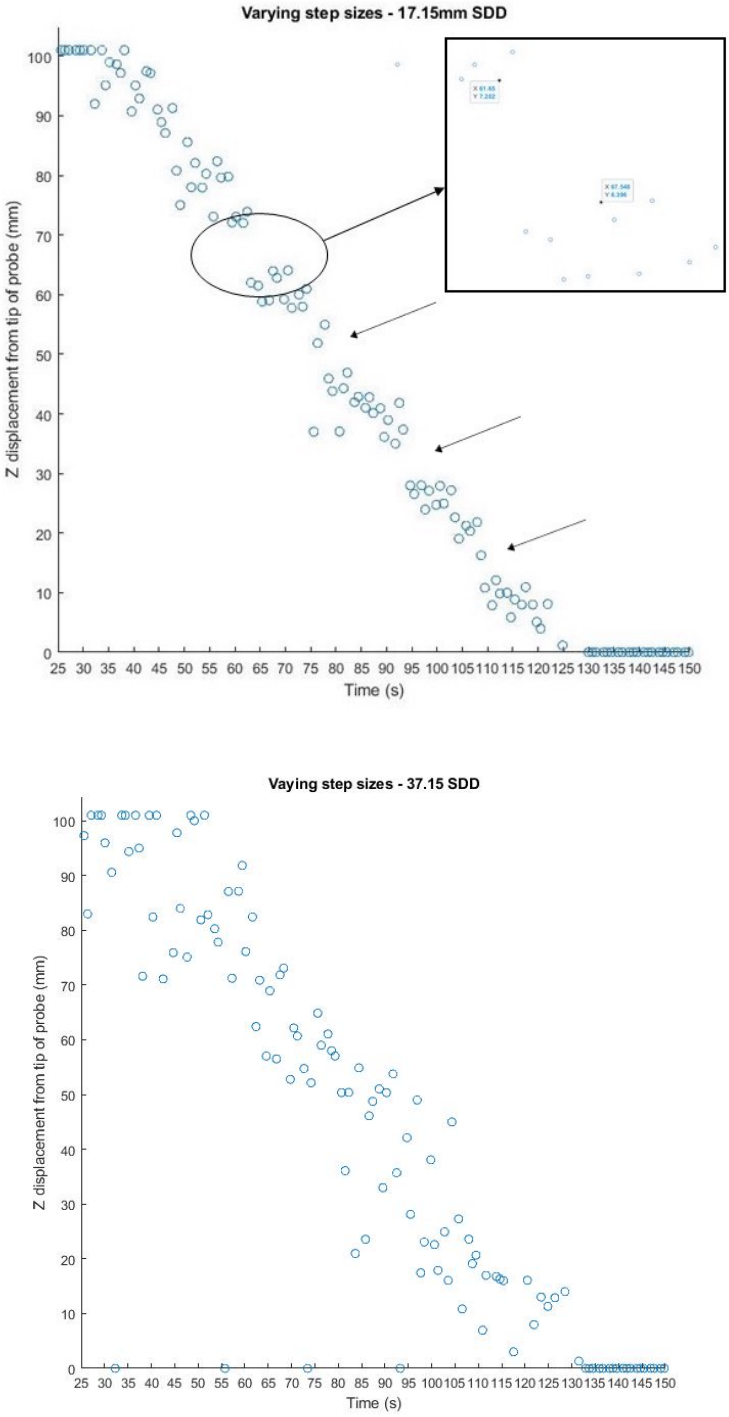

Figure 5.5.1: Varying step sizes at 17.15mm SDD and 37.15mm SDD

the observed pattern. The exact timing of these individual step sizes cannot be determined due to the spread of the data. Both the 2mm and 5mm step size cannot be distinguished. The inability to observe these steps sizes is likely due to the characteristics of the MO*Skin* dosimeters; a low temporal resolution combined with an angular dependence. The system cannot differentiate points if they occur within 10mm. Further, there exists a characteristic fluctuation in dose values obtained. Due to this fluctuation, the system is not able to resolve the smaller step sizes.

5.6 Feasibility for *In-vivo* rectal wall dosimetry using MO*Skin* dosimeters coupled with the TRUSProbe Tracker

Previously in this chapter, the use of the TRUSProbe Tracker in verification of treatment delivery by means of preliminary HDR BT source tracking was proven. In order to quantify the TRUSProbe Tracker's ability in performing IVTV during TRUS based HDR BT, the dose delivered to at risk organs must be verified.

This study hopes to achieve three objectives. The first is to verify findings from both Poder *et al* and Carrara *et al* in their previous rectal wall dose studies [67, 68, 69]. These studies both set out to quantify the differences between MO*Skin* dose measurements and the doses calculated on the pre-treatment plan. Secondly, it is hoped to perform catheter-by-catheter dose analysis to examine the feasibility of real-time measurement. Finally, a clinically relevant

error will be introduced and the systems ability to verify this error will be evaluated.

Method

The End-to-end phantom was used in conjunction with a 60cc Gel Prostate insert in this study. This provided an anthropomorphic phantom which allowed a complete HDR pBT treatment to be planed and delivered as per clinical procedure. Prior to the study, 5 MO*Skins* were placed longitudinally on the TRUSProbe Tracker, each with 15mm spacing in between. Due to the small rectal hole used in the E2E phantom, a endorectal balloon was not used. However, a condom was placed over the probe in order to protect the dosimeters (Figure 5.6.1).

Twenty treatment catheters were inserted under US guidance. A US based plan was not able to generated due to artefacts caused by the treatment catheters. The base of the prostate was chosen as a reference point to line up the first MO*Skin* dosimeter. A 120keV 50mA CT was acquired and a treatment plan was generated. A 9 Gy per fraction prescription was chosen after contouring the prostate and defining the urethra and rectal wall. For each of the MO*Skin* diodes, a reference point was defined on the TPS which allowed the prescribed dose to these positions to be known.

The dose delivered to each dosimeter was monitored in real-time using the OneTouch readout system which was placed in the treatment room next to the phantom.

The introduction of a clinical relevant error was then applied to the experimental setup in order to quantify the TPT's ability to determine any large deviations from the treatment

(a) MO*Skins* placed along the TRUSProbe Tracker. The kapton tape can be seen securing the dosimeters.

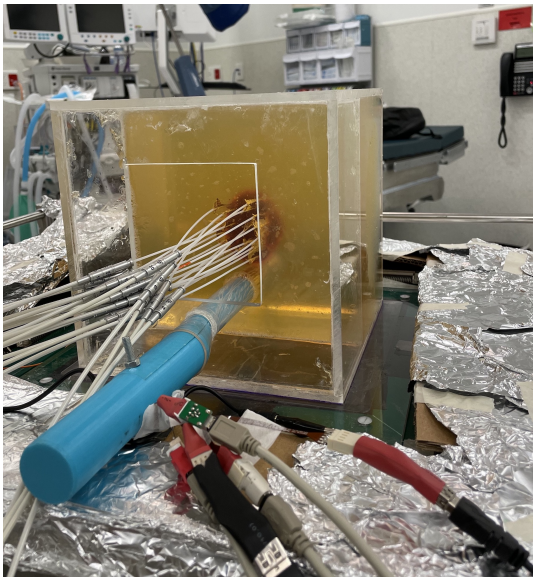

(b) The E2E and the 60cc Gel Prostate insert with the probe inserted prior to treatment.

Figure 5.6.1: An overview of the rectal wall dose study.

plan. This involved swapping catheters 1 and 3, an error which is both difficult to identify given current QA methods and clinical relevant due to the user specificity of connecting treatment catheters and the transfer tubes. The same treatment plan as previous tests was used.

Results

Of the five MO*Skin* dosimeters used on the TRUSProbe Tracker, one dosimeter returned a null reading, despite each dosimeter being tested before use. The malfunction may have arisen when inserting the TPT into the E2E phantom. Its measurements were neglected in any forthcoming calculations.

Over the course of each treatment, 2600 MO*Skin* data points were taken for each of the four functioning dosimeters across two fractions. The average response for all dosimeters across both fractions was (0.234cGy±0.382)cGy. The cumulative dose for each of the dosimeters was determined for each fraction and compared to the expected doses from the TPS. This can be seen in table 5.6.1.

The doses measured at each of the dosimeter positions all fall within 5% of the expected dose, with the largest being -4.49% and the smallest being 0.67%. The average $\Delta_{TPTvsTPS}$ was found to be (-2.34±6.3)%.

Table 5.6.1: A comparison of the measured dose deposited in each dosimeter and the expected doses determined from the TPS.

	Total Dose (cGy)					
Dosimeter	Fraction 1	Fraction 2	Mean	Error	TPS	$\Delta_{TPTvsTPS}$ (%)
1	437.56	447.41	447.41	±9.9	467.54	-4.49
3	434.91	429.34	429.34	±5.6	426.45	0.67
4	268.91	261.42	261.42	±7.5	268.50	-2.71
5	158.81	146.33	156.33	±2.5	160.72	-2.81

For the analysis of the catheter by catheter doses, twenty catheters per fraction over two fractions were used. The doses for each catheter were determined for each of the 4 functioning dosimeters and compared to the expected catheter doses for each of the dosimeters from the TPS. The average catheter dose measured was between 2.58 cGy to 133.60cGy, with the average being (16.17±19.50)cGy.

A histogram comparing the $\Delta_{TPTvsTPS}$ can be seen in Figure 5.6.2. When comparing the catheter by catheter doses between the dosimeter and the TPS values, the average relative dose difference was determined to be -2.4%. The maximum and minimum $\Delta_{TPTvsTPS}$ was found to be 19.66% and -21.36% respectively.

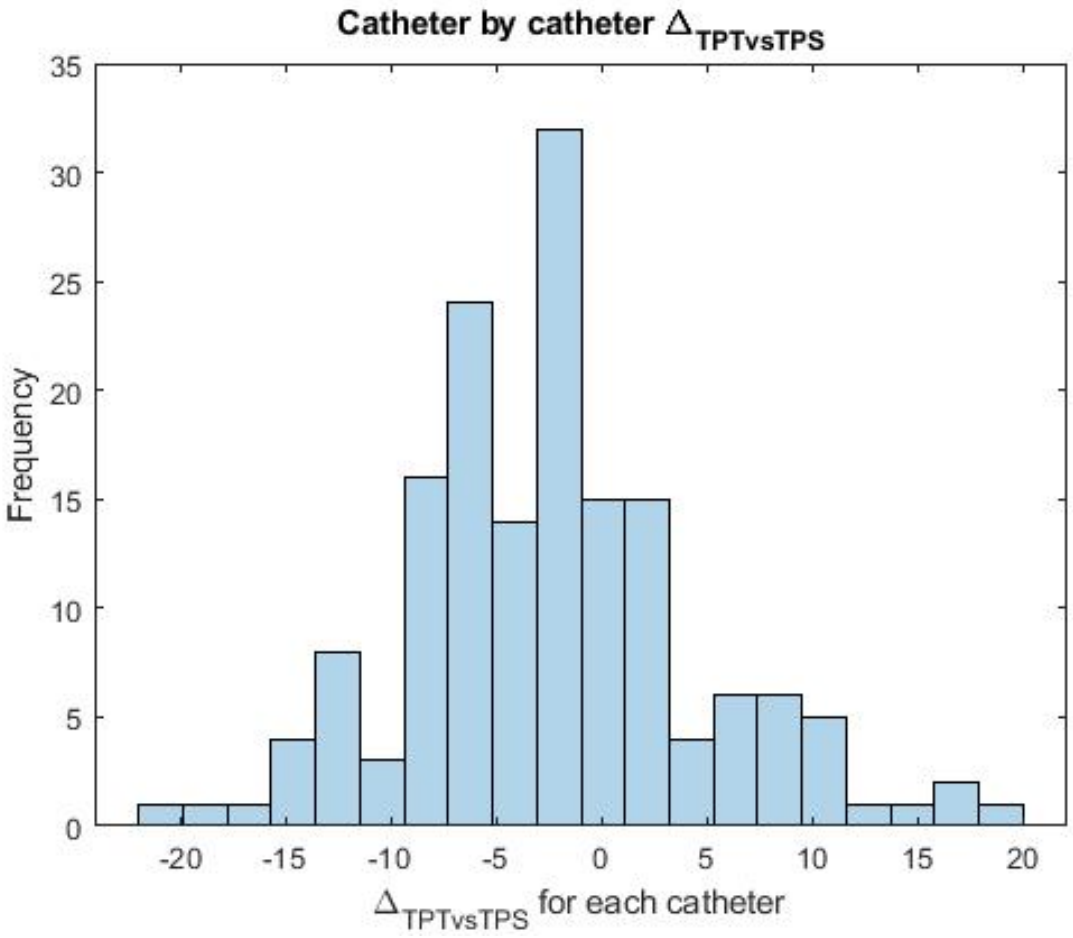

Figure 5.6.2: Histogram showing the $\Delta_{TPTvsTPS}$ for each catheter. The analysis uses 160 points which were taken using 20 catheters over 2 treatments measured with 4 MO*Skin* dosimeters.

When comparing the dose measurements from the error run and the TPS doses, the average relative dose difference was determined to be -5.29%. The maximum and minimum

$\Delta_{TPTvsTPS}$ was found to be 47.21% and -237.65% respectively. These results can be seen in Figure 5.6.3.

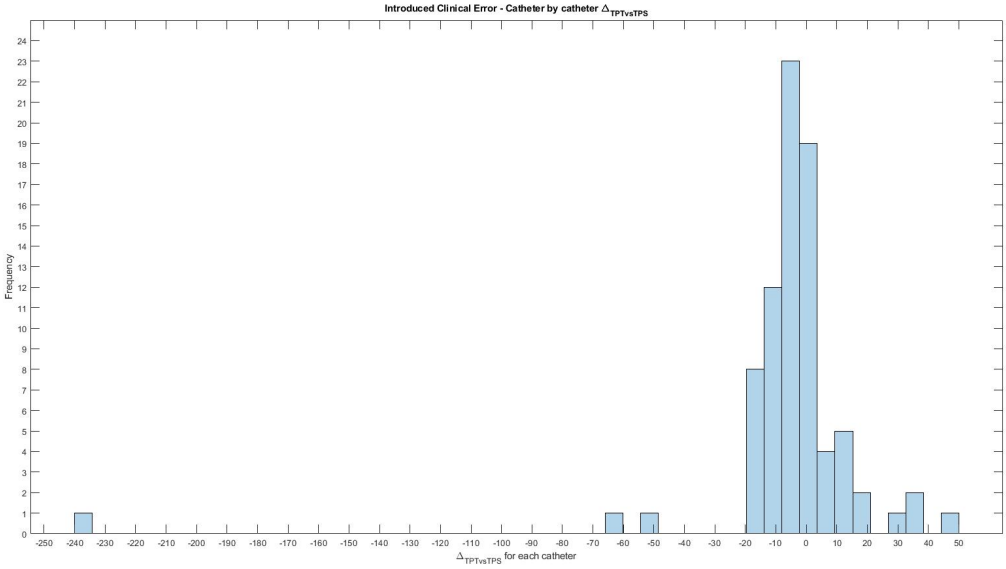

Figure 5.6.3: Histogram showing the $\Delta_{TPTvsTPS}$ for each catheter after the catheter swap had been performed.

Discussion

In order to validate the feasibility of the TRUSProbe Tracker (TPT) for *in-vivo* dosimetry, the first objective of the study was to obtain similar findings from earlier MO*Skin* studies. Poder *et al*'s 2020 study which utilised the Duel Purpose Probe obtained an average relative dose difference of (-1.6±11.1)% across 20 measured fractions [69]. Similar results were obtained by Carrara *et al.* Over 18 fractions, the measured doses returned an agreement with the TPS doses of (-2.1±8.3)% [67].

In this study, the average $\Delta_{TPTvsTPS}$ found across 2600 MO*Skin* data points taken from four

dosimeters across 2 fractions was (-2.34±6.3)%. This value shows a close correspondence to those results obtained in the previous studies. As a result, the use of MO*Skin* dosimeters for *in-vivo* dosimetry is further proven.

In order to validate real-time dose measurement, a catheter-by-catheter dose analysis was performed. Twenty catheters per fraction over 2 fractions were used. The doses were determined in each dosimeter for each catheter and compared to the TPS calculated doses. The average $\Delta_{TPTvsTPS}$ per catheter was found to be -2.4%, with a maximum of 19.66% and a minimum of -21.36%. At the end of the procedure, the relative difference observed was -1.8%.

The measured and TPS dose in each catheter is shown in Figure 5.6.4. The data shows a close correlation to the expected dose, with any deviations clearly visible by the existence of a difference in step. For the second half of the procedure when the catheters are further away from the dosimeters, it can be seen that there exists a clear difference in cumulative catheter dose by the presence of a step in Figure 5.6.4. This step may be attributed to the decrease in sensitivity of the dosimeters at this large SDD; errors associated with the fluctuations in dose caused from limitations in the MO*Skin* dosimeters are highlighted at large SDD.

Another factor which may contribute to the differences observed is the limitations in readout time for the OneTouch system. For smaller dwell times, the system is unable to to distinguish between. This may have resulted in the total dose for each catheter to miss some dose values or for some dose values to be contributed to the next catheter total.

The response of the TRUSProbe Tracker was evaluated when a clinically relevant error was introduced to the treatment. The error chosen to introduce was a catheter swap, which involved swapping catheter 1 and 3 prior to treatment delivery. The catheter by catheter

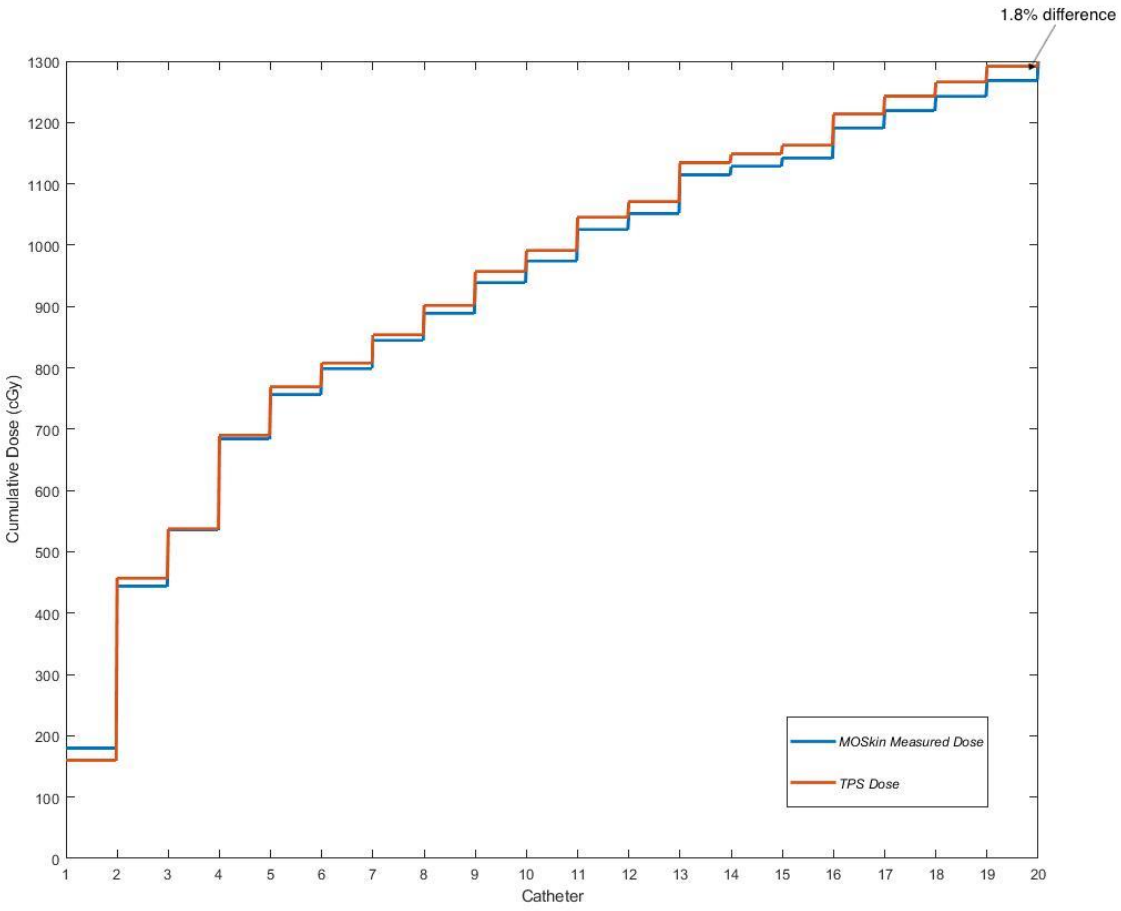

Figure 5.6.4: The cumulative dose for each catheter for both the TPS predicted (orange) and MO*Skin* (blue) measured doses.

cumulative dose can be seen in Figure 5.6.5.

A comparison of the dose measured in each dosimeter for each catheter can be seen in Figure 5.6.6. The measured, the TPS and the introduced run are all displayed.

From the graphs as well as the cumulative dose representation, the error introduction can be qualitatively seen; a large dose difference of ≈20cGy is evident for each dosimeter. Each dosimeter returned a different response to the error, based on where it is in relation to the catheter. Dosimeter 1 and 3 both showed an under response while dosimeter 4 and 5 shower

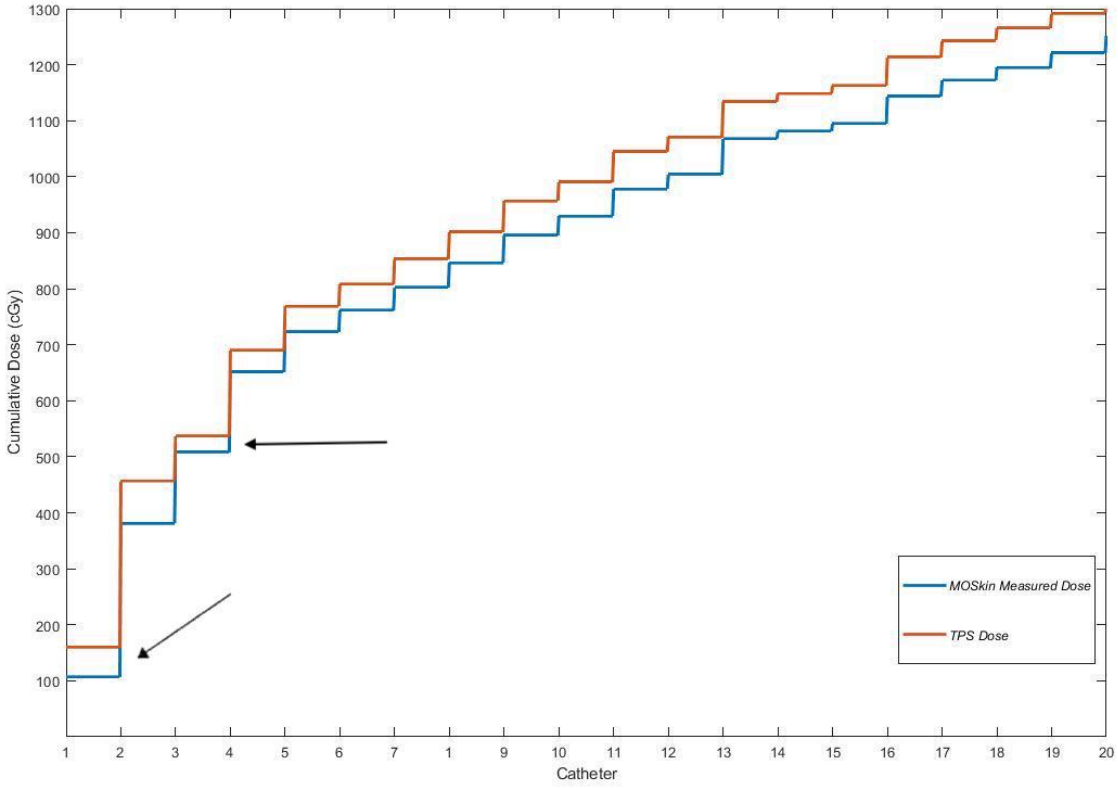

Figure 5.6.5: The cumulative dose for each catheter for both the TPS predicted (orange) and MO*Skin* (blue) measured. Prior to treatment, catheter 1 and 3 were swapped.

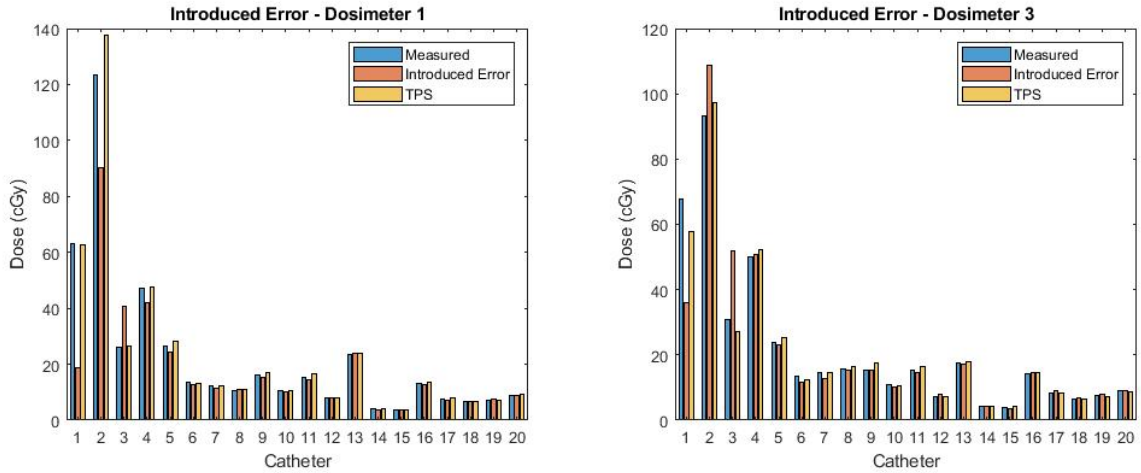

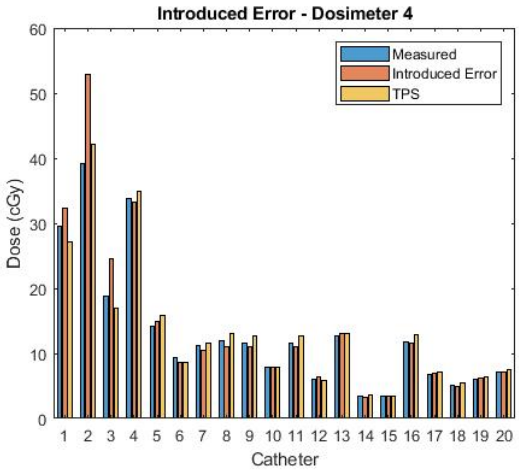

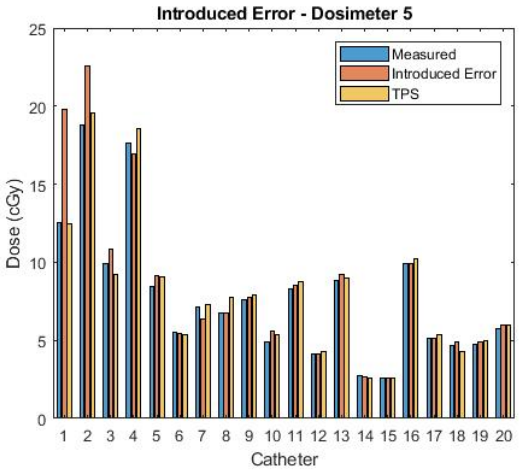

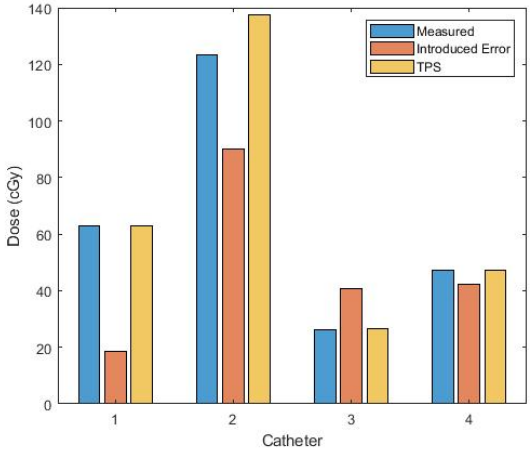

(b) A closeup of catheters 1,2,3 and 4

Figure 5.6.6: Dose deposited in each dosimeter in the initial measurement, the TPS and the introduced error measurement.

an over response.

The effect of a catheter swap can be observed in two different ways; timing and distance. Each catheter has its own total dwell time. Any increase, say from a catheter swap with a longer total dwell time, will cause measured dose for this catheter to increase and vice versa. the distance between the catheter and the dosimeters will also influence the dose deposited. Those catheters further away will deposit less dose than those which are closer. These two effects have both an additive and subtractive influence on dose.

For catheter 1, we see that we have an decrease in dose compared to the TPS. This is attributed to the difference in catheter 1 and 3 channel time: catheter 1 has a total dwell time of 42.6s and catheter 3 has a timing of 34.4s. By swapping the two, we would expect to see a decrease in dose for catheter 1 based on the timing differences.

For catheter 3, based on this difference in timing we would expect to see a large increase in dose. However, we only see a small increase. This small difference in dose may be a result in the other effect which influences detected dose; distance. Catheter 3 is located above catheter 1, with a difference in SDD. Based on this increased SDD, the dose deposited will be less. This may have been an attributing factor to a lower dose being detected for catheter 3.

Although the system was able to detect this difference, the difference in measured dose for catheter 2 cannot be explained. From Figure 5.6.6, the dose for catheter 2 can be seen to be lower than the expected. Due to the catheter not being swapped or changed, it is expected that its dose value was not to change. This difference may have been attributed to some level of dose spill from the surrounding catheters or a movement in catheter within the phantom during the catheter swap.

Although the system can be used to observe an introduced error, more testing at different heights and dwell timing needs to be conducted.

5.7 Conclusion

The purpose of this chapter was to investigate the potential of the TRUSProbe Tracker as a tool for *in-vivo* treatment verification for HDR PBT.

The source localisation section of this chapter hoped to prove a novel means of source tracking utilising MO*Skin* dosimeters. It was shown that preliminary source tracking was achieved with a varying degree of accuracy based on which axis was being investigate and the SDD. Based on limitations of the MO*Skin* dosimeter however, it is shown that the choice of detector needs to be revised. A more superior detector choice would be silicon diodes, similar to those used in the MP987 as they have a larger sensitive volume and are much easier to obtain a real-time readout. By using this detector type, an array of 12 detectors could be used in the probe to achieve its full source tracking potential. These diodes do not have the same fluctuations and angular dependence that MO*Skins* exhibit which would produce a more accurate source localisation.

The TRUSProbe Trackers ability to perform *in-vivo* dosimetry was evaluated in the second half of this chapter. The results obtained mirrored those that were obtained in previous studies, verifying the systems use as an *in-vivo* dosimetry tool. However, more studies are required to further verify findings found. Patient and retrospective studies would also serve as great importance in the commissioning of this device.

Chapter 6

Conclusion

The aim of this thesis was to develop a system which could accurately perform *in-vivo* treatment verification for HDR pBT in a clinical setting. This aim was achieved through the successful development of the E2E phantom with anatomically correct Gel Prostate insert which allowed subsequent studies to be conducted under clinically relevant conditions. The phantom was then used in the following chapters in conjunction with the MP987 detector system and the TRUSProbe Tracker to investigate their potential in IVTV. It was shown that the MP was capable of source localisation for clinically relevant treatment plans as well as its use in the identification of clinically relevant treatment errors. The TRUSProbe Tracker proved its ability to perform *in-vivo* dosimetry using MOSkin dosimeters and the abilities and limitations in source HDR source tracking were established.

6.1 Final Summary

In Chapter 3 of this thesis, it was successfully shown that the E2E phantom would be suitable for clinically relevant treatments. The Gel Prostate insert were proven to be an appropriate anthropomorphic phantom, with its US compatibility proven with a successful volumetric study conducted. It was further demonstrated that the phantom was compatible with the Proguide treatment catheters, with clear visibility shown on CT and US images. The importance of phantom mixture consistency was identified with the evaluation of catheter identification on US imaging.

The feasibility of using the MP987 to track clinically relevant HDR pBT treatment plans was proven in Chapter 4 of this thesis. The statistically significant property of repeatability between successive acquisitions was firstly evaluated, with results indicating that 95% of data collected for a single dwell position would fall within 2.6mm. The variance(σ) was calculated for varying SDD and dwell times, to evaluate their effect on the acquired data. It was shown that the variance decreased with increasing dwell time and increased with increasing SDD. It was then demonstrated that the calibration factor is dependent on the reference depth that it is calculated from, causing deviations on z output positions by up to 90%. It was then determined that the MP987 could localise a HDR source when comparing to the known source positions from the TPS on average to within (3.60±0.14)mm, (3.70±0.15)mm, (3.53±0.12)mm and (0.30±0.06)s for the x, y, z and t coordinates respectively. The systems ability to detect a clinically relevant error was also evaluated, with the catheter swap clearly evident in the returned dwell position differences.

Finally, in Chapter 5 the ability of the TRUSProbe Tracker coupled with MO*Skin* dosimeters to perform IVTV was evaluated. The tracking capabilities by means of dose rate comparison of the system was evaluated; using the times of maximum dose rates and the separation of the dosimeters the feasibility of using dose rate to localise a source was proven. The source tracking algorithm's use in source localisation was also demonstrated, with its performance evaluated for varying SDD along the z axis. The coordinates determined for an SDD of 17.15mm resulted in a relative difference when measuring the time taken between a pre-defined positions to be 1.3%. An increase of SDD to 51.15mm saw an increase in relative difference to 23.5%. The x axis and step size tracking abilities were evaluated, highlighting the systems source tracking limitations for these coordinates.

The feasibility of *in-vivo* rectal wall dosimetry using the TRUSProbe Tracker was then evaluated, with $\Delta_{TPTvsTPS}$ found to be (-2.34±6.3)% across 2 fractions. This is in close agreement with results found in previous MO*Skin* studies [67, 68]. Catheter-by-catheter dose analysis was then proven, with the average $\Delta_{TPTvsTPS}$ per catheter was found to be -2.4%. The plausibility of using the TRUSProbe tracker in determining a catheter swap was then shown, with a clear increase in relate difference in the swapped catheters.

6.2 Future Work

Although the use of the MP987 detector system and the TRUSProbe Tracker in IVTV was demonstrated successfully, there are a number of studies and alterations which need to be made before routine clinical application.

Firstly, as demonstrated in Section 4.2 and 4.3, the need for a more robust method of equalisation is apparent. The z coordinate output from the tracking software relies on pixel response, so a uniform response for each diode is a necessity. If each pixel across the plate responded uniformly, a calibration factor determined at any SDD and position above the plate should hold true for all measurements. This was not the case. A more reliable source of equalisation should be applied to the system before further studies. One such possibility positioning a source above each pixel individual at a fixed SDD, utilising treatment catheters and a remote afterloader. By doing so, each pixels response to the same source will be known and adjusted accordingly. Another factor which needs to be addressed in further studies is the influence of dead pixels in the COM calculation which returns position data. By creating a non-uniform distribution of the top 30% of pixel values, the COM calculation may produce an incorrect position which is not directly below the source. To avoid this, the source tracking algorithm needs to be altered in such a way as to remove the dead pixel's response entirely and replace it with an average of its neighbours responses.

Furthermore, a more appropriate means of shielding of the electronics should be investigated. The use of aluminium foil, although crude, did provide an appropriate level of RF shielding. However, the manufacture of a more permanent solution is required in order to reduce any miss-reads or noise into the system.

In order to obtain a more clinically relevant system, the way in which the co-registration of the MP and TPS coordinate system needs also to be investigated.

Finally, further studies for the TRUSProbe Tracker need to be conducted in order to further refine its use in IVTV. Retrospective and patient studies should be carried out to test its

in-vivo dosimetric properties. The source tracking capability of the TPT is limited however due to the use of MO*Skin* dosimeters as a means of source localisation. Future studies should replace MO*Skin*s with SI diodes to maximise the systems source tracking abilities. This will allow more detectors to be used in the TPT as well as a more accurate means of source localisation.

Bibliography

[1] Prostate cancer in australia. *Australian Institute of Health and Welfare*, Canberra, Australia:2013.

[2] Cancer fact sheets. *World Health Organisation* -, International Agency for Research on Cancer:2015.

[3] Fang-Zhi Chen and Xiao-Kun Zhao. Prostate cancer: current treatment and prevention strategies. *Iranian Red Crescent medical journal*, 15(4):279–284, 04 2013.

[4] Jack Venselaar. *Comprehensive brachytherapy: physical and clinical aspects*. CRC Press, 2016.

[5] Dimos Baltas Peter J. Hoskin Jack Venselaar, Ali S. Meigooni. *Comprehensive Brachytherapy: Physical and Clinical Aspects*.

[6] Elaine Nicpon Marieb and Suzanne M. Keller. *Essentials of human anatomy and physiology / Elaine N. Marieb, R.N., Ph.D., Holyoke Community College, Suzanne M. Keller, Ph.D., Indian Hills Community College*. Pearson, NY, NY, twelfth edition, global edition. edition, 2018.

[7] MaryBeth B. Culp, Isabelle Soerjomataram, Jason A. Efstathiou, Freddie Bray, and Ahmedin Jemal. Recent global patterns in prostate cancer incidence and mortality rates". *European Urology*, 2019.

[8] Peter Grimm, Ignace Billiet, David Bostwick, Adam P. Dicker, Steven Frank, Jos Immerzeel, Mira Keyes, Patrick Kupelian, W. Robert Lee, Stefan Machtens, Jyoti Mayadev, Brian J. Moran, Gregory Merrick, Jeremy Millar, Mack Roach, Richard Stock, Katsuto Shinohara, Mark Scholz, Ed Weber, Anthony Zietman, Michael Zelefsky, Jason Wong, Stacy Wentworth, Robyn Vera, and Stephen Langley. Comparative analysis of prostate-specific antigen free survival outcomes for patients with low, intermediate and high risk prostate cancer treatment by radical therapy. results from the prostate cancer results study group. *BJU International*, 109(s1):22–29.

[9] D. Jeffrey Demanes, Alvaro A. Martinez, Michel Ghilezan, Dennis R. Hill, Lionel Schour, David Brandt, and Gary Gustafson. High-dose-rate monotherapy: Safe and effective brachytherapy for patients with localized prostate cancer. *International Journal of Radiation Oncology*Biology*Physics*, 81(5):1286 – 1292, 2011.

[10] H. Dale Kubo, Glenn P. Glasgow, Timothy D. Pethel, Bruce R. Thomadsen, and Jeffrey F. Williamson. High dose-rate brachytherapy treatment delivery: Report of the aapm radiation therapy committee task group no. 59. *Medical Physics*, 25(4):375–403.

[11] A Challapalli, E Jones, C Harvey, G O Hellawell, and S A Mangar. High dose rate prostate brachytherapy: an overview of the rationale, experience and emerging applications in the treatment of prostate cancer. *The British Journal of Radiology*, 85(Spec Iss

1):S18–S27, 11 2012.

[12] Atefeh Rostami, Mahdi Hoseini, Mahdi Ghorbani, and Courtney Knaup. Dosimetric investigation of a new high dose rate (192)ir brachytherapy source, irasource, by monte carlo method. *Reports of practical oncology and radiotherapy : journal of Greatpoland Cancer Center in Poznan and Polish Society of Radiation Oncology*, 25(1):139–145, Jan-Feb 2020.

[13] E Browne. Comments on evaluation of 192 ir beta - and electron-capture decay data, Oct 2017.

[14] Stefan Strohmaier and Grzegorz Zwierzchowski. Comparison of (60)co and (192)ir sources in hdr brachytherapy. *J Contemp Brachytherapy*, 3(4):199–208, Dec 2011.

[15] Daniel G. Petereit, Steven J. Frank, Akila N. Viswanathan, Beth Erickson, Patricia Eifel, Paul L. Nguyen, and David E. Wazer. Brachytherapy: Where has it gone? *Journal of Clinical Oncology*, 33(9):980–982, 2015. PMID: 25667278.

[16] Joel Poder and May Whitaker. Robustness of ipsa optimized high-dose-rate prostate brachytherapy treatment plans to catheter displacements. *Journal of Contemporary Brachytherapy*, 3:201–207, 2016.

[17] Alexandru Nicolae, Jure Murgic, Ivan Kruljac, Lior Dubnitzky, Laura Dalimonte, Lin Lu, Aaron Cumal, Niki Law, Gerard Morton, Andrew Loblaw, and et al. Dosimetric impact of inter-observer catheter reconstruction variability in ultrasound-based high-dose-rate prostate brachytherapy. *Brachytherapy*, 17(2):306–312, 2018.

[18] Shyam Bharat, Cynthia Kung, Ehsan Dehghan, Ananth Ravi, Niranjan Venugopal, Antonio Bonillas, Doug Stanton, and Jochen Kruecker. Electromagnetic tracking for catheter reconstruction in ultrasound-guided high-dose-rate brachytherapy of the prostate. *Brachytherapy*, 13(6):640 – 650, 2014.

[19] Ravinder Nath, Lowell L. Anderson, Gary Luxton, Keith A. Weaver, Jeffrey F. Williamson, and Ali S. Meigooni. Dosimetry of interstitial brachytherapy sources: Recommendations of the aapm radiation therapy committee task group no. 43. *Medical Physics*, 22(2):209–234, 1995.

[20] Mark J. Rivard, Bert M. Coursey, Larry A. DeWerd, William F. Hanson, M. Saiful Huq, Geoffrey S. Ibbott, Michael G. Mitch, Ravinder Nath, and Jeffrey F. Williamson. Update of aapm task group no. 43 report: A revised aapm protocol for brachytherapy dose calculations. *Medical Physics*, 31(3):633–674, 2004.

[21] Luc Beaulieu, A[U+0085]sa Carlsson Tedgren, Jean Franasois Carrier, Stephen D. Davis, Firas Mourtada, Mark J. Rivard, Rowan M. Thomson, Frank Verhaegen, Todd A. Wareing, and Jeffrey F. Williamson. Report of the task group 186 on model-based dose calculation methods in brachytherapy beyond the tg-43 formalism: Current status and recommendations for clinical implementation. *Medical Physics*, 39(10):6208–6236, 2012.

[22] M Saiful Huq, Benedick A Fraass, Peter B Dunscombe, Jr Gibbons, John P, Geoffrey S Ibbott, Arno J Mundt, Sasa Mutic, Jatinder R Palta, Frank Rath, Bruce R Thomadsen, Jeffrey F Williamson, and Ellen D Yorke. The report of task group 100 of the aapm: Application of risk analysis methods to radiation therapy quality management. *Medical*

physics, 43(7):4209–4209, 07 2016.

[23] Claire Dempsey, Ryan Smith, Thulani Nyathi, Abdurrahman Ceylan, Lisa Howard, Virendra Patel, Ram Das, and Annette Haworth. Acpsem brachytherapy working group recommendations for quality assurance in brachytherapy. *Australasian Physical & Engineering Sciences in Medicine*, 36(4):387–396, 2013.

[24] R Nath, L L Anderson, J A Meli, A J Olch, J A Stitt, and J F Williamson. Code of practice for brachytherapy physics: report of the aapm radiation therapy committee task group no. 56. american association of physicists in medicine. *Med Phys*, 24(10):1557–1598, Oct 1997.

[25] D A Wilkinson. High dose rate (hdr) brachytherapy quality assurance: a practical guide. *Biomed Imaging Interv J*, 2(2):e34, Apr 2006.

[26] Margaret. Bidmead, Jack. Venselaar, José. Pérez-Calatayud, European Society for Therapeutic Radiology, and Oncology. *A practical guide to quality control of brachytherapy equipment*. ESTRO, Brussels, 2004.

[27] Bradley R. Beeksma. Source tracking and quality assurance of high dose rate (hdr) brachytherapy. 2014.

[28] Kari Tanderup, Sam Beddar, Claus E. Andersen, Gustavo Kertzscher, and Joanna E. Cygler. In vivo dosimetry in brachytherapy. *Medical Physics*, 40(7):070902.

[29] Claudia Waldhausl, Andre Wambersie, Richard Potter, and Dietmar Georg. In-vivo dosimetry for gynaecological brachytherapy: physical and clinical considerations. *Ra-*

diother Oncol, 77(3):310–317, Dec 2005.

[30] G Anagnostopoulos, D Baltas, A Geretschlaeger, T Martin, P Papagiannis, N Tselis, and N Zamboglou. In vivo thermoluminescence dosimetry dose verification of transperineal 192ir high-dose-rate brachytherapy using ct-based planning for the treatment of prostate cancer. *Int J Radiat Oncol Biol Phys*, 57(4):1183–1191, Nov 2003.

[31] Evelina Jaselskė, Diana Adlienė, Viktoras Rudžianskas, Benas Gabrielis Urbonavičius, and Arturas Inčiūra. In vivo dose verification method in catheter based high dose rate brachytherapy. *Physica Medica*, 44:1 – 10, 2017.

[32] Kari Tanderup, Sam Beddar, Claus E. Andersen, Gustavo Kertzscher, and Joanna E. Cygler. In vivo dosimetry in brachytherapy. *Medical Physics*, 40(7):070902, 2013.

[33] Takayuki Nose, Masahiko Koizumi, Ken Yoshida, Kinji Nishiyama, Junichi Sasaki, Takeshi Ohnishi, Takuyo Kozuka, Kotaro Gomi, Masahiko Oguchi, Iori Sumida, Yutaka Takahashi, Akira Ito, and Takashi Yamashita. ¡em¿in vivo¡/em¿ dosimetry of high-dose-rate interstitial brachytherapy in the pelvic region: Use of a radiophotoluminescence glass dosimeter for measurement of 1004 points in 66 patients with pelvic malignancy. *International Journal of Radiation Oncology *Biology *Physics*, 70(2):626–633, 2018/10/29 2008.

[34] Sun Young Moon, Jaeman Son, Myonggeun Yoon, EunHee Jeang, Young Kyung Lim, Weon Kyu Chung, and Dong Wook Kim. Applicability of glass dosimeters for in-vivo dosimetry in brachytherapy. *Journal of the Korean Physical Society*, 72(11):1320–1325, 2018.

[35] Shih-Ming Hsu, Chien-Yi Yeh, Tien-Chi Yeh, Ji-Hong Hong, Annie Y. H. Tipton, Wei-Li Chen, Shung-Shung Sun, and David Y. C. Huang. Clinical application of radiophotoluminescent glass dosimeter for dose verification of prostate hdr procedure. *Medical Physics*, 35(12):5558–5564, 2008.

[36] Claus E. Andersen, Søren Kynde Nielsen, Steffen Greilich, Jakob Helt-Hansen, Jacob Christian Lindegaard, and Kari Tanderup. Characterization of a fiber-coupled luminescence dosimetry system for online in vivo dose verification during brachytherapy. *Medical Physics*, 36(3):708–718.

[37] Gustavo Kertzscher, Claus E. Andersen, Frank-André Siebert, Søren Kynde Nielsen, Jacob C. Lindegaard, and Kari Tanderup. Identifying afterloading pdr and hdr brachytherapy errors using real-time fiber-coupled al$_2$o$_3$:c dosimetry and a novel statistical error decision criterion. *Radiotherapy and Oncology*, 100(3):456–462, 2018/10/30 2011.

[38] Francois Therriault-Proulx, Tina M. Briere, Firas Mourtada, Sylviane Aubin, Sam Beddar, and Luc Beaulieu. A phantom study of an in vivo dosimetry system using plastic scintillation detectors for real-time verification of 192ir hdr brachytherapy. *Medical Physics*, 38(5):2542–2551.

[39] Zhen-Yu Qi, Xiao-Wu Deng, Shao-Min Huang, Jie Lu, Michael Lerch, Dean Cutajar, and Anatoly Rosenfeld. Verification of the plan dosimetry for high dose rate brachytherapy using metal–oxide–semiconductor field effect transistor detectors. *Medical Physics*, 34(6Part1):2007–2013, 2007.

[40] Jacob Graversen Johansen, Susanne Rylander, Simon Buus, Lise Bentzen, Steffen Bjerre

Hokland, Christian Skou Søndergaard, Anders Karl Mikael With, Gustavo Kertzscher, and Kari Tanderup. Time-resolved in vivo dosimetry for source tracking in brachytherapy. *Brachytherapy*, 17(1):122–132, 2018. Treatment Delivery Verification in Brachytherapy: Prospects of Technology Innovation.

[41] P. Guiral, J. Ribouton, P. Jalade, R. Wang, J.-M. Galvan, G.-N. Lu, P. Pittet, A. Rivoire, and L. Gindraux. Design and testing of a phantom and instrumented gynecological applicator based on gan dosimeter for use in high dose rate brachytherapy quality assurance. *Medical Physics*, 43(9):5240–5251, 2016.

[42] François Therriault-Proulx, Sam Beddar, and Luc Beaulieu. On the use of a single-fiber multipoint plastic scintillation detector for 192ir high-dose-rate brachytherapy. *Medical Physics*, 40(6Part1):062101, 2013.

[43] R. Wang, J. Ribouton, P. Pittet, P. Guiral, P. Jalade, and G.N. Lu. Implementation of gan based real-time source position monitoring in hdr brachytherapy. *Radiation Measurements*, 71:293–296, 2014. Proceedings of the 17th Solid State Dosimetry Conference (SSD17).

[44] Yusuke Watanabe, Hiroshi Muraishi, Hideyuki Takei, Hidetake Hara, Tsuyoshi Terazaki, Nobuaki Shuto, Takahiro Shimo, Marika Nozawa, Hiromichi Ishiyama, Kazushige Hayakawa, and Tsutomu Gomi. Automated source tracking with a pinhole imaging system during high-dose-rate brachytherapy treatment. *Physics in Medicine & Biology*, 63(14):145002, jul 2018.

[45] M. Petasecca, K. J. Loo, M. Safavi-Naeini, Z. Han, P. E. Metcalfe, S. Meikle, S. Pospisil,

J. Jakubek, J. A. Bucci, M. Zaider, M. L. F. Lerch, Y. Qi, and A. B. Rosenfeld. Brachyview: Proof-of-principle of a novel in-body gamma camera for low dose-rate prostate brachytherapy. *Medical Physics*, 40(4):041709, 2013.

[46] S. Alnaghy, D.L. Cutajar, J.A. Bucci, K. Enari, M. Safavi-Naeini, M. Favoino, M. Tartaglia, F. Carriero, J. Jakubek, S. Pospisil, M. Lerch, A.B. Rosenfeld, and M. Petasecca. Brachyview: Combining ldr seed positions with transrectal ultrasound imaging in a prostate gel phantom. *Physica Medica*, 34:55–64, 2017.

[47] Christoph Bert, Markus Kellermeier, and Kari Tanderup. Electromagnetic tracking for treatment verification in interstitial brachytherapy. *J Contemp Brachytherapy*, 8(5):448–453, Oct 2016.

[48] Markus Kellermeier, Jens Herbolzheimer, Stephan Kreppner, Michael Lotter, Vratislav Strnad, and Christoph Bert. Electromagnetic tracking (emt) technology for improved treatment quality assurance in interstitial brachytherapy. *Journal of Applied Clinical Medical Physics*, 18(1):211–222, 2017.

[49] Jun Zhou, Evelyn Sebastian, Victor Mangona, and Di Yan. Real-time catheter tracking for high-dose-rate prostate brachytherapy using an electromagnetic 3d-guidance device: A preliminary performance study. *Medical Physics*, 40(2):021716, 2013.

[50] Eric Poulin, Emmanuel Racine, Dirk Binnekamp, and Luc Beaulieu. Fast, automatic, and accurate catheter reconstruction in hdr brachytherapy using an electromagnetic 3d tracking system. *Medical Physics*, 42(3):1227–1232, 2015.

[51] R. L. Smith, M. L. Taylor, L. N. McDermott, A. Haworth, J. L. Millar, and R. D.

Franich. Source position verification and dosimetry in hdr brachytherapy using an epid. *Medical Physics*, 40(11):111706, 2013.

[52] Ryan L Smith, Jeremy Laurence Millar, Leah N McDermott, and Rick D Franich. Initial clinical experience with hdr treatment verification using a flat panel detector. *Journal of Contemporary Brachytherapy*, 6(1):123, May 2014. 23rd Annual Scientific Meeting of the Australasian Brachytherapy Group , ABG 2014 ; Conference date: 20-02-2014 Through 22-02-2014.

[53] Ryan L. Smith, Annette Haworth, Vanessa Panettieri, Jeremy L. Millar, and Rick D. Franich. A method for verification of treatment delivery in hdr prostate brachytherapy using a flat panel detector for both imaging and source tracking. *Medical Physics*, 43(5):2435–2442, 2016.

[54] Ryan L. Smith, Annette Haworth, Vanessa Panettieri, Jeremy L. Millar, and Rick D. Franich. 3d catheter reconstruction in hdr prostate brachytherapy for pre-treatment verification using a flat panel detector. *Physica Medica*, 39:121–131, 2017.

[55] Ryan L. Smith, Max Hanlon, Vanessa Panettieri, Jeremy L. Millar, Bronwyn Matheson, Annette Haworth, and Rick D. Franich. An integrated system for clinical treatment verification of hdr prostate brachytherapy combining source tracking with pretreatment imaging. *Brachytherapy*, 17(1):111–121, 2018. Treatment Delivery Verification in Brachytherapy: Prospects of Technology Innovation.

[56] G Fonseca, M Podesta, B Reniers, and F Verhaegen. Mo-ab-bra-03: Development of novel real time in vivo epid treatment verification for brachytherapy. *Medical Physics*,

43(6Part28):3691–3691, 2016.

[57] Gabriel P Fonseca, Mark Podesta, Murillo Bellezzo, Michiel R Van den Bosch, Ludy Lutgens, Ben G L Vanneste, Robert Voncken, Evert J Van Limbergen, Brigitte Reniers, and Frank Verhaegen. Online pretreatment verification of high-dose rate brachytherapy using an imaging panel. *Physics in Medicine & Biology*, 62(13):5440–5461, jun 2017.

[58] Gabriel P Fonseca, Michiel R Van den Bosch, Robert Voncken, Mark Podesta, and Frank Verhaegen. A novel system for commissioning brachytherapy applicators: example of a ring applicator. *Physics in Medicine & Biology*, 62(21):8360–8375, oct 2017.

[59] A Espinoza, B Beeksma, M Petasecca, I Fuduli, C Porumb, D Cutajar, S Corde, M Jackson, M L F Lerch, and A B Rosenfeld. The feasibility study and characterization of a two-dimensional diode array in "magic phantom" for high dose rate brachytherapy quality assurance. *Med Phys*, 40(11):111702, Nov 2013.

[60] Anthony Espinoza, Marco Petasecca, Iolanda Fuduli, A Howie, J Bucci, Stéphanie Corde, Michael Jackson, Michael Lerch, and Anatoly Rosenfeld. The evaluation of a 2d diode array in "magic phantom" for use in high dose rate brachytherapy pretreatment quality assurance. *Medical Physics*, 42:663–673, 02 2015.

[61] A. Espinoza, B. Beeksma, M. Petasecca, I. Fuduli, C. Porumb, D. Cutajar, S. Corde, M. Jackson, M. L. F. Lerch, and A. B. Rosenfeld. The feasibility study and characterization of a two-dimensional diode array in "magic phantom" for high dose rate brachytherapy quality assurance. *Medical Physics*, 40(11):111702, 2013.

[62] J. H. D. Wong, I. Fuduli, M. Carolan, M. Petasecca, M. L. F. Lerch, V. L. Perevertaylo,

P. Metcalfe, and A. B. Rosenfeld. Characterization of a novel two dimensional diode array the "magic plate" as a radiation detector for radiation therapy treatment. *Medical Physics*, 39(5):2544–2558, 2012.

[63] Joel Poder, Dean Cutajar, Susanna Guatelli, Marco Petasecca, Andrew Howie, Joseph Bucci, and Anatoly Rosenfeld. Hdr brachytherapy in vivo source position verification using a 2d diode array: A monte carlo study. *Journal of Applied Clinical Medical Physics*, 19(4):163–172, 2018.

[64] Joel Poder, Dean Cutajar, Susanna Guatelli, Marco Petasecca, Andrew Howie, Joseph Bucci, Mauro Carrara, and Anatoly Rosenfeld. A monte carlo study on the feasibility of real-time in vivo source tracking during ultrasound based hdr prostate brachytherapy treatments. *Physica Medica*, 59:30 – 36, 2019.

[65] I. S. Kwan, D. Wilkinson, D. Cutajar, M. Lerch, A. Rosenfeld, A. Howie, J. Bucci, Y. Chin, and V. L. Perevertaylo. The effect of rectal heterogeneity on wall dose in high dose rate brachytherapy. *Medical Physics*, 36(1):224–232, 2009.

[66] C. Tenconi, M. Carrara, M. Borroni, A. Cerrotta, D. Cutajar, M. Petasecca, M. Lerch, J. Bucci, G. Gambarini, E. Pignoli, and A. Rosenfeld. Trus-probe integrated moskin detectors for rectal wall in vivo dosimetry in hdr brachytherapy: In phantom feasibility study. *Radiation Measurements*, 71:379–383, 2014. Proceedings of the 17th Solid State Dosimetry Conference (SSD17).

[67] Mauro Carrara, Chiara Tenconi, Giulio Rossi, Marta Borroni, Annamaria Cerrotta, Simone Grisotto, Davide Cusumano, Brigida Pappalardi, Dean Cutajar, Marco Petasecca,

Michael Lerch, Grazia Gambarini, Carlo Fallai, Anatoly Rosenfeld, and Emanuele Pignoli. In vivo rectal wall measurements during hdr prostate brachytherapy with moskin dosimeters integrated on a trans-rectal us probe: Comparison with planned and reconstructed doses. *Radiotherapy and Oncology*, 118(1):148–153, 2016.

[68] M. Carrara, C. Tenconi, D. Mazzeo, A. Romanyukha, M. Borroni, E. Pignoli, D. Cutajar, M. Petasecca, M. Lerch, J. Bucci, G. Gambarini, A. Cerrotta, C. Fallai, and A. Rosenfeld. Study of the correlation between rectal wall in vivo dosimetry performed with moskins and implant modification during trus-guided hdr prostate brachytherapy. *Radiation Measurements*, 106:385–390, 2017. Proceedings of the 18th International Conference on Solid State Dosimetry (SSD18), Munich, Germany, 3 – 8 July 2016.

[69] Joel Poder, Andrew Howie, Ryan Brown, Joseph Bucci, Anatoly Rosenfeld, Komiti Enari, Kristine Schreiber, Mauro Carrara, Andrej Bece, David Malouf, and Dean Cutajar. Towards real time in-vivo rectal dosimetry during trans-rectal ultrasound based high dose rate prostate brachytherapy using moskin dosimeters. *Radiotherapy and Oncology*, 151:273–279, 2020.

[70] Ida Bagus O W Putra, Agus R A H Hamid, Chaidir A Mochtar, and Rainy Umbas. Relationship of age, prostate-specific antigen, and prostate volume in indonesian men with benign prostatic hyperplasia. *Prostate Int*, 4(2):43–48, Jun 2016.

[71] Ronald Bude and Ronald S. Adler. An easily made, low-cost, tissue-like ultrasound phantom material.

[72] Practical guide for the validation, quality control, and uncertainty assessment of an

alternative oenological analysis method.

[73] Wei Loong Jong, Jeannie Hsiu Ding Wong, Ngie Min Ung, Kwan Hoong Ng, Gwo Fuang Ho, Dean L. Cutajar, and Anatoly B. Rosenfeld. Characterization of moskin detector for in vivo skin dose measurement during megavoltage radiotherapy. *Journal of Applied Clinical Medical Physics*, 15(5):120–132, 2014.

[74] Paolo Brandimarte. Neighbourhood search-based optimization algorithms for production scheduling: a survey. *Computer Integrated Manufacturing Systems*, 5(2):167–176, 1992.